

# REVEALING THE ORIGIN OF CHEMICAL WEAPONS

## SUPPLEMENTARY DATA



Mirjam de Bruin-Hoegée

# CHAPTER 2

## SUPPLEMENTARY DATA



Supplementary material

# Chemical Attribution of Fentanyl: The Effect of Human Metabolism

Mirjam de Bruin-Hoegée<sup>a,b,\*</sup>, Djarah Kleiweg<sup>a</sup>, Daan Noort<sup>b</sup>, Arian C. Van Asten<sup>a,c</sup>

<sup>a</sup> van 't Hoff Institute for Molecular Sciences, Faculty of Science, University of Amsterdam, P.O. Box 94157, 1090GD Amsterdam, The Netherlands

<sup>b</sup> TNO Defence, Safety and Security, Dep. CBRN Protection, Lange Kleiweg 137, 2288GJ Rijswijk, The Netherlands

<sup>c</sup> CLHC, Amsterdam Center for Forensic Science and Medicine, University of Amsterdam, P.O. Box 94157, 1090GD Amsterdam, The Netherlands

\*Corresponding author. Email address: [mirjam.debruin@tno.nl](mailto:mirjam.debruin@tno.nl) (M. de Bruin-Hoegée)

## Contents

- Figure 1. Method for microsomal incubation and sample preparation
- Figure 2. Calibration curves
- Figure 3. Identification of a tentative structure by MS/MS
- Figure 4. Effect of leave-one-out validation on PCA performance



### PRE-INCUBATION

- 500 µL Buffer: 0.1 M K<sub>3</sub>PO<sub>4</sub>, 2.5 mM MgCl<sub>2</sub> (pH = 7.4)
  - 100 µL of 1 mg/mL fentanyl
  - 200 µL of 2.5 mg/mL human liver microsomes
- 3 min., 300 rpm @37 °C

### INCUBATION

- 200 µL NADPH-regenerating system:
    - 1 mM NADP+
    - 5 mM glucose-6-phosphate
    - 1 U/mL glucose-6-phosphate dehydrogenase
    - 2 mM UDPGA
- 72h, 300 rpm @37 °C

### SAMPLE PREPARATION

#### LC

- Collect 500 µL sample
  - Add 500 µL acetonitrile
- Vortex and centrifuging: 10 min., 14,000 rpm
- Collect supernatant (proteins precipitate)
  - Add 100 µL benzylfentanyl of 1 µg/mL
  - Add 400 µL MilliQ
  - Analyse by LC

#### GC

- Collect 500 µL sample
- Centrifuging: 10 min., 14,000 rpm
- Collect supernatant (proteins precipitate)
  - Add 400 µL DCM and vortex
  - Collect bottom layer
  - Add 100 µL d<sub>5</sub>-norfentanyl of 100 µg/mL
  - Analyse by GC

Figure 1. Method for microsomal incubation and sample preparation. LC-Orbitrap-MS © Thermo Fisher Scientific (Bremen). Printed with OTRS permission. GC-MS © Agilent Technologies, Inc. Reproduced with Permission.

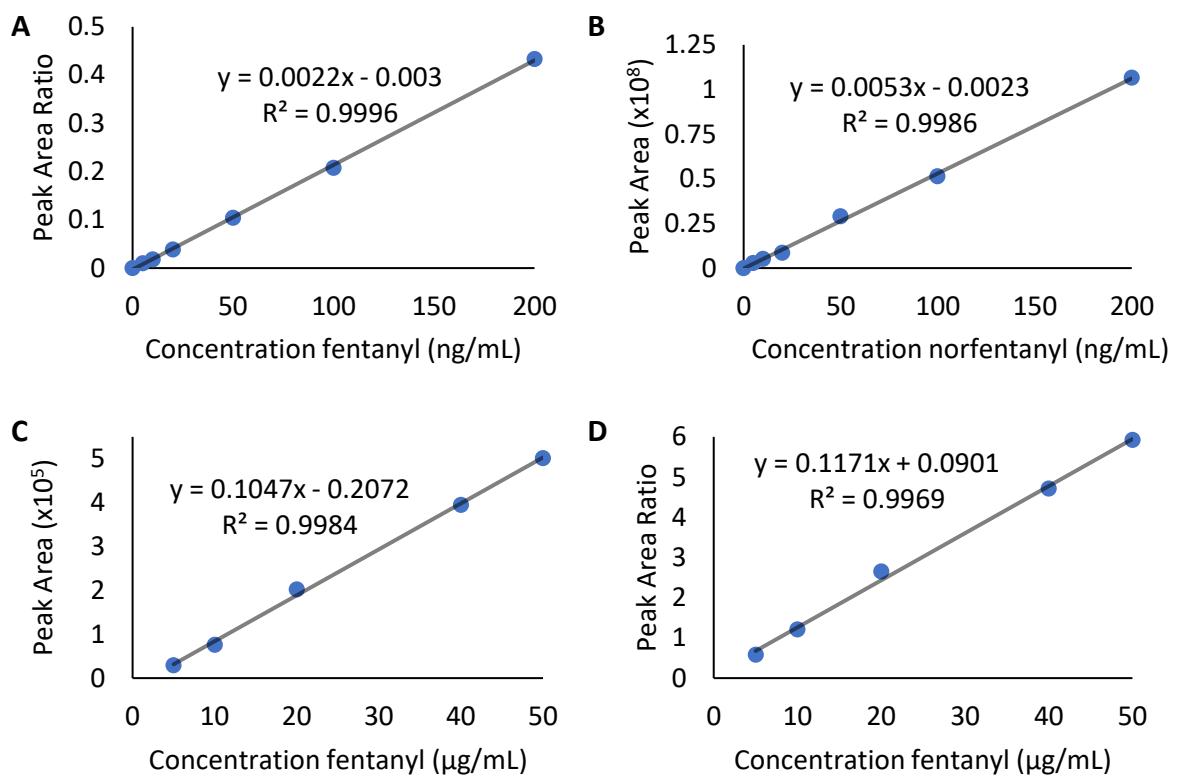
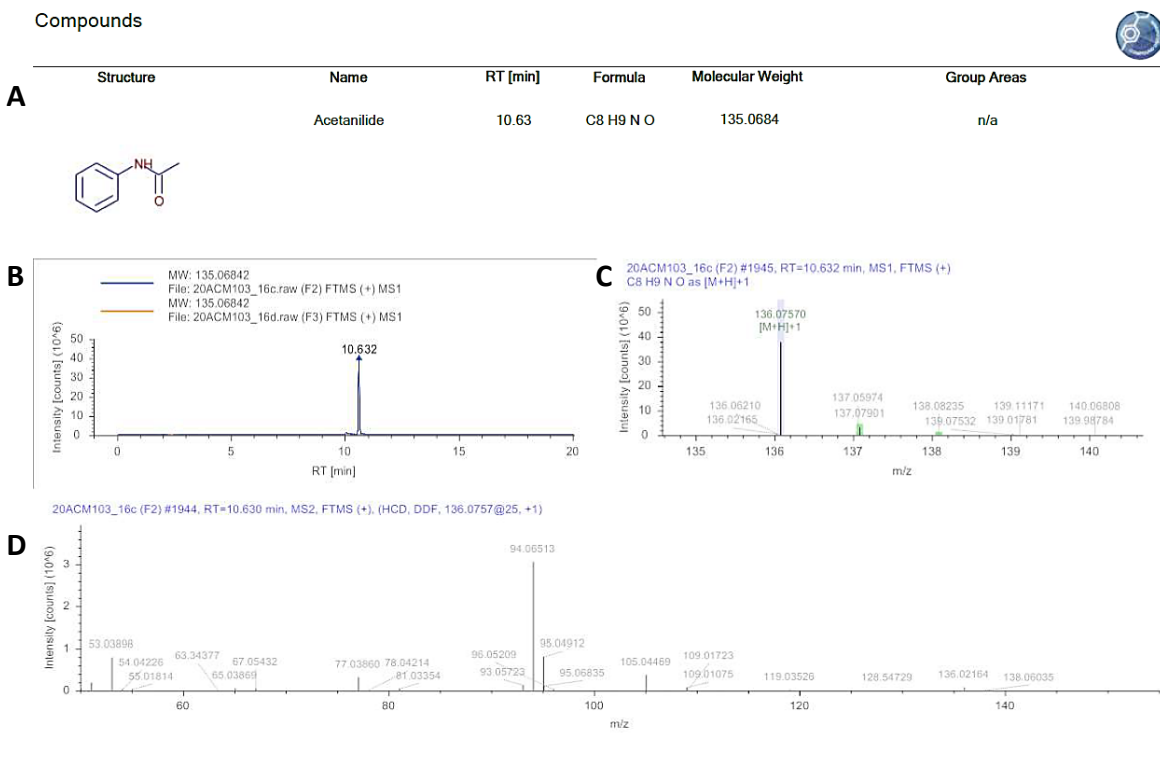


Figure 2. Calibration curves of A) Fentanyl with internal standard benzylfentanyl detected by LC-MS/MS. B) Norfentanyl detected by LC-MS/MS. C) Fentanyl detected by GC-MS. D) Norfentanyl with internal standard d<sub>5</sub>-norfentanyl detected by GC-MS.



© Reported with Compound Discoverer 2.1

Figure 3. Typical identification of a tentative structure by LC-Orbitrap-MS/MS reported by Compound Discoverer 2.1. The impurity identified as N-phenylacetamide (J) is presented. A) Summary of results. B) Chromatogram. C) Mass spectrum. D) MS/MS spectrum.

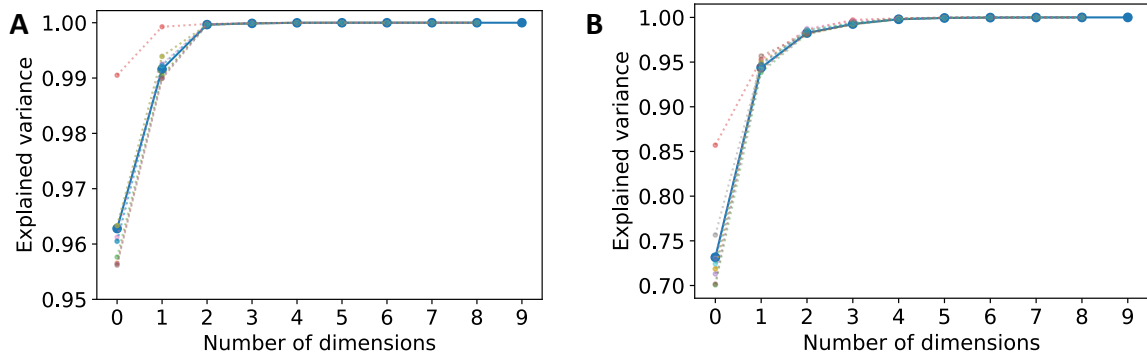


Figure 4. Effect of leave-one-out validation on PCA robustness. Blue line: PCA including all samples; dashed lines: PCA with one sample left out. For each dashed line another measurement is left out. The PCA model showed good robustness, since leaving out one sample resulted in similar explained variance. A) Pre-metabolism measured by LC-Orbitrap-MS. B) Post-metabolism measured by LC-Orbitrap-MS.

# CHAPTER 3

## SUPPLEMENTARY DATA



## Supplementary data

# Post-metabolism impurity profiling of carfentanil, remifentanil, sufentanil, and benzylfentanyl

Daan Vangerven<sup>a,1</sup>, Mirjam de Bruin-Hoegée<sup>a,b,1,\*</sup>, Fleur Kerstens<sup>c</sup>, Meike Kerklaan<sup>a</sup>, Rowdy P. T. Bross<sup>b</sup>, Alex Fidder<sup>b</sup>, Marcel van der Schans<sup>b</sup>, Daan Noort<sup>b,2</sup>, Arian C. Van Asten<sup>a,d</sup>

<sup>a</sup> van 't Hoff Institute for Molecular Sciences, Faculty of Science, University of Amsterdam, P.O. Box 94157, 1090GD Amsterdam, The Netherlands

<sup>b</sup> TNO Defence, Safety and Security, Dep. CBRN Protection, Lange Kleiweg 137, 2288GJ Rijswijk, The Netherlands

<sup>c</sup> Research group Analysis Techniques in Life Sciences, Avans University of Applied Sciences, Lovensdijkstraat 61-63, 4818 AJ, Breda, The Netherlands

<sup>d</sup> CLHC, Amsterdam Center for Forensic Science and Medicine, University of Amsterdam, P.O. Box 94157, 1090GD Amsterdam, The Netherlands

<sup>1</sup> Authors contributed equally to this manuscript.

<sup>2</sup> Current address: Organisation for the Prohibition of Chemical Weapons, Johan de Wittlaan 32, 2517 JR The Hague, The Netherlands

\*Corresponding author. Email address: [mirjam.debruin@tno.nl](mailto:mirjam.debruin@tno.nl) (M. de Bruin-Hoegée)

## Contents

1. Method validation LC-MS/MS .....	2
2. Impurities remifentanil.....	4
3. Impurities carfentanil .....	5
4. Match criterion approach.....	6
5. Multivariate analysis remifentanil.....	7
6. Multivariate analysis carfentanil .....	9
References.....	11

## 1. Method validation LC-MS/MS

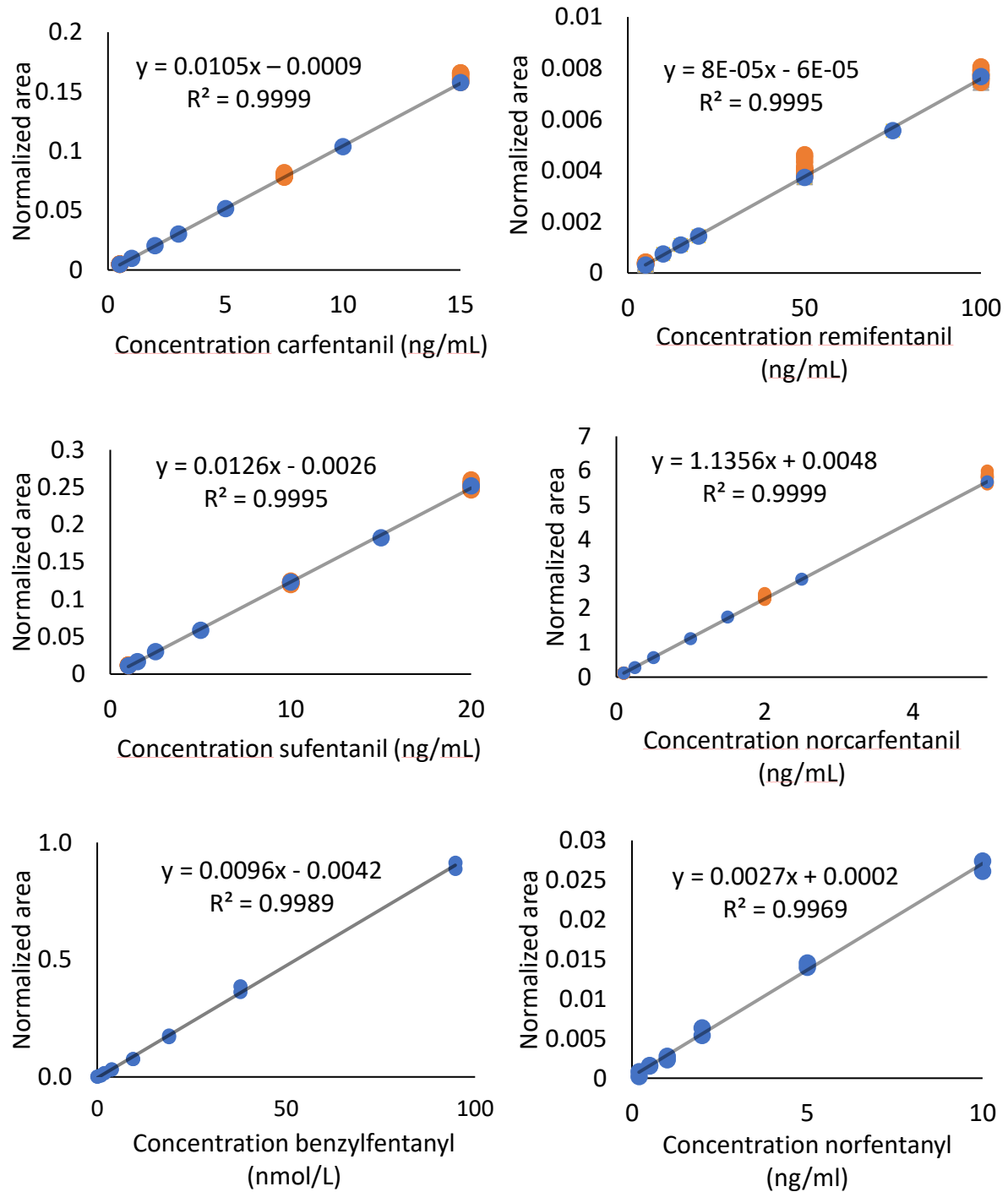


Figure S 1. Calibration curves and spiked quality controls of carfentanil, remifentanil, sufentanil, norcarfentanil, benzylfentanyl, and norfentanyl.

Table S 1. Quality control results for carfentanil, remifentanil, sufentanil, norcarfentanil ( $n=10$ ), and benzylfentanyl ( $n=9$ ).

Analyte	Level	Concentration (ng/mL)	Accuracy (% of true value)	Precision (RSD%)
<b>Carfentanil</b>	Low	0.5	8	1.5
	Medium	7.5	1.9	1.5
	High	15	3	1.9
<b>Remifentanil</b>	Low	5	11	8
	Medium	50	5	7
	High	100	2.5	2.5
<b>Sufentanil</b>	Low	1	15	2.1
	Medium	10	1.0	1.0
	High	20	1.2	1.6
<b>Norcarfentanil</b>	Low	0.1	2.4	3.4
	Medium	2	2.8	2.7
	High	5	1.7	2.1
<b>Benzylfentanyl</b>	Low	0.5	6	7
	Medium	5	-3	2.3
	High	50	-10	12

## 2. Impurities remifentanil

*Table S 2. Additional pre- and post-metabolism impurities detected by LC-HRMS/MS for remifentanil synthesized according to the 7-step and Ugi-method.*

Ref.	Name/ biotransformation	Chemical formula	m/z	t <sub>r</sub> (min)	Pre, post	Method	Tentative structure
R.E	Hydroxylation of C <sub>13</sub> H <sub>21</sub> NO <sub>3</sub>	C <sub>13</sub> H <sub>21</sub> NO <sub>3</sub>	240.160	7.774	Post	Ugi	n.a.
R.F	n.a.	C <sub>12</sub> H <sub>15</sub> NO	190.123	5.836	Post	Ugi	n.a.
R.G	n.a.	C <sub>12</sub> H <sub>27</sub> NO <sub>2</sub>	218.212	6.768	Pre, post	7-step	n.a.
R.H	n.a.	C <sub>12</sub> H <sub>14</sub> N <sub>2</sub> O <sub>2</sub>	219.113	6.039	Post	Ugi	n.a.
R.I	n.a.	C <sub>13</sub> H <sub>21</sub> NO <sub>2</sub>	224.165	11.027	Pre, post	7-step, Ugi	n.a.
R.J	n.a.	C <sub>12</sub> H <sub>27</sub> NO <sub>3</sub>	234.207	7.041	Pre	7-step	n.a.
R.K	n.a.	C <sub>14</sub> H <sub>29</sub> NO <sub>2</sub>	244.228	8.739	Pre	7-step	n.a.
R.L	n.a.	C <sub>14</sub> H <sub>31</sub> NO <sub>2</sub>	246.243	8.487	Pre	7-step	n.a.
R.M	n.a.	C <sub>12</sub> H <sub>27</sub> NO <sub>4</sub>	250.202	21.75	Post	7-step	n.a.
R.N	n.a.	C <sub>16</sub> H <sub>19</sub> NO <sub>2</sub>	258.149	12.253	Post	Ugi	n.a.
R.O	n.a.	C <sub>13</sub> H <sub>26</sub> N <sub>2</sub> O <sub>3</sub>	259.202	7.450	Post	Ugi	n.a.
R.P	n.a.	C <sub>15</sub> H <sub>33</sub> NO <sub>2</sub>	260.259	9.248	Pre	7-step	n.a.
R.Q	n.a.	C <sub>16</sub> H <sub>35</sub> NO <sub>2</sub>	274.275	9.938	Pre	7-step	n.a.
R.R	n.a.	C <sub>17</sub> H <sub>23</sub> NO <sub>3</sub>	290.176	12.252	Pre, post	Ugi	n.a.
R.S	n.a.	C <sub>16</sub> H <sub>35</sub> NO <sub>3</sub>	290.270	8.618	Pre	7-step	n.a.
R.T	n.a.	C <sub>15</sub> H <sub>21</sub> N <sub>3</sub> O <sub>3</sub>	292.166	4.655	Post	Ugi	n.a.
R.U	n.a.	C <sub>18</sub> H <sub>29</sub> N <sub>3</sub> O <sub>2</sub>	320.234	9.303	Post	Ugi	n.a.
R.V	n.a.	C <sub>19</sub> H <sub>20</sub> N <sub>6</sub> O	349.178	5.279	Post	7-step	n.a.

\*Identification with Compound Discoverer; †Identification and tentative structure determined by comparison with literature

### 3. Impurities carfentanil

Table S 3. Additional pre- and post-metabolism impurities detected by LC-HRMS/MS for carfentanil synthesized according to the 7-step and Ugi method.

Ref.	Name/ biotransformation	Chemical formula	m/z	t <sub>r</sub> (min)	Synthetic route	Pre, post	Tentative structure
C.H	n.a. [1]	C <sub>14</sub> H <sub>19</sub> NO	218.154	10.09	Ugi	Pre	n.a.
C.I	n.a. [1]	C <sub>13</sub> H <sub>19</sub> NO <sub>2</sub>	222.149	9.19	Ugi	Pre	n.a.
C.J	n.a.	C <sub>14</sub> H <sub>19</sub> NO <sub>2</sub>	234.149	18.04	Ugi	Pre, post	n.a.
C.K	Hydroxylation of C <sub>14</sub> H <sub>19</sub> NO <sub>2</sub> (C.J) OR dihydroxylation of C <sub>14</sub> H <sub>19</sub> NO (C.H)	C <sub>14</sub> H <sub>19</sub> NO <sub>3</sub>	250.144	4.98	Ugi	Post	n.a.
C.L	n.a. [1]	C <sub>16</sub> H <sub>19</sub> NO <sub>2</sub>	258.149	18.05	Ugi	Pre, post	n.a.
C.M	n.a. [1]	C <sub>17</sub> H <sub>56</sub> NO <sub>3</sub>	290.176	18.05	Ugi	Pre, post	n.a.
C.N	Hydroxylation of C <sub>17</sub> H <sub>23</sub> NO <sub>3</sub> ‡	C <sub>17</sub> H <sub>23</sub> NO <sub>4</sub>	306.171	8.54	Ugi	Post	n.a.
C.O	n.a.	C <sub>20</sub> H <sub>41</sub> NO	312.327	24.88	7-step	Pre, post	n.a.
C.P	n.a. [1]	C <sub>18</sub> H <sub>26</sub> N <sub>2</sub> O <sub>3</sub>	319.202	5.56	Ugi	Pre, post	n.a.
C.Q	n.a. [1]	C <sub>20</sub> H <sub>25</sub> N <sub>3</sub> O	324.208	11.04	Ugi	Pre, post	n.a.
C.R	n.a. [1]	C <sub>23</sub> H <sub>24</sub> N <sub>2</sub>	329.202	13.42	Ugi	Pre	n.a.
C.S	n.a. [1]	C <sub>20</sub> H <sub>28</sub> N <sub>2</sub> O <sub>2</sub>	329.223	11.38	Ugi	Post	n.a.
C.T	Hydroxylation of C <sub>18</sub> H <sub>26</sub> N <sub>2</sub> O <sub>3</sub> (C.P)	C <sub>18</sub> H <sub>26</sub> N <sub>2</sub> O <sub>4</sub>	335.197	4.79	Ugi	Post	n.a.
C.U	n.a.	C <sub>19</sub> H <sub>30</sub> N <sub>2</sub> O <sub>3</sub>	335.233	18.04	Ugi	Pre, post	n.a.
C.V	Hydroxylation of C <sub>19</sub> H <sub>30</sub> N <sub>2</sub> O <sub>3</sub> (C.U)	C <sub>19</sub> H <sub>30</sub> N <sub>2</sub> O <sub>4</sub>	351.228	8.54	Ugi	Post	n.a.
C.W	n.a. [1]	C <sub>22</sub> H <sub>26</sub> N <sub>2</sub> O <sub>3</sub>	367.202	16.87, 11.30	Ugi, 7-step	Pre	n.a.
C.X	n.a.	C <sub>25</sub> H <sub>31</sub> N <sub>3</sub>	374.260	14.64	Ugi	Pre	n.a.
C.Y	Dihydroxylation + glucuronidation of C <sub>20</sub> H <sub>41</sub> NO (C.O)‡	C <sub>26</sub> H <sub>49</sub> NO <sub>9</sub>	520.349	11.44	7-step	Post	n.a.

\*Identification with Compound Discoverer; †Identification and tentative structure determined by comparison with literature; ‡Metabolites from pre-metabolism impurities not included in list because area was below threshold, <sup>GC</sup>Compound also detected using GC-MS.

## 4. Match criterion approach

*Table S 4. Characteristic relative responses of remifentanil impurities for the 7-step and Ugi-method. The 95% confidence interval is shown (n=6). Responses are relative to the peak area of remifentanil acid.*

Impurity	7-step (%)	Ugi (%)
Aniline	0 - 1.01	16.1 - 17.8
R.T	0 - 0.01	17.3 - 30.6
R.U	0 - 0.082	6.7 - 7.2
R.R	0 - 0.082	1.89 - 3.31
R.H	0 - 0.008	0.54 - 2.91
R.P	0 - 0.0059	0.74 - 2.85
R.S	0 - 0.0052	1.19 - 1.32
R.M	0.17 - 0.34	0.17 - 0.25
R.D	0.012 - 0.037	0.0002 - 0.0077
R.L	0 - 0.19	0.0007 - 0.0009
R.V	0 - 0.007	0.011 - 0.04
R.N	0.003 - 0.007	0.0018 - 0.027

*Table S 5. Characteristic relative responses of carfentanil impurities for the 7-step (n=9) and Ugi-method (n=19). The 95% confidence interval is shown. Responses are relative to the peak area of carfentanil.*

Impurity	7-step (%)	Ugi (%)
C.AZ	24 - 732	42 – 210
C.AN	1.17 - 3.07	11.8 - 22.3
C.AK	2.69 - 6.54	6.54 - 13.85
C.AX	0.75 - 6.83	18.7 - 67.4
C.AE	0 – 294	0 - 585
C.AL	2.82 - 6.86	4.38 - 12.15
C.AS	34 - 315	0 - 57
C.AV	1.14 - 3.11	3.57 - 54.37
C.AW	0 - 27.5	5.9 - 25.2
C.AY	1.26 - 3.26	2.13 - 6.05
C.AM	1.28 - 3.32	1.67 - 18.03
C.AT	1.37 - 3.54	5.67 - 49.75
C.AU	1.42 - 3.65	5.45 - 39.54

## 5. Multivariate analysis remifentanil

### 5.1. PCA

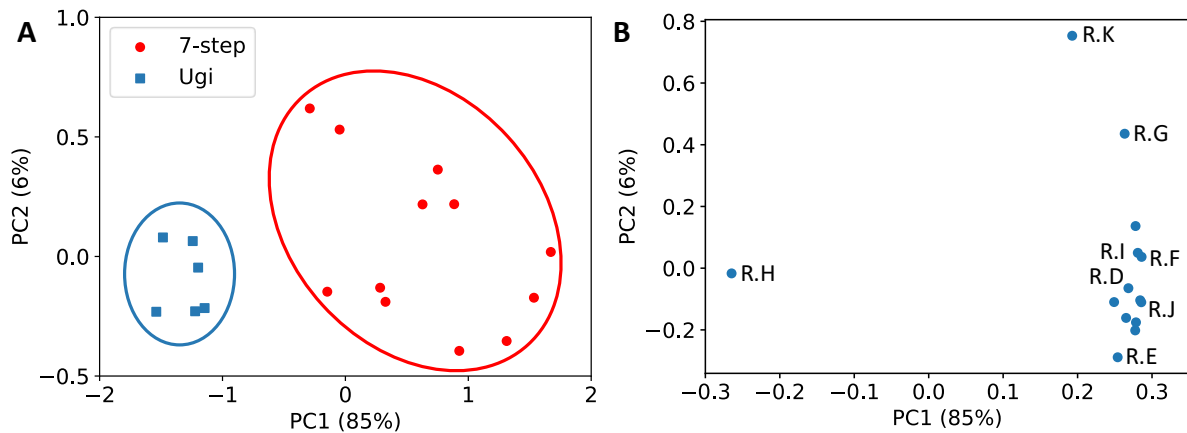


Figure S 2. PCA-score plot of pre-metabolism samples of remifentanil synthesized by the 7-step (red circle) and Ugi (blue square) method. B) Corresponding PCA loading plot with highlighted impurities.

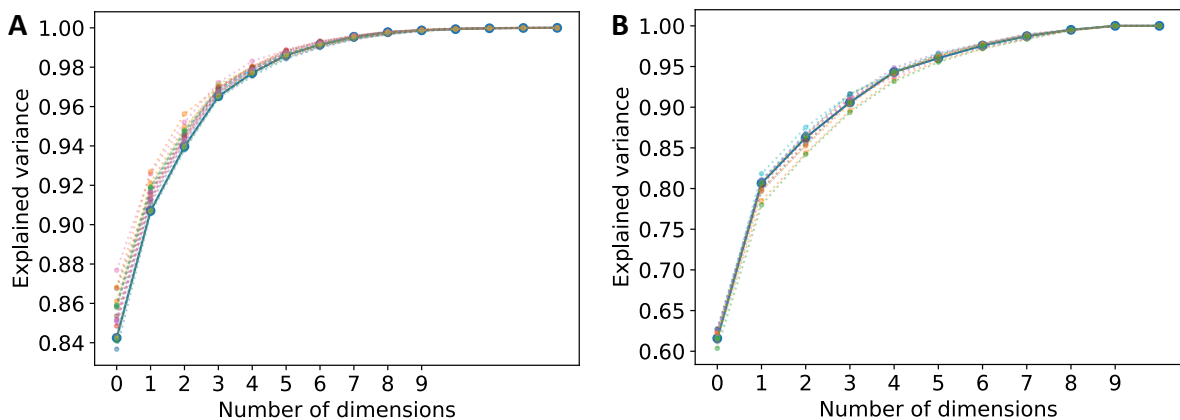


Figure S 3. Leave-one-out validation of PCA model for remifentanil samples A) pre-metabolism and B) post-metabolism. Blue line includes all samples. Dashed lines represent the variance when one sample is left out.

## 5.2. LDA

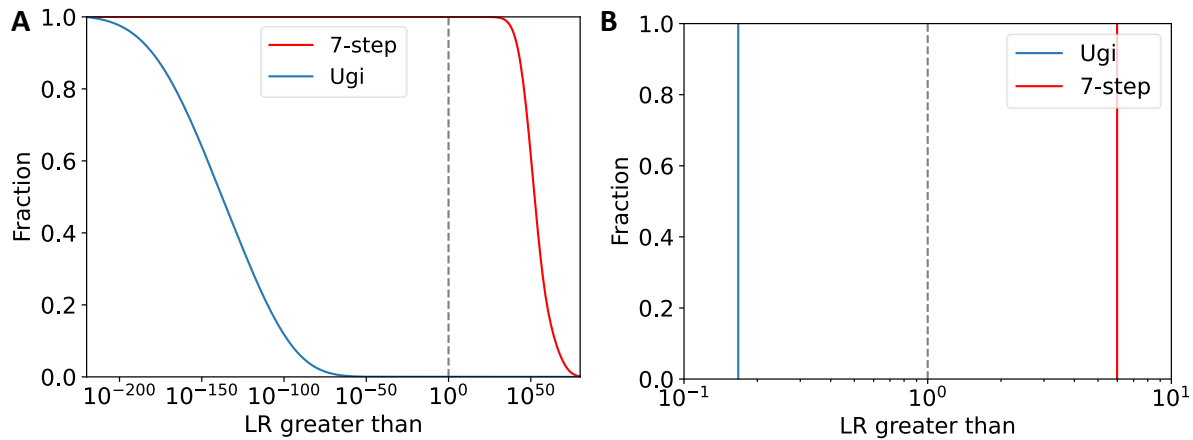


Figure S 4. Tippett plots with cumulative likelihood ratio (LR) distributions for post-metabolism remifentanil samples. A) Without correction. B) With ELUB bounds. The dashed lines show  $LR = 1$ .

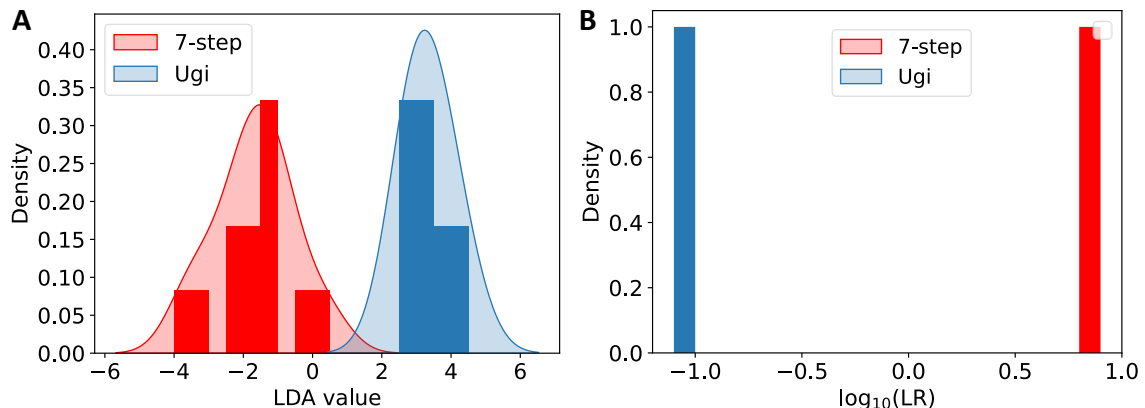


Figure S 5. LDA score plot of first four principal components of PCA (94% of the variance). B) Corrected distribution of  $\log_{10}(LR)$  with ELUB bounds, for remifentanil pre-metabolism samples of 7-step synthesis (red) and Ugi method (blue), analyzed with LC-HRMS/MS. The bars show the frequency of the measurements, and the shaded curves represent the kernel density estimations.

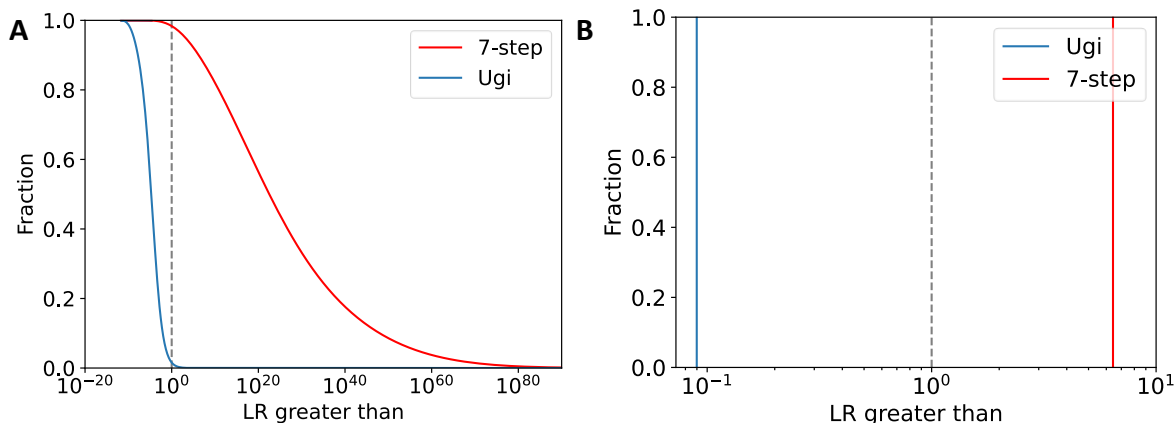


Figure S 6. Tippett plots with cumulative likelihood ratio (LR) distributions for pre-metabolism remifentanil samples. A) Without correction. B) With ELUB bounds. The dashed lines show  $LR = 1$ .

## 6. Multivariate analysis carfentanil

### 6.1. PCA

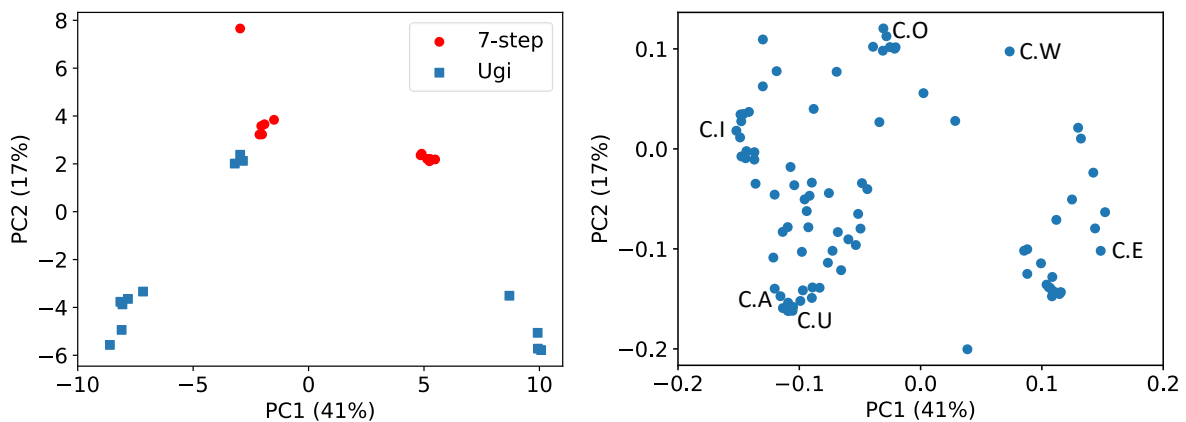


Figure S 7. PCA-score plot of pre-metabolism samples of carfentanil synthesized by the 7-step (red circle) and Ugi (blue square) method. B) Corresponding PCA loading plot with highlighted impurities.

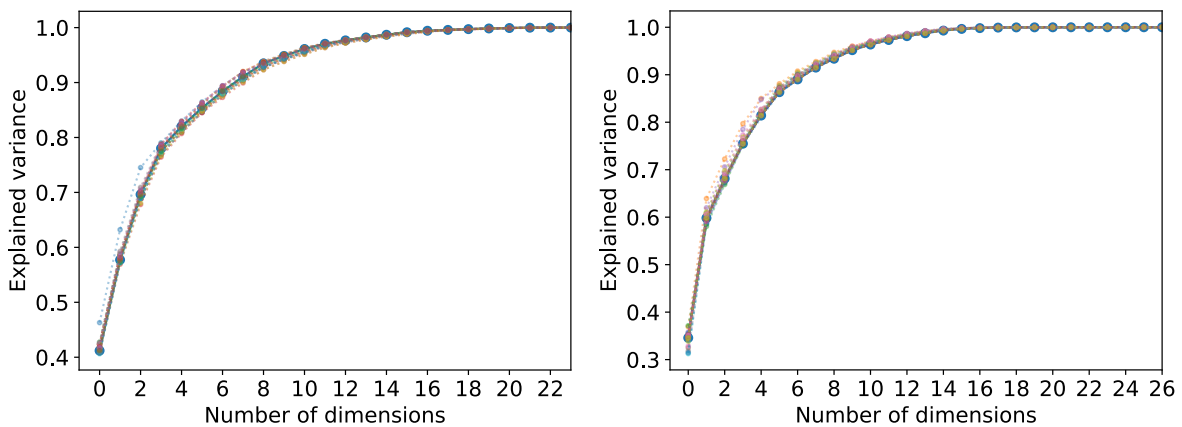


Figure S 8. Leave-one-out validation of PCA model for carfentanil samples A) pre-metabolism and B) post-metabolism. Blue line includes all samples. Dashed lines represent the variance when one sample is left out.

## 6.2. LDA

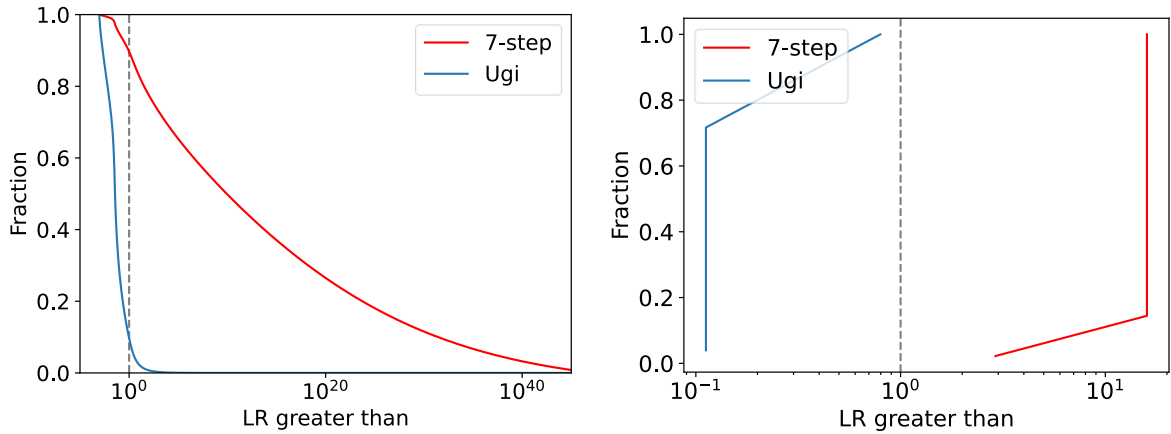


Figure S 9. Tippett plots with cumulative likelihood ratio (LR) distributions for post-metabolism carfentanil samples. A) Without correction. B) With ELUB bounds. The dashed lines show  $LR = 1$ .

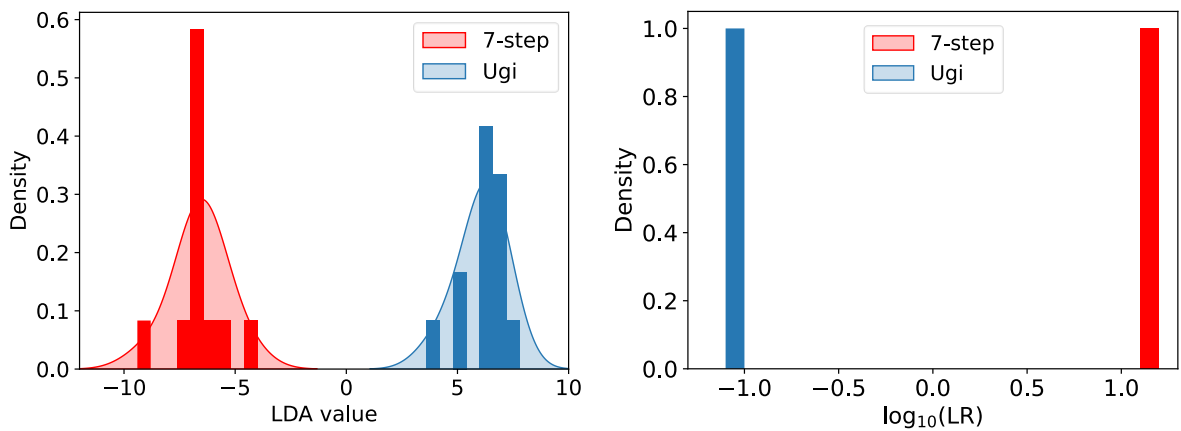


Figure S 10. LDA score plot of first six principal components of PCA (82% of the variance). B) Corrected distribution of  $\log_{10}(LR)$  with ELUB bounds, for carfentanil pre-metabolism samples of 7-step synthesis (red) and Ugi method (blue), analyzed with LC-HRMS/MS. The bars show the frequency of the measurements, and the shaded curves represent the kernel density estimations.

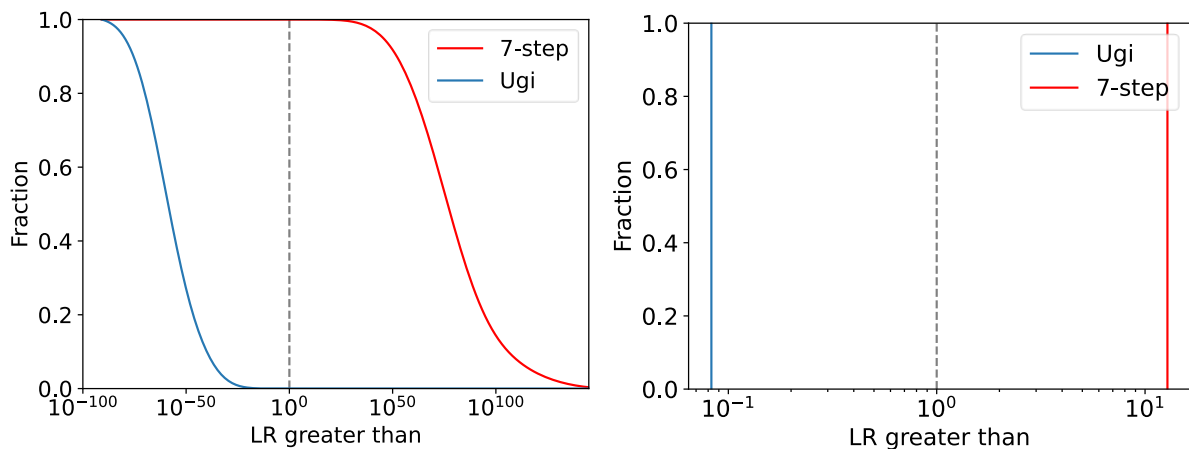


Figure S 11. Tippett plots with cumulative likelihood ratio (LR) distributions for pre-metabolism carfentanil samples. A) Without correction. B) With ELUB bounds. The dashed lines show  $LR = 1$ .

## References

- [1] L. Mörén, P. Lindén, J. Qvarnström, M. Engqvist, M. Carlsson, R. Afshin Sander, S. Lindberg, A. Larsson, A. Östin, Classification of carfentanil synthesis methods based on chemical impurity profile, *Forensic Chemistry* 26 (2021) 100355. <https://doi.org/10.1016/j.forc.2021.100355>.

# CHAPTER 4

## SUPPLEMENTARY DATA



# **Elucidation of in vitro chlorinated tyrosine adducts in blood plasma as selective biomarkers of chlorine exposure**

Mirjam de Bruin-Hoegée<sup>†,‡,\*</sup>, Irene M. van Damme<sup>†</sup>, Tomas van Groningen<sup>†</sup>, Debora van der Riet-van Oeveren<sup>†</sup>, Daan Noort<sup>†</sup>, Arian C. van Asten<sup>†,§</sup>

<sup>†</sup> van 't Hoff Institute for Molecular Sciences, Faculty of Science, University of Amsterdam, P.O. Box 94157, 1090GD Amsterdam, The Netherlands

<sup>‡</sup>TNO Defence, Safety and Security, Dep. CBRN Protection, Lange Kleiweg 137, 2288GJ Rijswijk, The Netherlands

<sup>§</sup> CLHC, Amsterdam Center for Forensic Science and Medicine, University of Amsterdam, P.O. Box 94157, 1090GD Amsterdam, The Netherlands

\*Corresponding author. Email address: [mirjam.debruin@tno.nl](mailto:mirjam.debruin@tno.nl) (M. de Bruin-Hoegée)

## **Supporting information**

### **Contents**

- S1. Method optimization and validation
- Figure S1. Calibration curves Cl-Tyr and di-Cl-Tyr
- Figure S2. Heatmap of peptides identified with LC-HRMS/MS after pepsin digestion
- Table S1. Extent of protein chlorination after pepsin digestion
- Table S2. Extent of protein chlorination after trypsin digestion
- Table S3. Identified biomarkers for chlorine exposure after trypsin and pepsin digestion.
- Figure S3. Protein coverage of human serum albumin and haptoglobin
- Figure S4. Extracted ion chromatograms of YLYEIAR
- S2. Isotope ratios
- Table S4. Theoretical compared to measured isotope values
- Table S5. Fragmentation pattern of peptide Y(Cl)LYEIAR
- Figure S5. MS/MS spectrum of parent ion K.Y(Cl)LY(Cl)EIAR
- Table S6. Fragmentation pattern of peptide Y(Cl)LY(Cl)EIAR
- Figure S6. MS/MS spectrum of parent ion K.Y(Cl)LY(Cl<sub>2</sub>)EIAR
- Table S7. Fragmentation pattern of peptide Y(Cl)LY(Cl<sub>2</sub>)EIAR
- Figure S7. Extracted ion chromatograms of HYEGSTVPEKK
- Table S8. Fragmentation pattern of peptide HY(Cl)EGSTVPEKK
- Figure S8. MS/MS spectrum of parent ion HY(Cl<sub>2</sub>)EGSTVPEKK.
- Table S9. Fragmentation pattern of peptide HY(Cl<sub>2</sub>)EGSTVPEKK

## S1. Method optimization and validation

The LC-MS/MS method was optimized for Cl-Tyr ( $t_r$ : 6.15 min) and di-Cl-Tyr ( $t_r$ : 6.57 min) with  $^{13}\text{C}_6$ -3-chloro-L-tyrosine ( $t_r$ : 6.14 min) as internal standard. Linear calibration curves were obtained in the range of 1-100 ng/mL with  $R^2 = 0.9992$ -0.9999 (Figure S1). The mean values for the quality controls were within 20% at 1 ng/mL and within 6% relative standard deviation at both 10 ng/mL and 100 ng/mL ( $n = 10$ , for each concentration). The stability of the analytes was assessed over two weeks and the concentration was within 15% of the nominal value. The sample preparation efficiency of the pronase digest, determined by spiking known concentrations of analyte into human plasma, were respectively  $59\% \pm 9\%$  for Cl-Tyr and  $56\% \pm 15\%$  for di-Cl-Tyr. The ionization efficiency was slightly improved by the addition of 0.5% formic acid solution of 10 v% in water.

In addition, the influence of the plasma surface area on the effect of the chlorine exposure was examined. It was found that increasing the surface area with a factor of approximately 10 by using the laboratory glass bottle setup instead of a 15 mL polypropylene Corning tube resulted in a 5-7-fold increase in detected Cl-Tyr level in plasma ( $n = 3$ ). Furthermore, it was found that increasing the exposure time from 2 hours to 48 hours did not significantly increase the degree of chlorination (concentrations were within the error range of  $\pm 1$  stdv.). This was expected because blood plasma rapidly consumes chlorine. Finally, prolonging the pronase digestion duration beyond 48 hours did not significantly affect the detected levels of Cl-Tyr and di-Cl-Tyr.

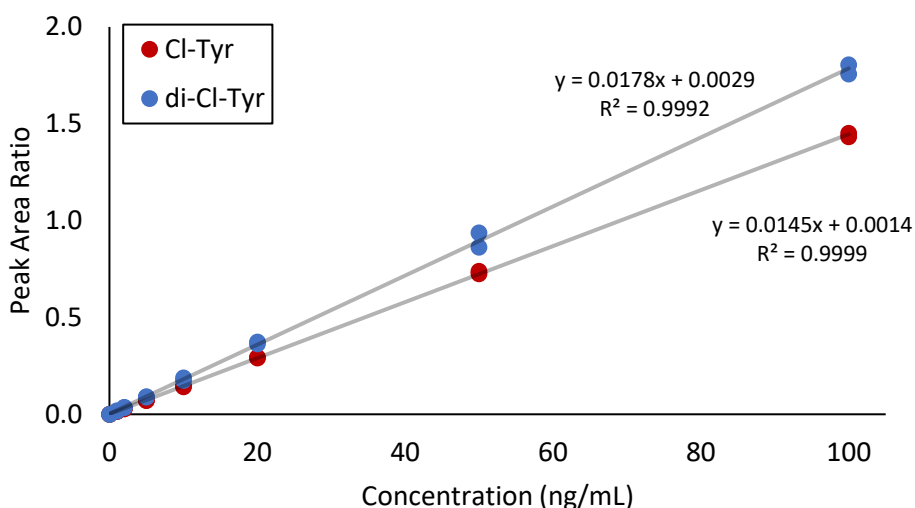


Figure S1. Calibration curves of 3-chlorotyrosine (Cl-Tyr) and 3,5-dichlorotyrosine (di-Cl-Tyr) with internal standard  $^{13}\text{C}_6$ -3-chloro-L-tyrosine, detected by LC-MS/MS.

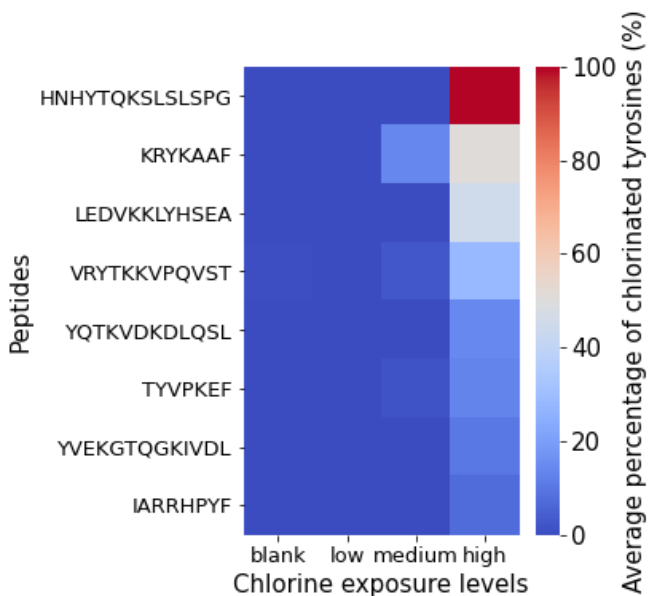


Figure S2. Heatmap of peptides identified with LC-HRMS/MS after pepsin digestion of human blood plasma, with corresponding average percentage of chlorinated tyrosines for non-exposed, low, medium, and high chlorine exposure.

Table S1. Extent of protein chlorination for various chlorine exposure levels after digestion by pepsin ( $n = 3, \pm SD$ ).

Chlorine exposure level	Average percentage of chlorinated tyrosines (%)
Blank	$1.2 \pm 0.4$
Low	$0.7 \pm 0.6$
Medium	$3.2 \pm 1.5$
High	$14 \pm 9$

Table S2. Extent of overall protein chlorination for various chlorine exposure levels after digestion by trypsin ( $n = 3, \pm SD$ ).

Chlorine exposure level	Average percentage of chlorinated tyrosines (%)
Blank	$0.2 \pm 0.3$
Low	$0.5 \pm 0.5$
Medium	$2.3 \pm 1.8$
High	$16.2 \pm 2.1$

Table S3. Identified biomarkers for chlorine exposure after trypsin and pepsin digestion.

Long peptide	Enzyme	Accession	Protein	Mass	t <sub>R</sub> (min)	Cl (#) <sup>a</sup>	N (#) <sup>b</sup>
AHY(Cl)GGFTVQNEANK	Trypsin	P02675   FIBB_HUMAN	Fibrinogen beta chain	1568.7	18.5	1	2
AIGY(Cl)LNTGYQR	Trypsin	P01023   A2MG_HUMAN	Alpha-2-macroglobulin	1288.6	20.2	1	1
ALSHAVNNY(Cl)HK	Trypsin	P04114   APOB_HUMAN	Apolipoprotein B-100	1286.6	15.3	1	2
ASAGLLGAHAAAITAY(Cl)	Trypsin	POCOL4   CO4A_HUMAN	Complement C4-A	1490.7	21.6	1	1
ATVLNY(Cl)LPK	Trypsin	P01023   A2MG_HUMAN	Alpha-2-macroglobulin	1051.5	21.9	1	3 <sup>c</sup>
AVRPGY(Cl)PK	Trypsin	n.a.	n.a.	920.5	15.9	1	4 <sup>c</sup>
DDLY(Cl)VSDAFHK	Trypsin	P01008   ANT3_HUMAN	Antithrombin-III	1342.6	20.4	1	3
FSVVY(Cl)AK	Trypsin	P02765   FETUA_HUMAN	Alpha-2-HS-glycoprotein	846.4	20.3	1	3
GEVPPRY(Cl)PR	Trypsin	P02790   HEMO_HUMAN	Hemopexin	1103.5	16.6	1	1
GGSTS(Y(Cl))GTGSETESPR	Trypsin	P02671   FIBA_HUMAN	Fibrinogen alpha chain	1605.6	16.3	1	2
GLSVY(Cl)ADKPETTK	Trypsin	P02763   A1AG1_HUMAN	Alpha-1-acid glycoprotein 1	1441.7	18.2	1	1
GVALHRPDVY(Cl).LLPPAR	Trypsin	P01871   IGHM_HUMAN	Immunoglobulin heavy constant mu	1159.6	19.1	1	2
GY(Cl)TQQLAFR	Trypsin	P01024   CO3_HUMAN	Complement C3	1116.5	20.5	1	2
AP.HGPGLIY(Cl)R	Trypsin	P02765   FETUA_HUMAN	Alpha-2-HS-glycoprotein	1113.5	19.2	1	1
HNHY(Cl)TQKSLSLSPG	Pepsin	P0DOX5   IGG1_HUMAN	Immunoglobulin gamma-1 heavy chain	1601.7	17.4	1	2
R.HPDY(Cl)SVVL.LLR	Trypsin	P02768   ALBU_HUMAN	Albumin	1500.8	21.5	1	1
HQLY(Cl)IDETVNSNIPTNLR	Trypsin	P02675   FIBB_HUMAN	Fibrinogen beta chain	1307.6	14.9	1	2
HY(Cl)EGSTVPEK.K	Trypsin	P00738   HPT_HUMAN	Haptoglobin	1307.6	14.9	1	5
HY(Cl2)EGSTVPEK.K	Trypsin	P00738   HPT_HUMAN	Haptoglobin	1341.6	15.1	2	3
YE.IARRHPY(Cl)F.Y(Cl)APEL	Pepsin	P02768   ALBU_HUMAN	Albumin	1360.6	20.8	2	1
L.IQPDSVKPY(Cl)R	Trypsin	P02675   FIBB_HUMAN	Fibrinogen beta chain	1435.7	18.6	1	2

IY(Cl)GNQDTSSQLK	Trypsin	P19823   ITIH2_HUMAN	Inter-alpha-trypsin inhibitor heavy chain H2	1386.6	17.9	1	1
FA.KRY(Cl2)KAAF	Pepsin	P02768   ALBU_HUMAN	Albumin	1168.5	19.5	1	2 <sup>c</sup>
FFA.KRY(Cl)KAAF	Pepsin	P02768   ALBU_HUMAN	Albumin	1281.6	20.6	1	4 <sup>c</sup>
LEDVKKLY(Cl)HSEA	Pepsin	P01009   A1AT_HUMAN	Alpha-1-antitrypsin	1464.7	18.3	1	2
KQL.INDY(Cl)V.EK	Trypsin	P01011   AACT_HUMAN	Alpha-1-antichymotrypsin	1041.5	18.7	1	3 <sup>c</sup>
LGEVNTY(Cl)AGDLQK	Trypsin	P06727   APOA4_HUMAN	Apolipoprotein A-IV	1440.7	20.0	1	2
LLIY(Cl)GASTR	Trypsin	n.a.	n.a.	1026.5	21.0	1	1
NSLFY(Cl)QK	Trypsin	P02671   FIBA_HUMAN	Fibrinogen alpha chain	1061.5	20.6	1	3
EEAPSLR.PAPPPISGGGY(Cl)R	Trypsin	P02675   FIBB_HUMAN	Fibrinogen beta chain	1984.0	19.6	1	3
SY(Cl)STTAVVTNPK	Trypsin	P02766   TTHY_HUMAN	Transthyretin	1300.6	18.1	1	2
TAQEGDHGSHVY(Cl).TK	Trypsin	P01023   A2MG_HUMAN	Alpha-2-macroglobulin	1562.7	14.8	1	3
TY(Cl)ETTLEK	Trypsin	P02768   ALBU_HUMAN	Albumin	1017.4	18.2	1	6
SALE.VDETY(Cl)VPK	Trypsin	P02768   ALBU_HUMAN	Albumin	1383.6	20.6	1	1
EVDE.TY(Cl)VPKE.F	Pepsin	P02768   ALBU_HUMAN	Albumin	1388.6	21.7	1	1
VGPEADKY(Cl)R	Trypsin	P02679   FIBG_HUMAN	Fibrinogen gamma chain	1067.5	16.3	1	1
IV.VRY(Cl)TKKVPQVST.PTL	Pepsin	P02768   ALBU_HUMAN	Albumin	1438.8	16.3	1	7 <sup>c</sup>
IV.VRY(Cl2)TKKVPQVST.PTL	Pepsin	P02768   ALBU_HUMAN	Albumin	1897.0	20.5	1	4 <sup>c</sup>
WY(Cl)VDGVEVH.NAK	Trypsin	P01857  IGHG1_HUMAN	Immunoglobulin heavy constant gamma 1	1449.6	16.0	1	4 <sup>c</sup>
Y(Cl)AATSQVLLPSK	Trypsin	P01871  IGHM_HUMAN	Immunoglobulin heavy constant mu	1310.7	20.2	1	2
F.Y(Cl)APELFFAK	Trypsin	P02768   ALBU_HUMAN	Albumin	1378.7	22.2	1	2
Y(Cl)EKPGSPPR	Trypsin	P02751   FINC_HUMAN	Fibronectin	1063.5	15.3	1	1
Y(Cl)GAATFTR	Trypsin	P01023   A2MG_HUMAN	Alpha-2-macroglobulin	919.4	18.8	1	2
SI.Y(Cl)KPGQTVK	Trypsin	P01023   A2MG_HUMAN	Alpha-2-macroglobulin	1153.6	17.4	1	4

YLQEIY(Cl)NSNNQK	Trypsin	P02679   FIBG_HUMAN	Fibrinogen gamma chain	1546.7	19.6	1	1
K.Y(Cl)LY(Cl)EIAR	Trypsin	P02768   ALBU_HUMAN	Albumin	994.4	21.6	2	3
KK.Y(Cl)LYEiar	Trypsin	P02768   ALBU_HUMAN	Albumin	960.4	20.8	1	4
Y(Cl)LY(Cl2)EIAR	Trypsin	P02768   ALBU_HUMAN	Albumin	1028.4	21.9	3	1
Y(Cl)QQHPGKAPK	Trypsin	P01704   LV214_HUMAN	Immunoglobulin lambda variable 2-14	1186.6	14.3	1	1
Y(Cl2)QQKPGKAPK	Trypsin	A0A0C4DH67   KV108_HUMAN	Immunoglobulin kappa variable 1-8	1594.8	15.2	2	1
Y(Cl)QQKPGQAPR	Trypsin	P01619   KV320_HUMAN	Immunoglobulin kappa variable 3-20	1205.6	14.8	1	5
Y(Cl)QTKVDKDLQLS	Pepsin	P02679   FIBG_HUMAN	Fibrinogen gamma chain	1470.7	20.0	1	1
Y(Cl)TFELSR	Trypsin	P02774   VTDB_HUMAN	Vitamin D-binding protein	948.4	20.9	1	2
Y(Cl)VEKGTQGKIVDL	Pepsin	P01009   A1AT_HUMAN	Alpha-1-antitrypsin	1482.7	20.0	1	1
Y(Cl)VGGQEHFAH	Trypsin	P02763   A1AG1_HUMAN	Alpha-1-acid glycoprotein 1	1177.5	16.8	1	1

<sup>a</sup>Number of attached chlorine atoms (Cl)

<sup>b</sup>Peptides detected in given number of repetitions (N)

<sup>c</sup>Not detected in all high chlorine exposure samples

A)



B)



Figure S3. Protein coverage, with sequences identified after pepsin digestion (blue) and trypsin digestion (red). A) Human serum albumin (56% coverage), B) Haptoglobin (33% coverage).

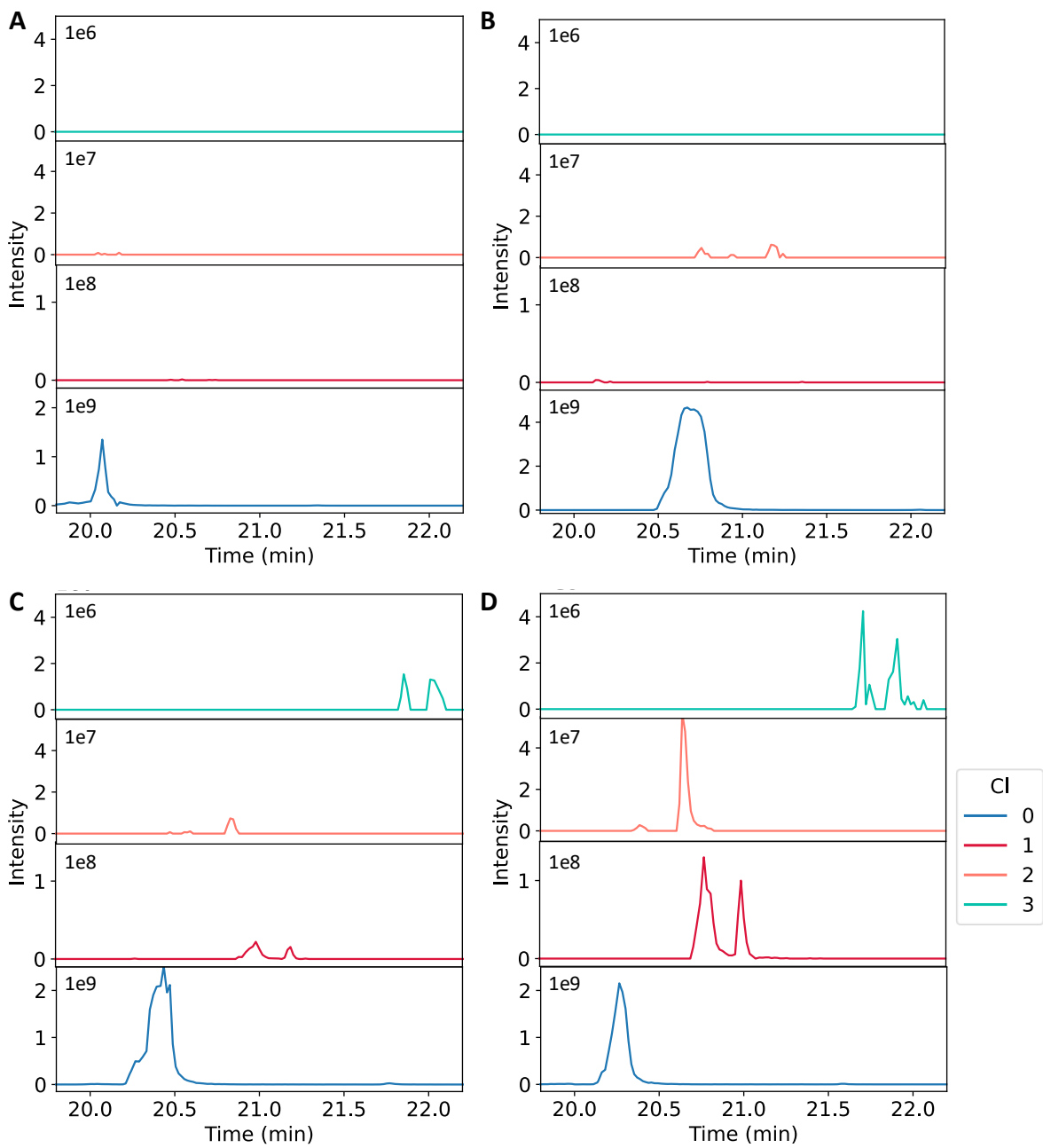


Figure S4. Extracted ion chromatograms of plasma exposed to various chlorine exposure concentrations analyzed by LC-HRMS/MS (Acclaim PepMap C18 column, mobile phase: H<sub>2</sub>O (A) and ACN (B) with 0.1% FA), with YLYEIAR at m/z 464.25 and t<sub>R</sub> = 20.1-20.7 min (blue), Y(Cl)LYEIAR and YLY(Cl)EIAR at m/z 481.23 and t<sub>R</sub> = 20.8-21.0 and 21.0-21.2 min (red), K.Y(Cl)LY(Cl)EIAR at m/z 562.26 and t<sub>R</sub> = 20.6-20.8 min (orange), and Y(Cl)LY(Cl<sub>2</sub>)EIAR and Y(Cl<sub>2</sub>)LY(Cl)EIAR at m/z 515.19 and t<sub>R</sub> = 21.7-21.9 and 21.9-22.0 min (green). A) Blank, B) Low exposure, C) Medium exposure, D) High exposure.

## S2. Isotope ratios

In the full scan MS spectrum of this doubly charged peptide, a distinct chlorine pattern is visible for single, double and triple chlorination (Figure 6B-D). The unchlorinated peptide showed a single peak as expected (Figure 6A). Because the  $^{35}\text{Cl}$  isotope has a natural occurrence of 76% and the  $^{37}\text{Cl}$  isotope of 24%, the isotope ratio for the chlorinated peptide can be calculated. When the influence of other isotopes, such as carbon, is also considered, the isotope ratio of a mono-, di- and tri-chlorinated peptide is 2:1 (Figure 6B), 5:4:1 (Figure 6C) and 11:12:5:1 (Figure 6D), respectively.<sup>49</sup> In Figure 6C, this last peak for the tri-chlorinated peptide was expected at a  $m/z$  518.19, but it was not visible presumably due to its low intensity.

Table S4. Theoretical compared to measured isotope values in full scan MS spectrum analyzed by LC-HRMS/MS of doubly charged chlorinated precursor Y\*LY\*EIAR.

Chlorination	Theoretical isotope value	Measured isotope value
0	1	1
1	2:1	2:1
2	5:4:1	5:4:1
3	11:12:5:1	11:13:4:0

Table S5. Fragmentation pattern of peptide Y(Cl)LYEIAR with y and b fragments.

#	b ( $m/z$ )	Peptide	y ( $m/z$ )	#
1	198.03	Y(+33.96)		7
2	311.12	L	764.43	6
3	474.18	Y	651.35	5
4	603.22	E	488.28	4
5	716.31	I	359.24	3
6	787.34	A	246.16	2
7		R	175.12	1

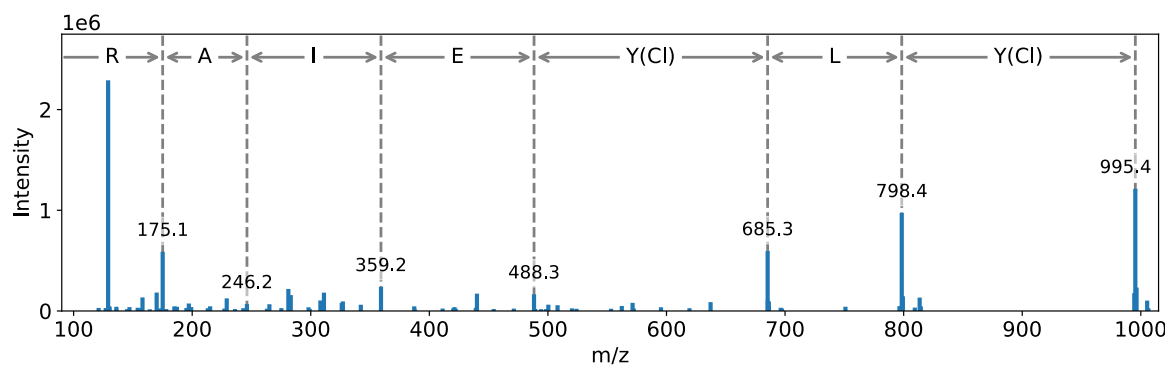


Figure S5. MS/MS spectrum of parent ion K.Y(Cl)LY(Cl)EIAR with  $m/z$  562.262 at an  $t_R = 20.64$  min., detected in the trypsin digest of a plasma sample exposed to 70 and 350 mmol/L chlorine gas. The  $m/z$  of the y-fragments and corresponding amino acids are shown.

Table S6. Fragmentation pattern of peptide Y(Cl)LY(Cl<sub>2</sub>)EIAR with y and b fragments.

#	b (m/z)	Peptide	Y (m/z)	#
1	129.10	K		8
2	326.13	Y(+33.96)	995.41	7
3	439.21	L	798.39	6
4	636.24	Y(+33.96)	685.31	5
5	765.28	E	488.28	4
6	878.36	I	359.24	3
7	949.40	A	246.16	2
8		R	175.12	1

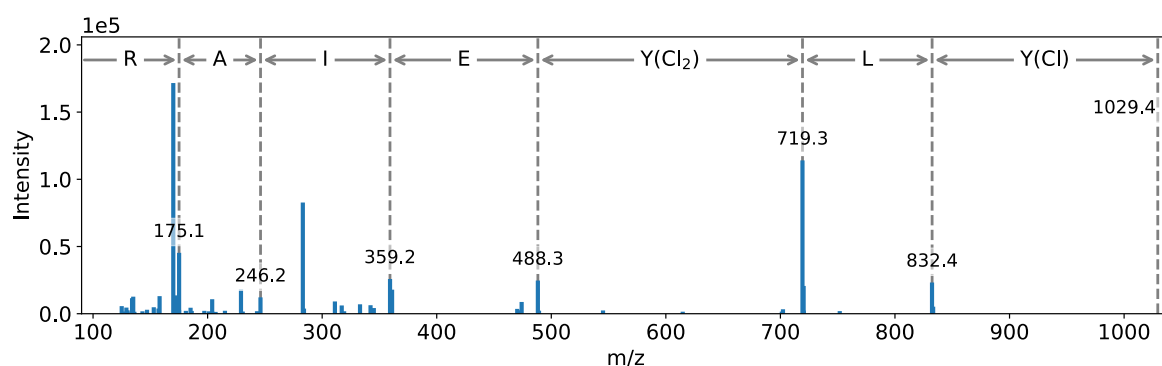


Figure S6. MS/MS spectrum of parent ion Y(Cl)LY(Cl<sub>2</sub>)EIAR with m/z 515.194 at an t<sub>R</sub> = 21.91 min., detected in the trypsin digest of a plasma sample exposed to 350 mmol/L chlorine gas. The m/z of the y-fragments and corresponding amino acids are shown.

Table S7. Fragmentation pattern of peptide Y(Cl)LY(Cl<sub>2</sub>)EIAR with y and b fragments.

#	b (m/z)	Peptide	Y (m/z)	#
1	198.03	Y(+33.96)	1029.4	7
2	311.12	L	832.36	6
3	542.10	Y(+67.92)	719.27	5
4	671.14	E	488.28	4
5	784.23	I	359.24	3
6	855.27	A	246.16	2
7		R	175.12	1

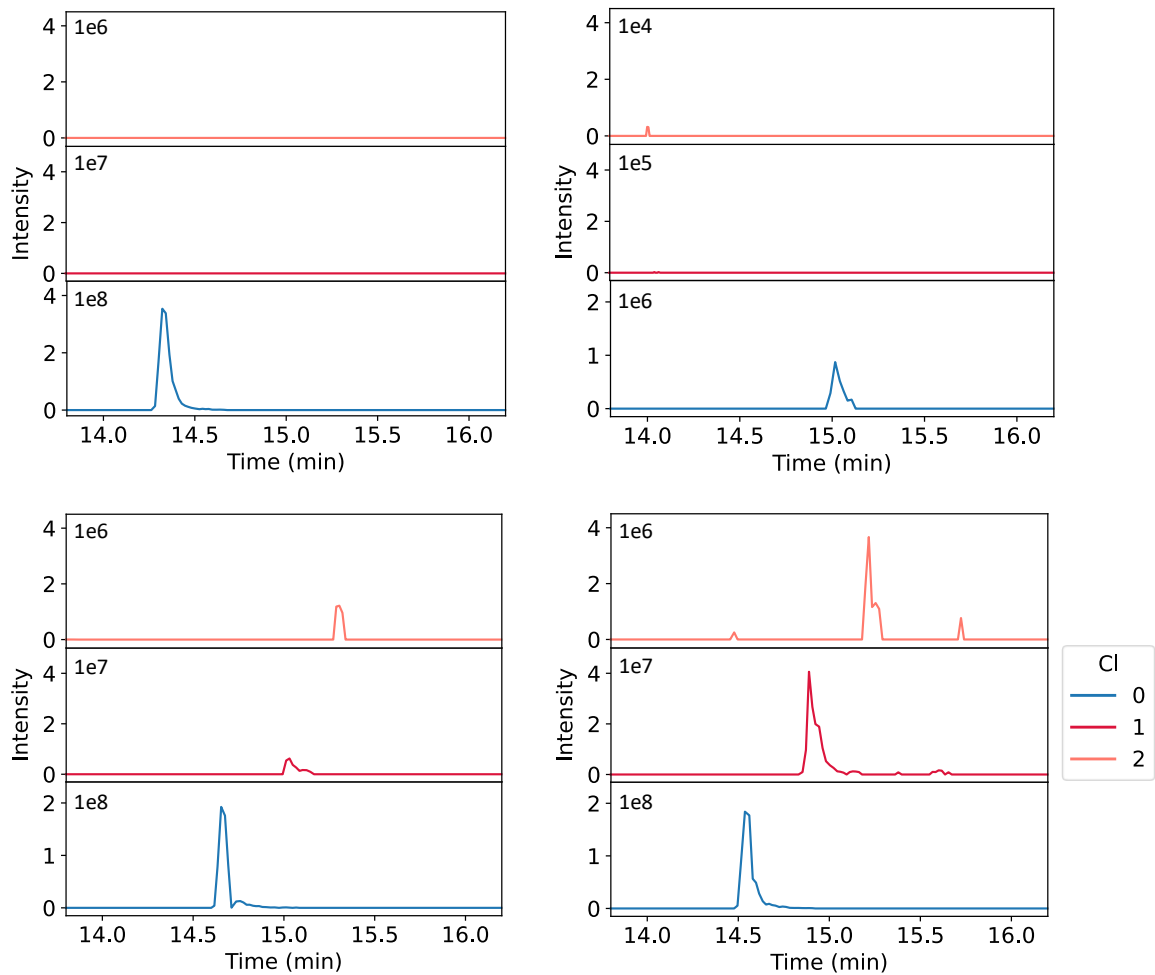


Figure S7. Extracted ion chromatograms of plasma exposed to various chlorine exposure concentrations analyzed by LC-HRMS/MS (Acclaim PepMap C18 column, mobile phase: H<sub>2</sub>O (A) and ACN (B) with 0.1% FA), with HYEGSTVPEKK at m/z 637.823 and t<sub>R</sub> = 14.3-15.0 min (blue), HY(Cl)EGSTVPEKK at m/z 654.805 and t<sub>R</sub> = 14.9-15.0 min (orange), and HY(Cl<sub>2</sub>)EGSTVPEKK at m/z 671.785 and t<sub>R</sub> = 15.2-15.3 min (green). A) Blank, B) Low exposure, C) Medium exposure, D) High exposure.

Table S8. Fragmentation pattern of peptide HY(Cl)EGSTVPEKK with y and b fragments.

#	<b>b</b>	<b>Peptide</b>	<b>y</b>	#
1	138.07	H	1308.60	11
2	335.09	Y(+33.96)	1171.54	10
3	464.14	E	974.52	9
4	521.15	G	845.48	8
5	608.19	S	788.45	7
6	709.24	T	701.42	6
7	808.30	V	600.37	5
8	905.36	P	501.30	4
9	1034.40	E	404.25	3
10	1162.48	K	275.21	2
11		K	147.11	1

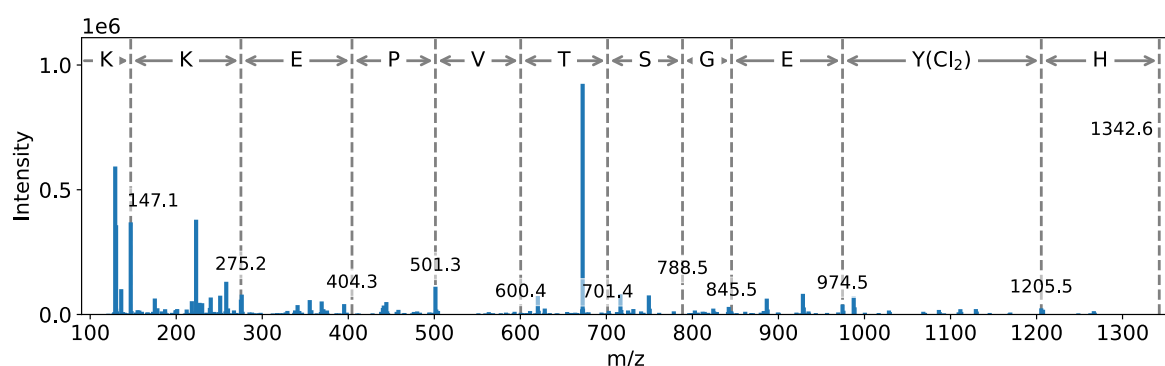


Figure S8. MS/MS spectrum of parent ion HY(Cl<sub>2</sub>)EGSTVPEKK with m/z 672.648 at an t<sub>R</sub> = 15.21 min., detected in the trypsin digest of a plasma sample exposed to 350 mmol/L chlorine gas. The m/z of the y-fragments and corresponding amino acids are shown.

Table S9. Fragmentation pattern of peptide HY(Cl<sub>2</sub>)EGSTVPEKK with y and b fragments.

#	<b>b</b>	<b>Peptide</b>	<b>y</b>	#
1	138.07	H	1342.6	11
2	369.05	Y(+67.92)	1205.5	10
3	498.09	E	974.52	9
4	555.12	G	845.47	8
5	642.15	S	788.45	7
6	743.20	T	701.42	6
7	842.26	V	600.37	5
8	939.32	P	501.30	4
9	1068.4	E	404.25	3
10	1196.5	K	275.21	2
11		K	147.11	1

# CHAPTER 5

## SUPPLEMENTARY DATA



## Supplemental Information

# On-site detection and laboratory verification of the presence of nerve agent biomarkers using dried blood spots

Mirjam de Bruin-Hoegée<sup>a,b,\*</sup>, Alex Fidder<sup>b</sup>, Tomas van Groningen<sup>b</sup>, Marcel J. van der Schans<sup>b</sup>, Daan Noort<sup>b,1</sup>, Arian C. van Asten<sup>a,c</sup>

<sup>a</sup> van 't Hoff Institute for Molecular Sciences, Faculty of Science, University of Amsterdam, P.O. Box 94157, 1090GD Amsterdam, The Netherlands

<sup>b</sup> TNO Defence, Safety and Security, Dep. CBRN Protection, Lange Kleiweg 137, 2288GJ Rijswijk, The Netherlands

<sup>c</sup> CLHC, Amsterdam Center for Forensic Science and Medicine, University of Amsterdam, P.O. Box 94157, 1090GD Amsterdam, The Netherlands

<sup>1</sup> Current address: Organisation for the Prohibition of Chemical Weapons, Johan de Wittlaan 32, 2517 JR The Hague, The Netherlands

\*Corresponding author. Email address: [mirjam.debruin@tno.nl](mailto:mirjam.debruin@tno.nl) (M. de Bruin-Hoegée)

## Contents

1.	Biotransformation pathways.....	2
2.	LC-MS/MS method optimization.....	4
3.	GC-MS/MS method optimization and validation .....	6
4.	Cholinesterase activity .....	8
5.	Analysis of free and regenerated nerve agent in liquid blood.....	9
6.	Analysis of free nerve agent in dried blood spots.....	10
7.	Analysis of hydrolysis metabolites in DBS .....	11

## 1. Biotransformation pathways

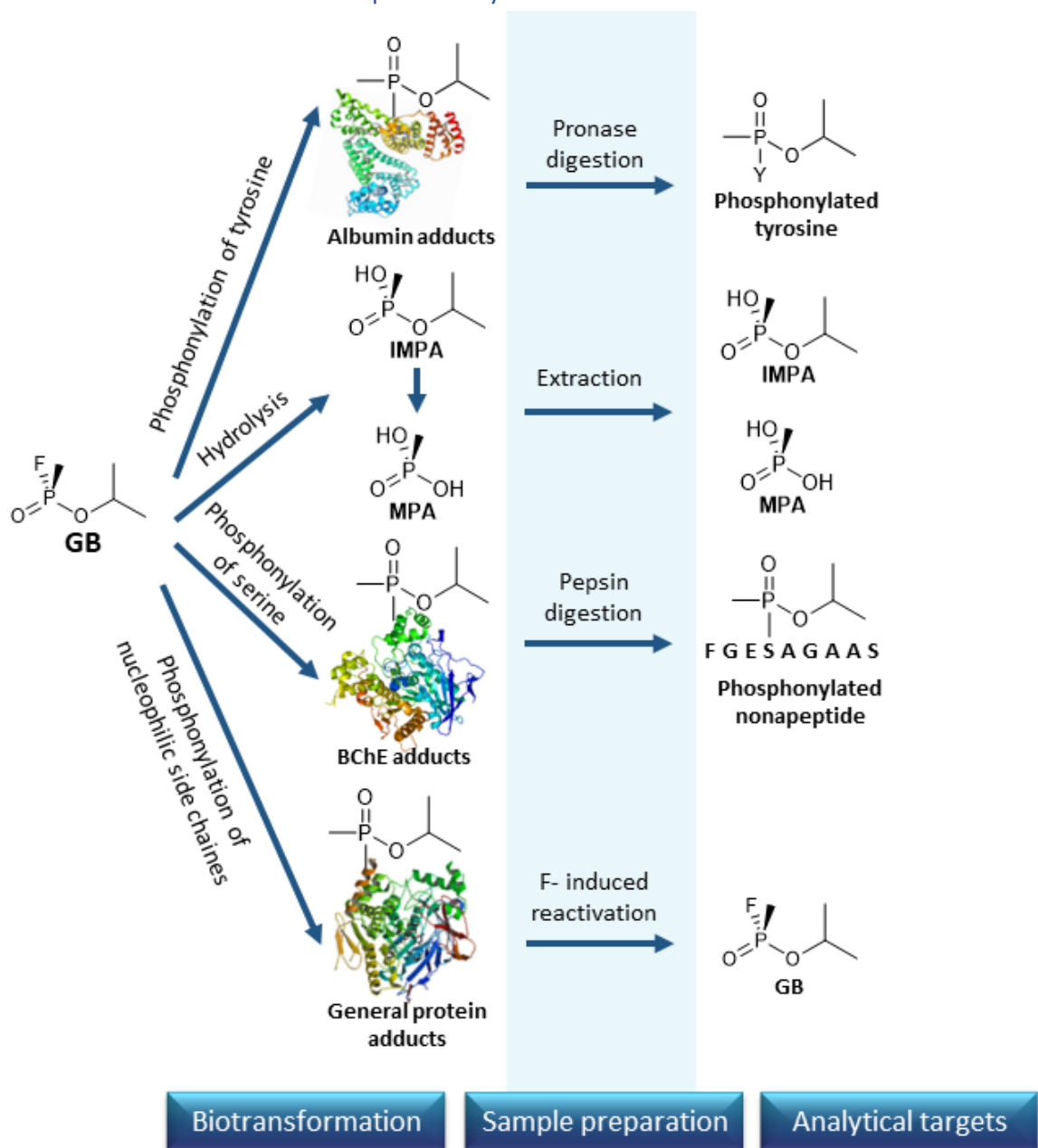


Figure S 1. Biotransformation pathways in humans after poisoning with sarin. Two main processes are hydrolysis, and the formation of protein adducts. Albumin, BChE and other protein adducts are then digested or reactivated by fluoride before the analysis.

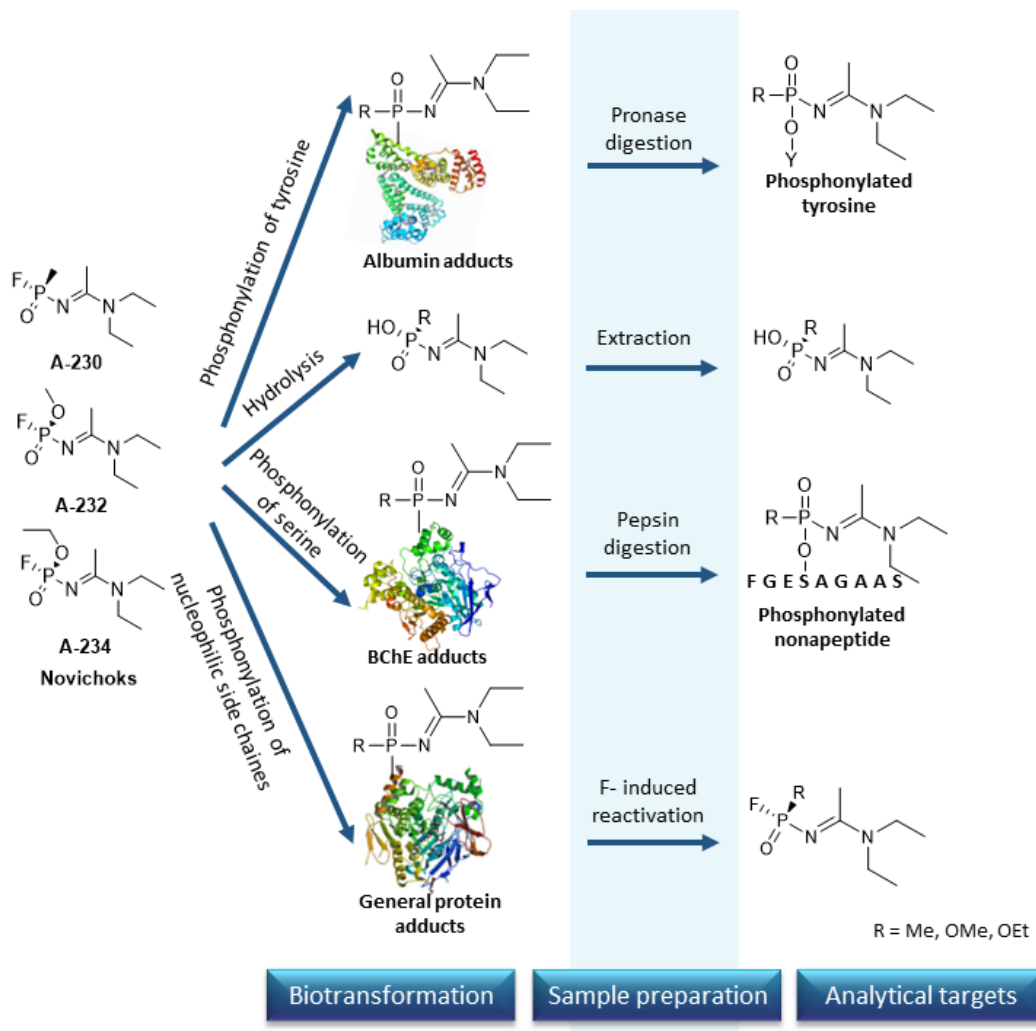


Figure S 2. To be investigated biotransformation pathways in humans after poisoning with Novichok nerve agents, based on sarin research. Two main processes are hydrolysis, and the formation of protein adducts. Albumin, BChE and other protein adducts are then digested or reactivated by fluoride before the analysis.

## 2. LC-MS/MS method optimization

Table S 1. Gradient elution settings for LC-MS/MS analyses. Eluent A is water with 0.2% v/v formic acid and eluent B is ACN with 0.2% v/v formic acid.

Analyte	Eluent A (%)	Linear ramping (min)	Eluent A (%)	Linear ramping (min)	Eluent A (%)
FGESAGAAS	100	20	20	0.1	100 (hold 5 min)
MPA-FGES(mpa)AGAAS					
GB-FGES(GB)AGAAS					
A-230-FGES(A-230)AGAAS					
A-232-FGES(A-232)AGAAS					
A-234-FGES(A-234)AGAAS					
MPA-Tyr	100 (hold 1 min)	10	50 (hold 2 min)	0.1	100 (hold 3 min)
GB-Tyr					
A-230-Tyr					
A-232-Tyr					
A-234-Tyr					
MPA	100	5	20 (hold 1 min)	0.1	100 (hold 3 min)
IMPA					
GB					
Methyl phosphate					
Ethyl phosphate					

Table S 2. Mass spectrometric parameters for nerve agent adducts and metabolites analyzed by LC-MS/MS

Analyte	Precursor ion (m/z)	Product ion (m/z)	Cone voltage (V)	Collision energy (eV)
<b>FGESAGAAS</b>	796.4	492.2	60	32
		620.3	60	32
		691.4	60	32
<b>FGES(mpa)AGAAS</b>	874.3	602.3	60	31
		673.3	60	27
		778.3	60	26
<b>FGES(GB)AGAAS</b>	916.3	602.3	60	31
		673.3	60	27
		778.3	60	26
<b>FGES(A-230)AGAAS</b>	970.4	602.3	60	31
		673.3	60	27
		778.3	60	26
<b>FGES(A-232)AGAAS</b>	986.4	602.3	60	31
		673.3	60	27
		778.3	60	26
<b>FGES(A-234)AGAAS</b>	1000.4	602.3	60	31
		673.3	60	27
		778.3	60	26
<b>MPA-Tyr</b>	260.1	197.1	40	13
		214.1	40	13
		260.1	40	13
<b>GB-Tyr</b>	302.1	214.1	40	13
		260.1	40	13
		313.0	40	15
<b>MPA</b>	97.0	65.0	20	26
		79.0	20	26
		97.0	20	7
<b>GB</b>	141.0	99.0	20	7
<b>A-230</b>	195.0	73.8	20	9
		121.6	20	10
		177.0	20	15
<b>A-232</b>	211.0	56.2	20	15
		73.8	20	10
		138.1	20	11
<b>A-234</b>	255.1	74.2	20	12
		123.9	20	13
		197.0	20	11

### 3. GC-MS/MS method optimization and validation

Table S 3. Mass spectrometric parameters for nerve agents analyzed by GC-MS/MS

Analyte	Retention time (min.)	Precursor ion (m/z)	Product ion (m/z)	Collision energy (V)
GB	7.70	125	99	10
		99	81	15
		99	47	30
A-230	19.19	194	72	5
		165	68	10
		122	81	10
A-232	20.00	210	181	10
		181	68	15
		138	97	15
A-234	20.65	224	195	5
		224	72	5
		195	68	10

Three different blood samples with a relatively low sarin inhibition of 20% were prepared for fluorite reactivation (n=3-5). Also, sarin standards, solvent blanks and blank samples without the addition of KF were added. OPCW criteria for signal-to-noise (S/N) and ion ratio were evaluated. The S/N should be larger than 5 and the ion ratio for a ratio of >50% should be maximum  $\pm 20\%$ . The standard has an ion-ratio, for 125 → 99 with respect to 99 → 81, of 83%. The variation must not be larger than  $\pm 20\%$ \* 83.2 =  $\pm 16.6\%$ . The obtained ion-ratios and the S/N as shown in Table S4 were according to the guidelines.

Table S 4. Evaluation of ion-ratios and signal-to-noise (S/N) ratios of blood incubated with 20% sarin after fluorite reactivation.

	99 → 81		125 → 99		Ion-ratio (%)	Deviation (%)
	Area	S/N	Area	S/N		
Solventblank1	0		0			
Standard_GB_0.5ng/mL	20964	612	17447	743	83	
Solventblank2	0		0			
Blood1_noKF	0		0			
Blood1_KF_1	26396	392	21500	1028	81	-2
Blood1_KF_2	22880	928	16395	251	72	-14
Blood1_KF_3	27267	1150	23724	202	87	5
Blood1_KF_4	31794	1617	26594	1735	84	1
Blood1_KF_5	31528	1201	25106	1682	80	-4
Solventblank3	0		0			
Blood2_noKF	0		0			
Blood2_KF_1	29042	7187	22301	341	77	-8
Blood2_KF_2	33697	522	26626	760	79	-5
Blood2_KF_3	31312	411	24139	304	77	-7
Solventblank4	0		0			
Blood3_noKF	0		0			
Blood3_KF_1	26677	534	18892	350	71	-15
Blood3_KF_2	30705	241	21918	298	71	-14
Blood3_KF_3	23437	190	18197	3067	78	-7
Solventblank5	0		0			

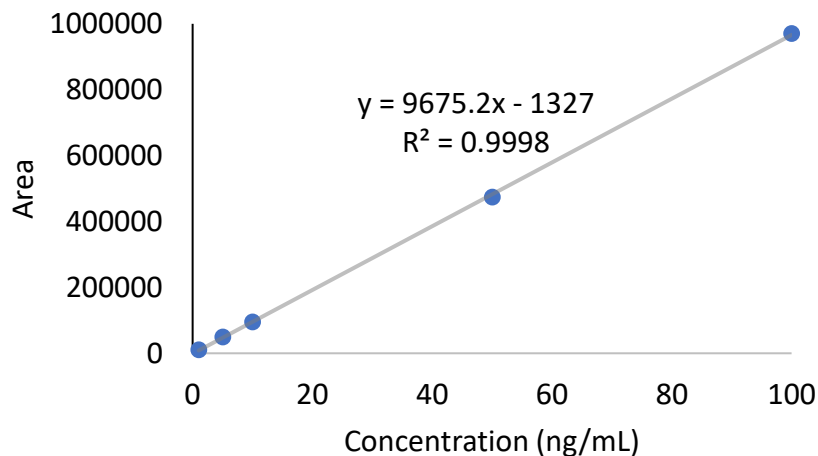


Figure S 3. Calibration curve of 1-100 ng/mL sarin analyzed by GC-MS/MS ( $n=1$ ,  $m/z$  99 → 81).

#### 4. Cholinesterase activity

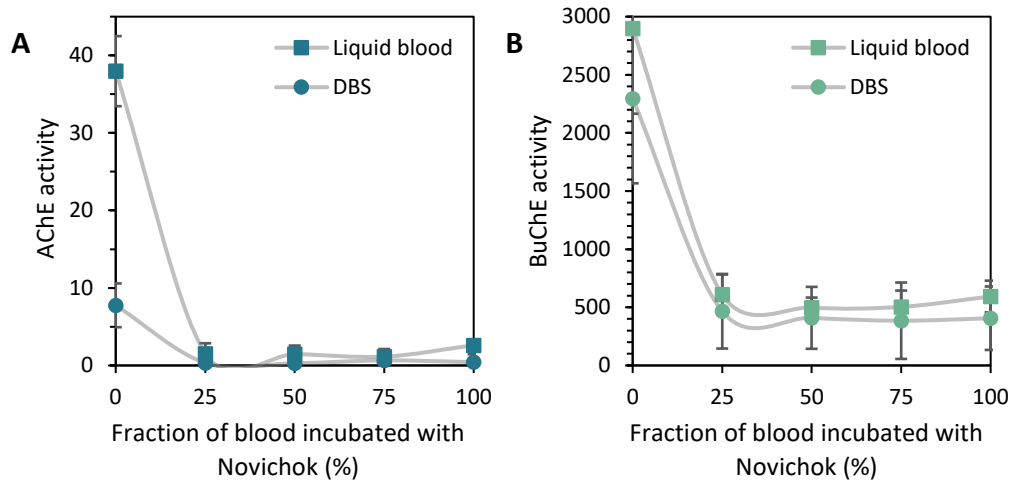


Figure S 4. Cholinesterase activity of 10 µL liquid blood (□) and 12.5 µL-based DBS (○) extracted after one month following nerve agent incubation. The ratio between blood incubated with 1.3 µM Novichok nerve agent and non-exposed blood is shown. A) AChE activity after Novichok inhibition ( $n=3$ ), B) BuChE activity after Novichok inhibition ( $n=3$ ). Line is of indicative nature only, error bars represent  $\pm 1$  standard deviation.

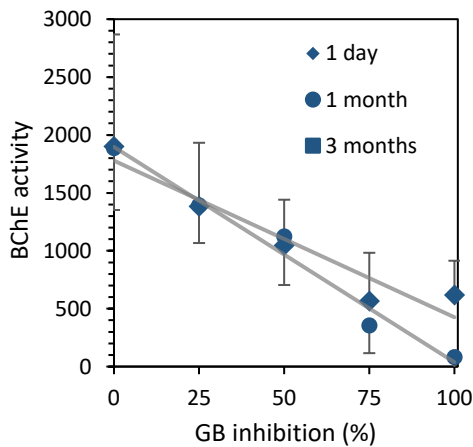


Figure S 5. BChE activity of DBS inhibited with sarin and extracted after one day ( $n=3$ , positive error bars), one month ( $n=8$ , negative error bars) and three months ( $n=1$ ) of storage at room temperature.

## 5. Analysis of free and regenerated nerve agent in liquid blood

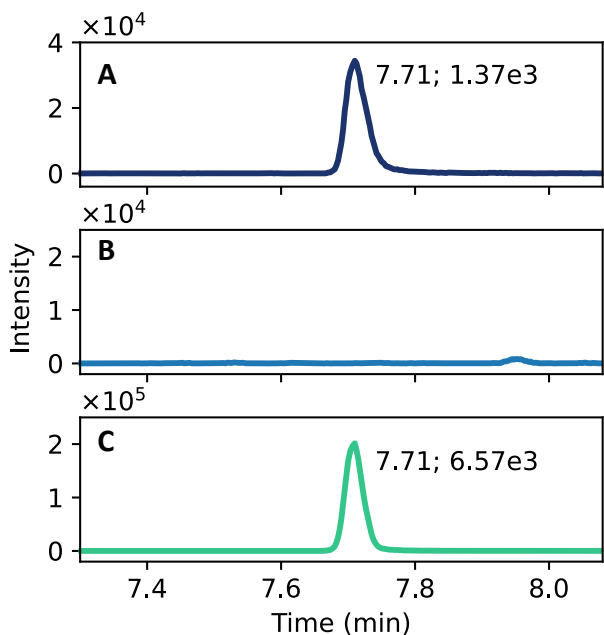


Figure S 6. Extracted ion chromatograms of regenerated sarin in 400  $\mu\text{L}$  liquid whole blood exposed to sarin, after fluoride reactivation analyzed by GC-MS/MS ( $m/z$  99 → 81, with corresponding area of the peak). A) Reference standard of sarin, B) Blood exposed to sarin without KF addition (control), C) Blood exposed to sarin with KF addition.

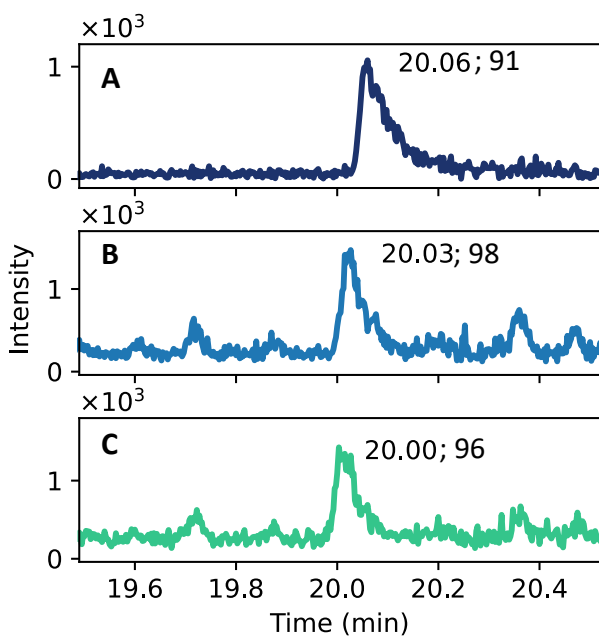


Figure S 7. Extracted ion chromatograms of intact Novichok A-232 in 400  $\mu\text{L}$  liquid whole blood exposed to A-232, after fluoride reactivation analyzed by GC-MS/MS ( $m/z$  138 → 97). A) Reference standard A-232, B) Dried blood spots exposed to A-232 without KF addition (control), C) DBS exposed to A-232 with KF addition.

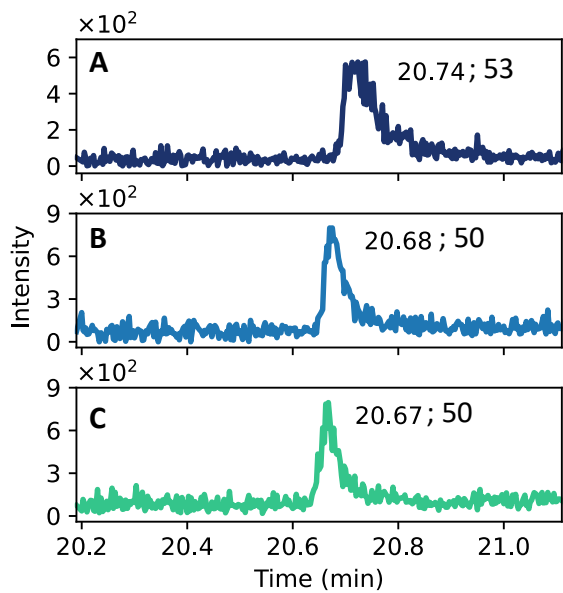


Figure S 8. Extracted ion chromatograms of intact Novichok A-234 in 400  $\mu\text{L}$  liquid whole blood exposed to A-234, after fluoride reactivation analyzed by GC-MS/MS ( $m/z$  224  $\rightarrow$  195). A) Reference standard A-234, B) Dried blood spots exposed to A-234 without KF addition (control), C) DBS exposed to A-234 with KF addition.

## 6. Analysis of free nerve agent in dried blood spots

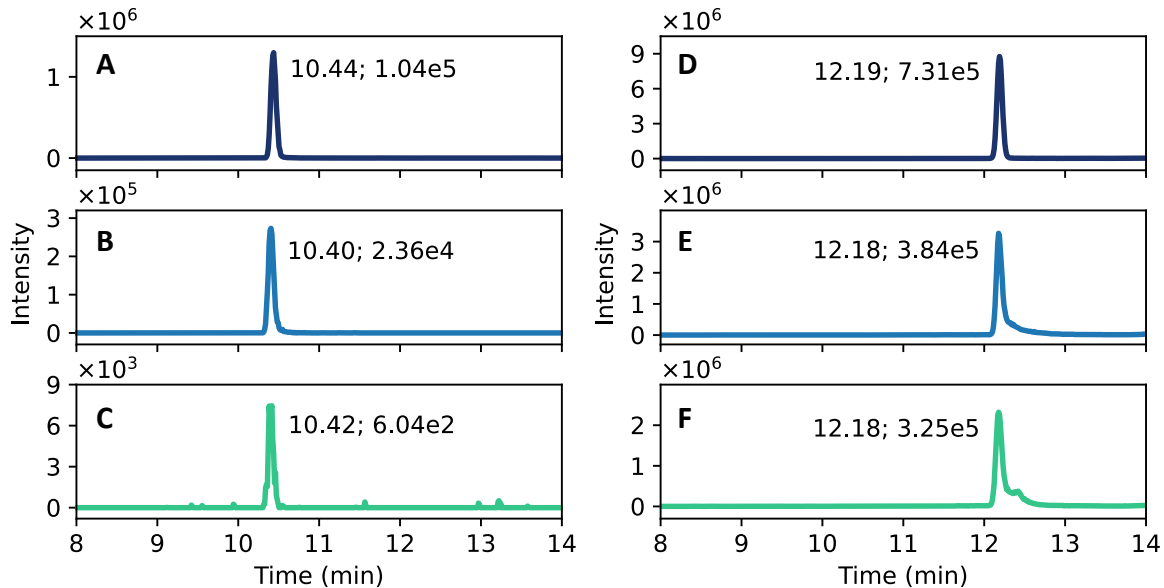


Figure S 9. Extracted ion chromatograms of intact Novichok A-C) A-230 ( $195.0 \rightarrow 73.8$ ) and D-F) A-234 ( $255.1 \rightarrow 74.2$ ) in dried blood spots (50  $\mu\text{L}$ ) analyzed by LC-MS/MS, three days after storage of the dried spots at ambient conditions. A, D) Reference standard, B, E) Dried blood spots exposed to nerve agent without KF addition (control), C, F) DBS exposed to nerve agent with KF addition.

## 7. Analysis of hydrolysis metabolites in DBS

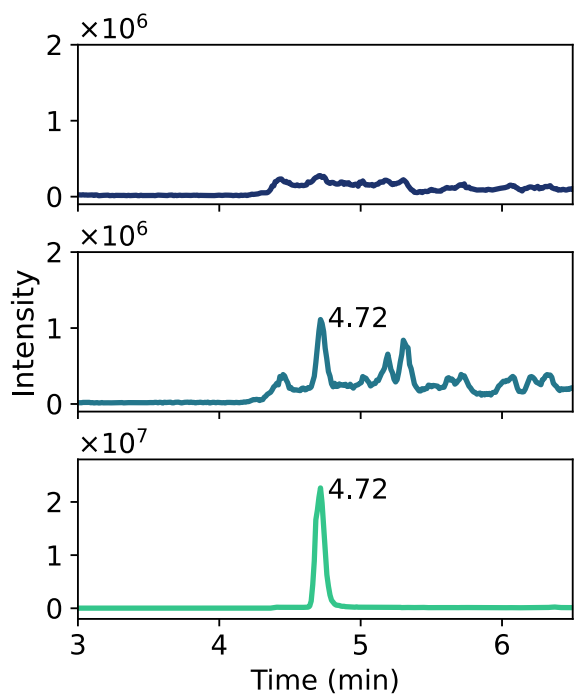


Figure S 10. Extracted ion chromatograms ( $139 \rightarrow 97$ ) of 100% inhibited dried blood spots after sarin exposure. A) sample preparation blank, B) potential presence of IMPA in dried blood spots, C) standard of IMPA.

# CHAPTER 6

## SUPPLEMENTARY DATA



## Supporting Information

# Verification of exposure to chemical warfare agents through analysis of persistent biomarkers in plants

Mirjam de Bruin-Hoegée<sup>a,b,\*</sup>, Latifa Lamriti<sup>a,b</sup>, Jan Langenberg<sup>b</sup>, René C. M. Olivier<sup>b</sup>, Lai Fun Chau<sup>b</sup>, Marcel van der Schans<sup>b</sup>, Daan Noort<sup>b</sup>, Arian C. van Asten<sup>a,c</sup>

<sup>a</sup> van 't Hoff Institute for Molecular Sciences, Faculty of Science, University of Amsterdam, P.O. Box 94157, 1090GD Amsterdam, The Netherlands

<sup>b</sup> TNO Defence, Safety and Security, Dep. CBRN Protection, Lange Kleiweg 137, 2288GJ Rijswijk, The Netherlands

<sup>c</sup> CLHC, Amsterdam Center for Forensic Science and Medicine, University of Amsterdam, P.O. Box 94157, 1090GD Amsterdam, The Netherlands

\*Corresponding author. Email address: [mirjam.debruin@tno.nl](mailto:mirjam.debruin@tno.nl) (M. de Bruin-Hoegée)

## Contents

- Section A.1. Method optimization and validation
  - Figure A.1. Calibration curves
- Section A.2. Visual examination of vegetation
  - Figure A.2. Physical state of nettle leaf upon liquid exposure to A-234
  - Figure A.3. Physical state of plants upon vapor exposure to 25 mg/m<sup>3</sup> of sarin
  - Figure A.4. Physical state of nettle upon vapor exposure to 250 mg/m<sup>3</sup> of sarin
- Section A.3. Chromatograms after three months
  - Figure A.5. Extracted ion chromatograms of phosphorylated tyrosine adduct
  - Figure A.6. Extracted ion chromatograms of chlorinated tyrosine adducts
  - Figure A.7. Extracted ion chromatograms of N1-HETE-His and N3-HETE-His adducts
- Table A.1. Identified biomarkers in plants after chlorine, sarin or sulfur mustard exposure

### A.1. Method optimization and validation

The gradient elution was optimized for each analyte (Table A.1). The chemicals could be analyzed with a single chromatographic method as well, which is the same as described for the A-234 and GB adducts.

Table A. 1. Gradient elution settings for LC-MS/MS analyses. Eluent A is water with 0.2% v/v formic acid and eluent B is ACN with 0.2% v/v formic acid.

Analyte	Eluent A (%)	Linear ramping (min)	Eluent A (%)	Eluent A (%)
A-234-Tyr GB-Tyr MPA-Tyr	100 (hold 1 min)	10	50 (hold 2 min)	100 (hold 3 min)
Cl-Tyr di-Cl-Tyr <sup>13</sup> C <sub>6</sub> -Cl-Tyr	100 (hold 2 min)	8	20 (hold 2 min)	100 (hold 3 min)
N1-HETE-His N3-HETE-His	100 (hold 3 min)	3	20 (hold 1 min)	100 (hold 3 min)

For GB-Tyr, linear calibration curves were obtained in the range of 0.05 – 20 ng/mL with  $R^2 = 0.9997 - 0.9999$  (Figure A.1A). The mean values for the quality controls were within 2.6% relative standard deviation at 0.1, 1 and 10 ng/mL ( $n=10$  for each concentration). The stability of the analyte was assessed over two weeks and the concentration was within 15% of the nominal value for 0.1 ng/mL and within 3.3% for 1 and 10 ng/mL.

In addition, linear calibration curves were obtained in the range of 1 – 100 ng/mL with  $R^2 = 0.9999 - 0.99995$  for Cl-Tyr and di-Cl-Tyr as well (Figure A.1B). The mean values for the quality controls were within 20% at 1 ng/mL and within 6% relative standard deviation at both 10 ng/mL and 100 ng/mL ( $n = 10$ , for each concentration). The stability of the analytes was assessed over two weeks and the concentration was within 18% of the nominal value for 1 ng/mL and within 3.8% for 10 and 100 ng/mL.

Third, the LC-MS/MS method was validated for N1-HETE-HIS and N3-HETE-HIS. Linear calibration curves were obtained in the range of 1 – 50 ng/mL with  $R^2 = 0.9987 - 0.9997$  (Figure A.1C). The mean values of the quality controls were within 5% for 1 and 10 ng/mL N1-HETE-HIS and N3-HETE-HIS ( $n = 10$ , for each concentration). The stability of the analytes was assessed over one week and the concentration was within 23% for 1 ng/mL N3-HETE-HIS and within 6% for 1 ng/mL N1-HETE-HIS and 10 mg/mL N1-HETE-HIS and N3-HETE-HIS.

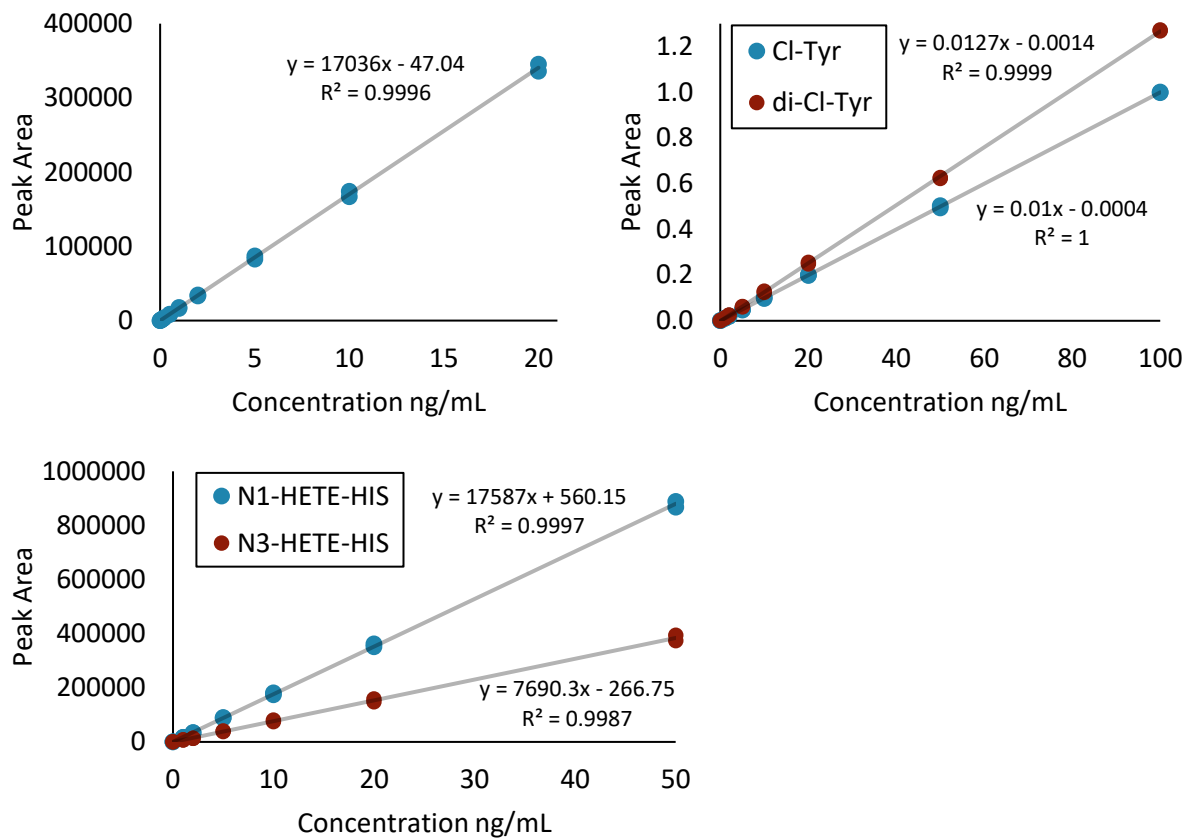
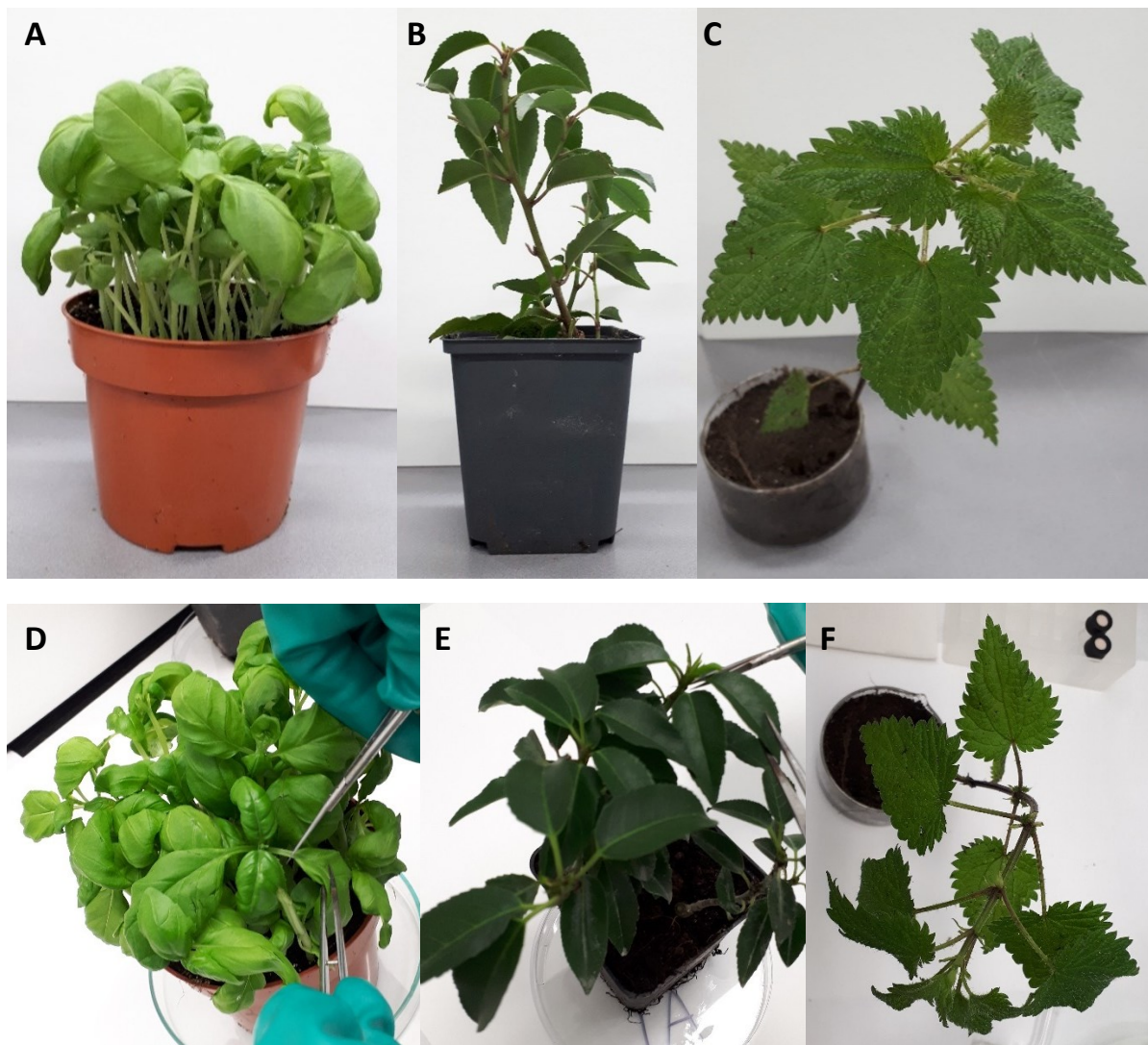


Figure A. 1. Calibration curves analyzed by LC-MS/MS of A) GB-Tyr, B) 3-chlorotyrosine (Cl-Tyr) and 3,5-dichlorotyrosine (di-Cl-Tyr) with internal standard 13C6-3-chloro-L-tyrosine, C) N1-HETE-HIS and N3-HETE-HIS adducts of sulfur mustard.

## A.2. Visual examination of vegetation



Figure A. 2. Physical state of nettle leaf upon liquid exposure to A-234.



*Figure A. 3. No notable differences were observed for A) Laurel, B) Basil and C) Nettle prior to exposure compared to D) Laurel, E) Basil and F) Nettle immediately after vapor exposure of 25 mg/m<sup>3</sup> sarin in the vapor generation set-up.*



*Figure A. 4. Nettle A) prior to exposure B) after 250 mg/m<sup>3</sup> exposure to sarin. It should be noted that the change could also be due to the dry atmosphere in the vapor generation set-up instead as a result of the chemical warfare agent exposure.*

### A.3. Chromatograms after three months

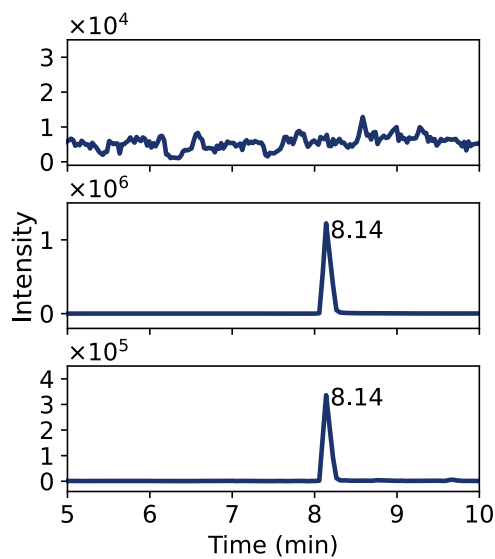


Figure A. 5. Extracted ion chromatograms of phosphorylated tyrosine adduct with  $t_R = 8.14$  three months after sarin vapor exposure. A) Sample preparation blank. B) Standard GB-Tyr. C) GB-Tyr measured after plant exposure to  $250 \text{ mg/m}^3$  sarin.

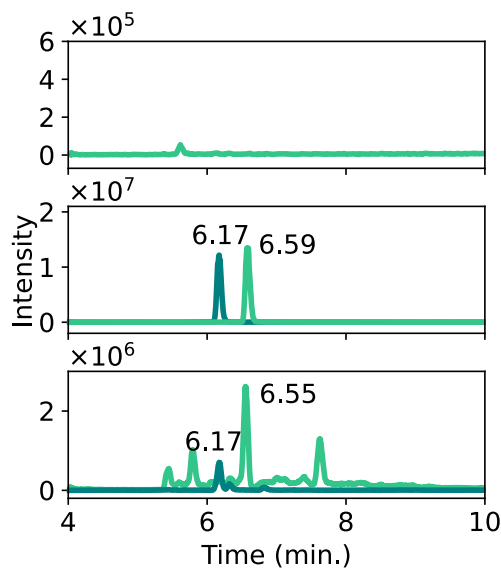


Figure A. 6. Extracted ion chromatograms of chlorinated tyrosine adducts three months after chlorine gas exposure. A) Sample preparation blank. B) Standard Cl-Tyr with  $t_R = 6.17 \text{ min}$  and di-Cl-Tyr with  $t_R = 6.59 \text{ min}$ . C) Cl-Tyr and di-Cl-Tyr after  $5 \text{ g/m}^3$  plant exposure.

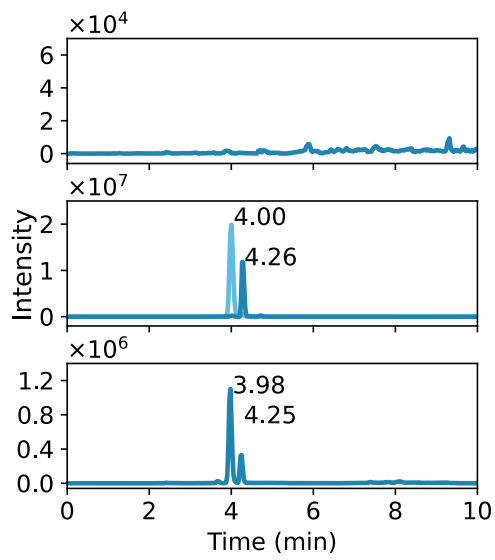


Figure A. 7. Extracted ion chromatograms of N1-HETE-His and N3-HETE-His adducts three months after sulfur mustard vapor exposure. A) Sample preparation blank. B) Standard N1-HETE-His with  $t_R = 4.00$  min and N3-HETE-His with  $t_R = 4.26$  min. C) N1-HETE-His and N3-HETE-His measured after 150 mg/m<sup>3</sup> plant exposure.

Table A. 2. Identified biomarkers in plants after chlorine, sarin or sulfur mustard exposure.

Peptide	Accession	Protein	Mass (Da)	t <sub>R</sub> (min)	Exposure	Species	N (#) <sup>a</sup>
Y(+120.03)FRLSSLEKCY(+120.03)SR	P93211 1433 6_SOLLC	14-3-3 protein	1890.9	16.4	GB	Basil	1
KSCSY(+33.96)ELETLSK	P29307 1433 _OENEH	14-3-3 protein	1549.7	16.0	Cl	Nettle	1
H(+105.04)DKHELQEAAHNK	P93784 1433 5_SOLTU	14-3-3 protein	1660.8	20.1	HD	Laurel	1
AEEAAEKY(+120.03)RKPAEEATAAPPR	P49608 ACOC _CUCMA	Aconitate hydratase, cytoplasmic	2417.2	16.1	GB	Basil	1
CY(+120.03)KLLPTTLVADKFAFAEHK	O65396 GCST _ARATH	Aminomethyltransferase, mitochondrial	2626.4	21.2	GB	Laurel	1
GYPGY(+33.96)LYTDLATIYER	B0K8E7 VATB _THEP3	ATP synthase	1927.9	21.3	Cl	Nettle	2
MY(+120.03)Y(+120.03)EAKETLELAEAVKR	Q0ZJ14 ATPE _VITVI	ATP synthase, chloroplastic	2283.1	21.6	GB	Laurel	1
QMLPLCH(+105.04)CQTLELAEAGGLR	Q2MI94 ATPE _SOLLC	ATP synthase, chloroplastic	2287.1	21.6	HD	Basil	1
EAQAVADDVFSLFISEEVDKVELLY(+33.96)TK	Q01908 ATPG 1_ARATH	ATP synthase, chloroplastic	3091.5	22.8	Cl	Nettle	2
WEHY(+120.03)FMESLASELAAR	P29790 ATPG _TOBAC	ATP synthase, chloroplastic	2058.9	20.2	GB	Laurel	1
KVEY(+120.03)MRVLMGDGLFLQEGSWK	A6MM21 ATP A_BUXMI	ATP synthase, chloroplastic	2605.3	22.0	GB	Basil	1
NY(+120.03)MQVDPFQESGVNLNEENLAESK	Q68RZ9 ATPB _PANGI	ATP synthase, chloroplastic	2760.2	18.8	GB	Basil	1
Y(+120.03)FKLATSGSGVSTLEK	Q68RZ9 ATPB _PANGI	ATP synthase, chloroplastic	1806.9	17.1	GB	Basil	1
Y(+120.03)VGPNAVPLDSTPNAVMMPR	Q68RZ9 ATPB _PANGI	ATP synthase, chloroplastic	2118.0	20.8	GB	Basil	1
RY(+120.03)PAVDPLDSFHVVMPR	Q85V35 ATPB _LACPU	ATP synthase, chloroplastic	2118.0	20.7	GB	Basil	1
VGLTALTIAEY(+33.96)FR	O03081 ATPB _PSINU	ATP synthase, chloroplastic	1486.8	21.2	Cl	Nettle	2
VGLTALTIAEY(+67.92)FR	O03081 ATPB _PSINU	ATP synthase, chloroplastic	1520.7	21.6	Cl	Nettle	1
QVY(+120.03)HLNEQNLAESK	Q2L917 ATPB _GOSHI	ATP synthase, chloroplastic	1791.9	16.6	GB	Laurel	1
Y(+120.03)NMCY(+120.03)RWWRLNEKNLA ESK	Q2L917 ATPB _GOSHI	ATP synthase, chloroplastic	2743.3	19.9	GB	Laurel	1
Y(+120.03)Y(+120.03)Y(+120.03)VVLSTEMG TLKER	Q2L917 ATPB _GOSHI	ATP synthase, chloroplastic	2311.1	20.1	GB	Laurel	1
KYY(+120.03)NMY(+120.03)SPAGYLENK	P19023 ATPB M_MAIZE	ATP synthase, mitochondrial	2079.9	19.8	GB	Basil	1
Y(+120.03)DADSGGVLYVK	Q41396 VATE _SPIOL	ATPase	1504.7	18.5	GB	Basil	1
AY(+120.03)ENGTLSVAGR	O80860 FTSH 2_ARATH	ATP-dependent zinc metalloprotease, chloroplastic	1356.6	23.1	GB	Basil	1
EALGKAELKEALASLEH(+105.04)KEETLK	Q655S1 FTSH 2_ORYSJ	ATP-dependent zinc metalloprotease, chloroplastic	2641.4	20.3	HD	Basil	1
Y(+33.96)AGVGAAIEYAVLHLK	P42737 BCA2 _ARATH	Carbonic anhydrase, chloroplastic	1707.9	20.9	Cl	Nettle	2
WY(+120.03)WY(+120.03)KLLSSVDLLEEKLR	B9N843 ACCC 2_POPTR	Biotin carboxylase, chloroplastic	2580.3	21.0	GB	Basil	1
H(+105.04)NLTDDQLSEFK	Q39752 CAL M_FAGSY	Calmodulin	1550.7	21.4	HD	Laurel	2
GPILEDY(+33.96)HLVEK	P48350 CAT A_1_CUCPE	Catalase	1558.8	20.7	Cl	Nettle	1

LPACCAY(+120.03)RLLEKENNK	P48350 CATA 1_CUCPE	Catalase	1984.0	16.0	GB	Laurel	1
Y(+120.03)FELEQENNKNVASSTGK	P48350 CATA 1_CUCPE	Catalase	2177.0	15.9	GB	Basil	1
GPLENLADHLADPVNNNAWAY(+33.96)ATKL CPGK	P09755 CB22 _SOYBN	Chlorophyll binding protein, chloroplastic	3125.5	22.3	Cl	Nettle	2
CY(+120.03)GDYLGPNPNLLVVPK	P09756 CB23 _SOYBN	Chlorophyll binding protein, chloroplastic	1883.9	20.5	GB	Laurel	1
GY(+120.03)CDYLGPNPSLVVPAR	P09756 CB23 _SOYBN	Chlorophyll binding protein, chloroplastic	1842.9	20.2	GB	Laurel	1
LVY(+120.03)FYLAPELLGK	P27522 CB13 _SOLLC	Chlorophyll binding protein, chloroplastic	1644.9	21.6	GB	Basil	1
DHVKPVSSGSY(+120.03)YGDPR	P04783 CB25 _PETSP	Chlorophyll binding protein, chloroplastic	1882.9	19.0	GB	Basil	1
Y(+120.03)Y(+120.03)PNATGDKGYPGGK	P36494 CB4_ SPIOL	Chlorophyll binding protein, chloroplastic	1826.8	17.8	GB	Basil	1
KLY(+120.03)RYLKFDLSDLQNLAK	Q07473 CB4A _ARATH	Chlorophyll binding protein, chloroplastic	2462.3	22.3	GB	Basil	1
NY(+120.03)WELLHGR	Q07473 CB4A _ARATH	Chlorophyll binding protein, chloroplastic	1306.6	17.8	GB	Basil	1
Y(+120.03)CMVQSTPFQDHRSQVLVLR	Q07473 CB4A _ARATH	Chlorophyll binding protein, chloroplastic	2526.2	21.8	GB	Laurel	1
Y(+120.03)GELLHGR	Q07473 CB4A _ARATH	Chlorophyll binding protein, chloroplastic	1306.6	17.8	GB	Basil	2
Y(+120.03)YHELLHGR	Q07473 CB4A _ARATH	Chlorophyll binding protein, chloroplastic	1306.6	18.0	GB	Basil	1
EFLVLH(+105.04)LQFELDSLQGGLAK	Q9XF88 CB4B _ARATH	Chlorophyll binding protein, chloroplastic	2476.3	22.3	HD	Basil	2
EVPYLH(+105.04)LQFDLDSLQDQNLAK	Q9XF88 CB4B _ARATH	Chlorophyll binding protein, chloroplastic	2462.2	22.1	HD	Basil	2
H(+105.04)GVFLWSWFH(+105.04)WFDNCA GLSADEPTFAK	P08221 CB21 _CUCSA	Chlorophyll binding protein, chloroplastic	3377.5	22.0	HD	Basil	1
Y(+120.03)GCDYLGPNPSLVVPAR	Q10HD0 CB2 3_ORYSJ	Chlorophyll binding protein, chloroplastic	1842.9	20.4	GB	Basil	1
RY(+33.96)VVDAGVLSR	P29357 HSP7 E_SPIOL	Chloroplast envelope membrane	1382.7	17.4	Cl	Nettle	1
KLLRY(+120.03)LPGESDSDFSDFSSK	Q9SA52 CP41 B_ARATH	Chloroplast stem-loop binding protein, chloroplastic	2410.1	19.2	GB	Laurel	1
KQPLAQKLY(+120.03)SDSDFSDFSSK	Q9SA52 CP41 B_ARATH	Chloroplast stem-loop binding protein, chloroplastic	2410.1	19.5	GB	Basil	1
RY(+120.03)LLKLPGESDSDFSDFSSK	Q9SA52 CP41 B_ARATH	Chloroplast stem-loop binding protein, chloroplastic	2410.1	19.5	GB	Basil	1
Y(+120.03)Y(+120.03)LLDVVYDLNGR	Q9SA52 CP41 B_ARATH	Chloroplast stem-loop binding protein, chloroplastic	1841.9	21.8	GB	Basil	1
VAVEAQWVADY(+120.03)AVK	Q0WLB5 CLA H2_ARATH	Clathrin	1667.8	17.8	GB	Basil	1
TPLTDAAAAY(+120.03)YRR	P25076 CY11 _SOLTU	Cytochrome	1587.8	19.7	GB	Laurel	1
H(+105.04)HLTFPLLSPDPTTK	A6MMV7 CYF _ILLOL	Cytochrome	1807.9	21.8	HD	Basil	2
QFY(+120.03)SVTVESAETLK	Q9SRZ6 ICDH C_ARATH	Cytosolic isocitrate dehydrogenase [NADP]	1791.9	18.5	GB	Laurel	1
GFVY(+120.03)DLLLPY	F4JLP5 PLPD2 _ARATH	Dihydrolipoyl dehydrogenase, chloroplastic	1424.8	22.8	GB	Basil	1
KYH(+105.04)VAEMNKR	P34824 EF1A 1_HORVU	Elongation factor	1379.7	15.3	HD	Laurel	1

LPLQDVY(+33.96)K	Q03033 EF1A_WHEAT	Elongation factor	1008.5	19.7	Cl	Nettle	1
DY(+120.03)LPGHKKLTTR	O24310 EFTU_PEA	Elongation factor, chloroplastic	1660.9	19.8	GB	Basil	1
KWSY(+120.03)LFAVEDVFSLTGR	Q43467 EFTU_1_SOYBN	Elongation factor, chloroplastic	2137.1	23.4	GB	Basil	1
H(+105.04)LEAPSRLAAQPK	Q6ZA06 GUN_20_ORYSJ	Endoglucanase	1634.9	20.1	HD	Laurel	1
ATLPAFY(+67.92)LKKLPLPLR	Q42971 ENO_ORYSJ	Enolase	1908.1	21.7	Cl	Nettle	1
KNEVHKY(+120.03)RDDTLADEELAK	P56337 IF5A5_SOLTU	Eukaryotic translation initiation factor	2506.2	20.3	GB	Basil	1
WPY(+120.03)Y(+120.03)LFDLFDDWLR	P23225 GLTB_MAIZE	Ferredoxin-dependent glutamate synthase, chloroplastic	2188.0	22.3	GB	Basil	1
NGY(+120.03)LSFLANLVSDLR	Q43155 GLTB_SPIOL	Ferredoxin-dependent glutamate synthase, chloroplastic	1800.9	21.0	GB	Basil	1
Y(+120.03)VMAAEKPAAADAPAAEPK	Q69RJ0 GLTB_ORYSJ	Ferredoxin-dependent glutamate synthase, chloroplastic	2020.0	17.7	GB	Basil	1
VVPILLEAY(+67.92)VPK	Q69RJ0 GLTB_ORYSJ	Ferredoxin-dependent glutamate synthase, chloroplastic	1294.6	20.5	Cl	Nettle	1
H(+105.04)DLLQLSGHDGGTGASPVSSLK	Q43155 GLTB_SPIOL	Ferredoxin-dependent glutamate synthase, chloroplastic	2280.1	18.7	HD	Basil	1
TY(+120.03)SNTGVKGAVNVQWDKK	P25851 F16P_1_ARATH	Fructose-1,6-bisphosphatase, chloroplastic	2114.1	19.1	GB	Laurel	1
H(+105.04)DELVLFVEHR	P46256 ALF1_PEA	Fructose-bisphosphate aldolase, cytoplasmic	1497.8	21.5	HD	Laurel	1
WKYWY(+120.03)VLKENNVLPGK	P46256 ALF1_PEA	Fructose-bisphosphate aldolase, cytoplasmic	2269.2	21.3	GB	Basil	1
QECKH(+105.04)TDVLQENNVLPGLK	O65581 ALFC_5_ARATH	Fructose-bisphosphate aldolase, cytosolic	2269.1	20.9	HD	Basil	1
RPLTY(+33.96)GLLLASLGLEWDNGGR	P16096 ALFC_SPIOL	Fructose-bisphosphate aldolase, cytosolic	2334.2	18.4	Cl	Nettle	1
Y(+120.03)Y(+120.03)LVFEVLQK	Q9XQ94 GLN_A2_MEDSA	Glutamine synthetase leaf isozyme, chloroplastic	1540.8	15.8	GB	Basil	1
H(+105.04)KLLNLDVTPTDK	O22506 GLN_A2_DAUCA	Glutamine synthetase, chloroplastic	1760.9	21.3	HD	Basil	1
HPY(+120.03)LSAYGEDGKR	O22506 GLN_A2_DAUCA	Glutamine synthetase, chloroplastic	1611.7	15.1	GB	Basil	1
QMY(+120.03)HVFEVLQK	O22506 GLN_A2_DAUCA	Glutamine synthetase, chloroplastic	1540.8	15.9	GB	Basil	1
RY(+120.03)WTPKGEGNER	O22506 GLN_A2_DAUCA	Glutamine synthetase, chloroplastic	1611.8	15.1	GB	Laurel	1
KHKY(+67.92)WDELFGGYLYFHK	O24338 ASNS_SANAU	Glutamine-dependent asparagine synthetase	2298.0	21.0	Cl	Nettle	1
Y(+120.03)LVRHYPLDVVVDFMR	P09044 G3PB_TOBAC	Glyceraldehyde-3-phosphate dehydrogenase B, chloroplastic	2141.1	22.9	GB	Basil	1
HSMLGTFY(+120.03)ER	P09044 G3PB_TOBAC	Glyceraldehyde-3-phosphate, chloroplastic	1359.6	15.8	GB	Basil	1
LTLFGDKPVAVY(+33.96)GPR	P08735 G3PC_1_MAIZE	Glyceraldehyde-3-phosphate, cytosolic	1665.9	22.1	Cl	Nettle	1
KGADVCH(+105.04)VVEAVR	O49954 GCSP_SOLTU	Glycine decarboxylase	1486.8	16.2	HD	Basil	1
WQQAAEKY(+120.03)RQPAAAETAPVPK	P26969 GCSP_PEA	Glycine dehydrogenase, mitochondrial	2530.3	17.3	GB	Basil	1

Y(+33.96)AASDLRKAK	Q01899 HSP7 M_PHAVU	Heat shock protein, mitochondrial	1155.6	17.3	Cl	Nettle	1
MSY(+120.03)AFFADYTEAHLK	Q9FE01 APX2 _ORYSJ	L-ascorbate peroxidase, cytosolic	1912.8	20.6	GB	Basil	1
LAEEAAEKRY(+120.03)KPAAAEDGVPAPK	P30184 AMPL 1_ARATH	Leucine aminopeptidase	2530.3	17.1	GB	Laurel	1
GY(+120.03)KLEGDGPGPTLKK	O24248 PRU1 _PRUAV	Major allergen Pru av 1	1638.8	15.7	GB	Laurel	1
H(+105.04)PELEGDGPGPTLK	O24248 PRU1 _PRUAV	Major allergen Pru av 2	1510.7	16.4	HD	Basil	1
KRQQY(+120.03)VCTSELPPPR	O24248 PRU1 _PRUAV	Major allergen Pru av 3	1921.0	21.2	GB	Laurel	1
LYY(+120.03)Y(+120.03)VLRFESLKPSTDLG SK	O49079 PSBO _FRIAG	Oxygen-evolving enhancer, chloroplastic	2733.3	21.0	GB	Basil	1
LSEELGKGH(+105.04)AK	P14226 PSBO _PEA	Oxygen-evolving enhancer, chloroplastic	1401.7	15.5	HD	Basil	1
H(+105.04)EGPLEVSVLKDR	P85194 PSBO _HELAN	Oxygen-evolving enhancer, chloroplastic	1582.8	20.0	HD	Laurel	1
SEQWNNEVY	Q40459 PSBO _TOBAC	Oxygen-evolving enhancer, chloroplastic	1595.7	18.9	Cl	Nettle	1
H(+105.04)GENWLEYPGQVLR	P16059 PSBP _PEA	Oxygen-evolving enhancer, chloroplastic	1801.9	20.8	HD	Basil	1
Y(+120.03)MQWLEYPGQVLR	P16059 PSBP _PEA	Oxygen-evolving enhancer, chloroplastic	1801.9	21.1	GB	Basil	1
Y(+120.03)WWWEYPGKVLR	P85189 PSBP _HELAN	Oxygen-evolving enhancer, chloroplastic	1801.9	21.0	GB	Laurel	1
DGDATEH(+105.04)HKLLSATVNDGK	Q04127 PSBP 3_TOBAC	Oxygen-evolving enhancer, chloroplastic	2112.0	16.4	HD	Basil	1
EAVH(+105.04)AH(+105.04)APSDELEYPGQV LR	Q04127 PSBP 3_TOBAC	Oxygen-evolving enhancer, chloroplastic	2427.2	20.3	HD	Basil	1
SY(+120.03)NDELEYPGKVLR	Q04127 PSBP 3_TOBAC	Oxygen-evolving enhancer, chloroplastic	1801.9	21.2	GB	Basil	1
Y(+120.03)CVTPNVVVAADNAAPPR	P83218 PME DAUCA	Pectinesterase	1976.0	20.1	GB	Laurel	1
Y(+120.03)TWASLAAEAKK	O49006 PME 3_ARATH	Pectinesterase	1457.7	18.8	GB	Laurel	1
HVVFGQVVEPY(+33.96)GLPK	Q39613 CYPH CATRO	Peptidyl-prolyl cis-trans isomerase	1701.9	19.1	Cl	Nettle	1
QLVNY(+120.03)VGTEAVAK	P50318 PGKH 2_ARATH	Phosphoglycerate kinase, chloroplastic	1510.8	18.4	GB	Laurel	1
REVLPTTLVVADKFAY(+120.03)NSK	P41758 PGKH _CHLRE	Phosphoglycerate kinase, chloroplastic	2383.3	22.0	GB	Basil	1
HY(+120.03)VFAVGTEAVAK	Q42961 PGK H_TOBAC	Phosphoglycerate kinase, chloroplastic	1510.8	18.7	GB	Basil	1
H(+105.04)ELAGFQYLGGPETGEK	P0DKC3 PGP1 A_ARATH	Phosphoglycolate phosphatase, chloroplastic	1936.9	22.0	HD	Laurel	1
H(+105.04)MQEPLVVGALK	P0DKC3 PGP1 A_ARATH	Phosphoglycolate phosphatase, chloroplastic	1425.8	17.4	HD	Laurel	1
KFY(+120.03)Y(+120.03)DGTGLFQTLVGLK	P26302 KPPR _WHEAT	Phosphoribulokinase, chloroplastic	2189.1	22.3	GB	Basil	1
WLYGY(+33.96)CPYYHVSLEFDGQFDR	P26302 KPPR _WHEAT	Phosphoribulokinase, chloroplastic	2790.2	22.0	Cl	Nettle	1
WH(+105.04)EPAYPGGPLFNPLGFGK	Q9SY97 LHCA 3_ARATH	Photosystem chlorophyll binding protein, chloroplastic	2188.1	22.2	HD	Basil	1
KHY(+120.03)WALAPELLGK	Q9SY97 LHCA 3_ARATH	Photosystem chlorophyll binding protein, chloroplastic	1644.9	21.7	GB	Basil	1
KTY(+120.03)HPLVYDTWESPK	P12372 PSAD _SOLLC	Photosystem I reaction center, chloroplastic	1983.0	20.3	GB	Laurel	1
RRNNVTEALH(+105.04)TYH(+105.04)YFYW PLFGGSTGGLLR	P36213 PSAD _HORVU	Photosystem I reaction center, chloroplastic	3634.8	22.3	HD	Basil	1

Y(+120.03)AHPADGLPHLLVSTAQR	P13192 PSAF_HORVU	Photosystem I reaction center, chloroplastic	2065.1	21.4	GB	Basil	1
AAEEAAEKY(+120.03)RKPAEEATPVAPK	P12354 PSAE_SPIOL	Photosystem I reaction center, chloroplastic	2488.3	16.1	GB	Laurel	1
WSFAAEH(+105.04)HPENLLFPEEVLPK	Q2MIA5 PSB_D_SOLLC	Photosystem II D2	2622.3	20.5	HD	Basil	2
AAEDPEFETFY(+33.96)TK	Q3MA59 PSB_D_TRIV2	Photosystem II D2	3877.4	20.7	Cl	Nettle	1
WKY(+120.03)VY(+120.03)Y(+120.03)PKSV GRATELNNAVNVSPR	POC367 PSBC_ORYSJ	Photosystem II reaction center	3319.6	21.1	GB	Basil	1
Y(+120.03)AEDGTLALAGR	Q09G50 PSBC_PLAOC	Photosystem II reaction center	1355.6	23.6	GB	Laurel	1
QRDLWHAPY(+67.92)KVLVGGVATELNNAVNY VSPR	Q09G50 PSBC_PLAOC	Photosystem II reaction center	3319.6	21.0	Cl	Nettle	1
QSFDH(+105.04)TLAVGWLGHPLFR	P56777 PSBB_ARATH	Photosystem II reaction center	2185.1	21.1	HD	Basil	1
LMVVY(+33.96)ERTFPVVLVDGDGLVR	Q06FP2 PSBB_PELHO	Photosystem II reaction center	2410.2	22.5	Cl	Nettle	1
VPVY(+33.96)FETFPVVLVDGDGLVR	Q06FP2 PSBB_PELHO	Photosystem II reaction center	2254.1	22.7	Cl	Nettle	1
FVDPSDPLDFY(+120.03)R	Q7OXY1 PSBB_AMBTC	Photosystem II reaction center	1702.8	22.1	GB	Basil	1
GY(+120.03)HLGDGNAVGWLGHPLFR	P56777 PSBB_ARATH	Photosystem II reaction center	2185.1	21.5	GB	Basil	1
VFDPSDPLDFY(+120.03)R	P56777 PSBB_ARATH	Photosystem II reaction center	1702.8	22.1	GB	Basil	1
RY(+120.03)FGKVEDEDFVEFAGVDVSK	P11970 PLAS_2_POPNI	Plastocyanin B, chloroplastic	2555.2	20.1	GB	Laurel	1
ERPY(+33.96)EFMLNAPGEVYVTLSEK	P00288 PLAS_VICFA	Plastocyanin	2592.2	21.4	Cl	Nettle	1
GPEVY(+33.96)PMYLNAPGEVYVTLSEK	P00288 PLAS_VICFA	Plastocyanin	2576.2	21.3	Cl	Nettle	1
KVY(+120.03)VSY(+120.03)VVFDEDEVPARD VAK	P07030 PLAS_SILLB	Plastocyanin, chloroplastic	2667.3	19.3	GB	Laurel	1
Y(+120.03)CMTQDQEGLVPEMTVPK	Q9FHQ6 UBQ_9_ARATH	Polyubiquitin	2173.9	20.4	GB	Laurel	1
LEGAYDRY(+33.96)FQLEASQQFNGYELDGR	Q9LJL3 PREP1_ARATH	Presequence protease 1, chloroplastic/mitochondrial	3073.4	22.2	Cl	Nettle	1
VVAEAAKAQFSNKAY(+120.03)YDK	Q2JRU4 AMP_A_SYNJA	Probable cytosol aminopeptidase	2122.0	17.4	GB	Laurel	1
Y(+120.03)RKMVMGLDKSLEAEFLDR	P83344 XYNB_PRUPE	Putative beta-D-xylosidase	2420.2	22.8	GB	Laurel	1
Y(+120.03)TLPGHKK AFLPR	P83344 XYNB_PRUPE	Putative beta-D-xylosidase	1646.9	18.6	GB	Laurel	2
Y(+120.03)HNHY(+120.03)LLVGQLEWR	P31414 AVP1_ARATH	Pyrophosphate-energized vacuolar membrane proton pump	2067.0	16.5	GB	Basil	1
MCVVY(+120.03)DLTDPFGLLTDHK	Q40521 RB11_B_TOBAC	Ras-related protein Rab11B	2299.1	21.9	GB	Basil	1
RRKRY(+120.03)YVELSEVLYNR	P28644 ROC1_SPIOL	ribonucleoprotein, chloroplastic	2263.2	22.6	GB	Basil	1
RY(+120.03)KDEAAPAKRPAEAPK	Q4FP12 RS16_PELUB	ribosomal protein	2017.1	15.8	GB	Basil	1
RKY(+120.03)ADAPAEAPK	O22518 RSSA_SOYBN	ribosomal protein	1435.7	15.7	GB	Basil	1
TPKFLEGSVY(+120.03)ELVEK	Q4FG71 RR3_RANMC	ribosomal protein, chloroplastic	1915.0	19.6	GB	Laurel	1
AEERDKY(+120.03)RKPAEEAPAEAPK	P24929 RK12_TOBAC	ribosomal protein, chloroplastic	2417.2	16.1	GB	Basil	1
VAY(+33.96)PIDLFEEGSVTNLFTSIVGNVFGFK	P48711 RBL_PICAB	RuBisCO	3096.5	23.0	Cl	Nettle	2

GHYNATAATC(+67.92)EEMLKR	Q1KVV0 RBL_TETO	RuBisCO	1974.8	16.2	Cl	Nettle	2
DY(+120.03)MEVHSGTVVGK	P19163 RBL_NEUMU	RuBisCO	1540.7	15.1	GB	Basil	1
EY(+120.03)FDPSGTVVGK	P19163 RBL_NEUMU	RuBisCO	1417.7	15.6	GB	Basil	1
MVENY(+120.03)KY(+120.03)Y(+120.03)DDENVNSKPFMR	P19163 RBL_NEUMU	RuBisCO	2901.2	19.0	GB	Basil	1
MWV(+120.03)VHSGTVVGQLEWR	P19163 RBL_NEUMU	RuBisCO	2067.0	16.5	GB	Basil	1
TY(+120.03)WTKDDENVNSQPETR	P19163 RBL_NEUMU	RuBisCO	2202.0	20.3	GB	Basil	1
WY(+120.03)MVHSGTVVGQLEWR	P19163 RBL_NEUMU	RuBisCO	2067.0	16.5	GB	Basil	2
WY(+120.03)PDHSGTVVGKLEWR	P19163 RBL_NEUMU	RuBisCO	2049.0	16.5	GB	Basil	1
NNAAQSH(+105.04)KWDLAAEGANLLR	P28420 RBL_UNCGR	RuBisCO	2283.1	19.2	HD	Basil	1
LTYTPEY(+33.96)NPKDTDILAAFR	P28438 RBL_PASQU	RuBisCO	2424.1	22.5	Cl	Nettle	1
LTYTPEY(+33.96)ETK	P48706 RBL_LACSA	RuBisCO	1440.6	19.4	Cl	Nettle	2
MAVWTKH(+105.04)WYRSDVWTDGLTLSDR	Q33438 RBL_ERYCG	RuBisCO	2927.4	20.6	HD	Basil	1
AVYY(+120.03)FLTAGREDDKTFDANSQPFMR	P19163 RBL_NEUMU	RuBisCO	3061.4	20.5	GB	Laurel	1
WY(+120.03)Y(+120.03)SGVNVVNSQPFMR	P19163 RBL_NEUMU	RuBisCO	2186.0	20.9	GB	Laurel	1
DEDNVNSQPFY(+33.96)DPK	P19163 RBL_NEUMU	RuBisCO	1700.7	18.9	Cl	Nettle	1
EAAATDAEALY(+33.96)K	P19163 RBL_NEUMU	RuBisCO	1285.6	22.7	Cl	Nettle	1
EEENVNSKPY(+33.96)PR	P19163 RBL_NEUMU	RuBisCO	1494.7	18.6	Cl	Nettle	1
Y(+67.92)TSASGLHAGTVVGK	P19163 RBL_NEUMU	RuBisCO	1514.7	15.7	Cl	Nettle	1
RY(+120.03)MDTDLLAAFR	P48708 RBL_MOROL	RuBisCO	1590.8	21.7	GB	Laurel	1
WY(+120.03)DHTAGAVEEMLKR	Q32303 RBL_GALLU	RuBisCO	1924.9	17.8	GB	Basil	1
Y(+120.03)HLLEQDR	Q33438 RBL_ERYCG	RuBisCO	1192.6	17.0	GB	Basil	1
GYY(+120.03)LADAASKEDLKAR	P21239 RUB1_BRANA	RuBisCO	1889.9	18.6	GB	Laurel	1
KKDCY(+120.03)RLLEELEQK	P34794 RUB2_BRANA	RuBisCO	1914.0	21.5	GB	Basil	1
KVY(+33.96)LSFLAYKFKDYR	P19310 RBS4_LEMGI	RuBisCO	1974.0	19.9	Cl	Nettle	1
H(+105.04)ELSESLKEGK	Q08185 RBS5_MESCR	RuBisCO	1489.7	16.4	HD	Laurel	1
WRWY(+120.03)DVSDDKKDLAR	O98997 RCA_VIGRR	RuBisCO activase	2072.0	19.9	GB	Laurel	1
H(+105.04)WDYMLVQEQQENVK	Q01587 RCA_CUCSA	RuBisCO activase	1922.9	21.4	HD	Basil	1
Y(+120.03)NDEDKKTVDATPK	Q40281 RCA_MALDO	RuBisCO activase	1813.8	17.7	GB	Laurel	1
LY(+33.96)SEAALGDANQDLAK	Q40281 RCA_MALDO	RuBisCO activase	1711.8	19.5	Cl	Nettle	1
CY(+120.03)PEDPTAEGFY LAPAFFDK	Q7X9A0 RCA_1_LARTR	RuBisCO activase	2400.0	21.9	GB	Basil	1
RY(+120.03)Y(+120.03)FLVQEQQERGRK	Q7X9A0 RCA_1_LARTR	RuBisCO activase	2111.0	19.3	GB	Basil	1

Y(+120.03)AQVGKCLVQEQQENVK	Q7X9A0 RCA 1_LARTR	RuBisCO activase	1955.0	20.0	GB	Basil	1
Y(+120.03)TNTDRWNLLEDVSDDQKDLAR	Q7X9A0 RCA 1_LARTR	RuBisCO activase	2786.3	20.9	GB	Basil	1
H(+105.04)GNLEDVSDDKQDLAR	Q7X999 RCA2 _LARTR	RuBisCO activase	1915.9	20.9	HD	Laurel	1
KLVAVY(+33.96)DLSLNENANGLAR	A9P822 METHIONINE K1_POPTR	S-adenosylmethionine	2093.1	19.3	Cl	Nettle	1
TADY(+67.92)RRHKLLSATVK	P09439 LOX2 _SOYBN	Seed linoleate 9S-lipoxygenase-2	1825.9	16.4	Cl	Nettle	1
SSAKVAEY(+120.03)VKAK	Q94C74 GLY M2_ARATH	Serine hydroxymethyltransferase, mitochondrial	1399.7	16.0	GB	Basil	1
LDESTGYIDY(+33.96)DQLEK	P50433 GLY M_SOLTU	Serine hydroxymethyltransferase, mitochondrial	1821.8	18.7	Cl	Nettle	1
CPEAAEKY(+120.03)RKPAEEATVPAPK	Q940H6 SRK2 E_ARATH	Serine/threonine-protein kinase	2417.2	16.1	GB	Basil	1
RDEAAEKY(+120.03)RQPAAEATVPAPK	Q940H6 SRK2 E_ARATH	Serine/threonine-protein kinase	2488.2	16.2	GB	Basil	1
Y(+33.96)NLSLGLGLNK	P84187 SGAT _MAIZE	Serine-glyoxylate aminotransferase	1224.6	18.9	Cl	Nettle	2
H(+105.04)DVYMWVVATANLLEESTPTVDGK	Q9THX6 TL29 _SOLLC	Thylakoid lumenal, chloroplastic	2779.3	22.2	HD	Basil	1
KNQY(+120.03)LEAEWNAK	O20250 TKTC _SPIOL	Transketolase, chloroplastic	1612.8	17.8	GB	Laurel	2
YPRY(+120.03)NWTAGSYK	O20250 TKTC _SPIOL	Transketolase, chloroplastic	1624.7	16.0	GB	Basil	1
KHLNYMAAKSHNY(+33.96)LLLGTGSELELAA K	Q8RWV0 TKT C1_ARATH	Transketolase, chloroplastic	3005.5	20.9	Cl	Nettle	1
SPEAAAEKY(+120.03)RKPAEEATAVPPK	F4IW47 TKTC 2_ARATH	Transketolase, chloroplastic	2530.3	17.2	GB	Basil	1
RY(+120.03)KAKEVHSLCGGK	Q9M4S8 TPIC _FRAAN	Triosephosphate isomerase, chloroplastic	1694.9	18.9	GB	Basil	1

<sup>a</sup> Peptides detected in given number of repetitions (N)

# CHAPTER 7

## SUPPLEMENTARY DATA



## Supporting Information

# **Biomarker profiling in plants to distinguish between exposure to chlorine gas and bleach using LC-HRMS/MS and chemometrics**

## Contents

1.	LC-MS/MS parameters .....	2
2.	Overview of tentatively identified biomarkers .....	3
3.	Machine learning analysis .....	6
4.	LC-MS/MS chromatograms .....	10
5.	NMR spectra.....	14
6.	LC-HRMS/MS isotope ratios .....	20
7.	LC-HRMS/MS mass spectra .....	22
	References.....	23

## 1. LC-MS/MS parameters

Table S 1. Chromatographic and mass spectrometric parameters for plant biomarkers analyzed by LC-MS/MS.

Analyte	Retention time (min)	Precursor ion (m/z)	Product ion (m/z)	Collision energy (eV)	Cone voltage (V)	Chemical structure
Cl-Tyr	6.3	216.2	170.3	15	10	
			135.3	25		
di-Cl-Tyr	6.7	250.1	204.0	15	10	
			169.0	30		
Cl-Phe	6.9	200.0	183.0	10	30	
			165.0			
			153.9			
Cl-Cyt	4.6	146.0	129.0	15	30	
			101.0	15		
			74.0	17		
Cl-Ade	5.9	170.0	133.8	15	30	
			107.0	20		
			80.0	22		
Cl-dopamine	5.7	188.0	171.0	7	30	
			153.0	10		
		171.0	125.0	17		
			89.0	22		
2Cl-dopamine	6.0, 6.7	222.0	205.0	8	30	
			159.0	12		
		205.0	159.0	20		
3Cl-dopamine	6.7	239.0	256.0	239.0	8	
			204.0	204.0	22	
			193.0	193.0	21	

## 2. Overview of tentatively identified biomarkers

Table S 2. Biomarkers tentatively identified by Compound Discover after LC-HRMS/MS analysis of green spire, stinging nettle and feathergrass after chlorine and bleach exposure. Chemicals are sorted by their molecular mass.

#	Name	Formula	Mass (g/mol)
<b>1</b>	AL8225000	C2 H2 Cl N	74.9876
<b>2</b>	Imidazole + Cl*	C3 H3 Cl N2	101.9985
<b>3</b>	H-beta-Chloro-Ala-OH	C3 H6 Cl N O2	123.0085
<b>4</b>	2-pyridone + Cl*	C5 H4 Cl N O	128.9981
<b>5</b>	Valerolactam + Cl*	C5 H8 Cl N O	133.0294
<b>6</b>	Pentanamide + Cl*	C5 H10 Cl N O	135.0451
<b>7</b>	Bis(2-chloroethyl)amine*,†	C4 H9 Cl2 N	141.0110
<b>8</b>	SJ5700000	C6 H6 Cl N O	143.0136
<b>9</b>	2-Amino-5-chlorophenol	C6 H6 Cl N O	143.0138
<b>10</b>	2,4-Diamino-6-chloropyrimidine	C4 H5 Cl N4	144.0203
<b>11</b>	5-chlorocytosine	C4 H4 Cl N3 O	145.0043
<b>12</b>	Histamine + Cl*	C5 H8 Cl N3	145.0404
<b>13</b>	2-Pyrrolidone + 2Cl*	C4 H5 Cl2 N O	152.9748
<b>14</b>	p-Chloroacetophenone	C8 H7 Cl O	154.0183
<b>15</b>	2-Chlorobenzoic acid§	C7 H5 Cl O2	155.9977
<b>16</b>	2,4-Dichlorophenol	C6 H4 Cl2 O	161.9639
<b>17</b>	Valerolactam + 2Cl*	C5 H7 Cl2 N O	166.9904
<b>18</b>	2-Amino-6-chloropurine‡	C5 H4 Cl N5	169.0170
<b>19</b>	N1-(3-chlorophenyl)acetamide§	C8 H8 Cl N O	169.0291
<b>20</b>	NSC 444	C8 H8 Cl N O	169.0292
<b>21</b>	Tyramine + Cl*	C8 H10 Cl N O	171.0449
<b>22</b>	1-Methyl-1,4-dihydronicotinamide + Cl*	C7 H9 Cl N2 O	172.0402
<b>23</b>	2-amino-5-chloro-cis,cis-muconic 6-semialdehyde	C6 H6 Cl N O3	175.0036
<b>24</b>	cloxyquin	C9 H6 Cl N O	179.0137
<b>25</b>	Valine + 2Cl*	C5 H9 Cl2 N O2	185.0009
<b>26</b>	Guanine + Cl*	C5 H4 Cl N5 O	185.0105
<b>27</b>	4-CPA	C8 H7 Cl O3	186.0082
<b>28</b>	Dopamine + Cl*	C8 H10 Cl N O2	187.0398
<b>29</b>	DG6650000§	C7 H4 Cl2 O2	189.9587
<b>30</b>	Acetyl proline + Cl*	C7 H10 Cl N O3	191.0346
<b>31</b>	Guvacine + 2Cl*	C6 H7 Cl2 N O2	194.9854
<b>32</b>	clominorex	C9 H9 Cl N2 O	196.0404
<b>33</b>	Fenclonine	C9 H10 Cl N O2	199.0397
<b>34</b>	Quinoclamine	C10 H6 Cl N O2	207.0086
<b>35</b>	6-Chloro-7-nitroquinoxaline‡,§	C8 H4 Cl N3 O2	208.9992
<b>36</b>	Chlortoluron	C10 H13 Cl N2 O	212.0713
<b>37</b>	4-acetamindobutyric acid + 2Cl*	C6 H9 Cl2 N O3	212.9959
<b>38</b>	Carmustine	C5 H9 Cl2 N3 O2	213.0068

<b>39</b>	3-Chlorotyrosine	C9 H10 Cl N O3	215.0346
<b>40</b>	Dopamine + 2Cl*	C8 H9 Cl2 N O2	221.0009
<b>41</b>	ciproximide	C11 H8 Cl N O2	221.0243
<b>42</b>	4-(4-chlorophenoxy)-3,5-dimethyl-1H-pyrazole	C11 H11 Cl N2 O	222.0527
<b>43</b>	Arecoline + 2Cl*	C8 H11 Cl2 N O2	223.0164
<b>44</b>	seclazone	C10 H8 Cl N O3	225.0192
<b>45</b>	2-Chloro-N-(2,6-diethylphenyl)acetamide	C12 H16 Cl N O	225.0915
<b>46</b>	1-(3-Chloro-2-fluorophenyl)-3-(dimethylamino)prop-2-en-1-one	C11 H11 Cl F N O	227.0478
<b>47</b>	2-(2-chlorophenyl)-1H-indole <sup>†,‡</sup>	C14 H10 Cl N	227.6910
<b>48</b>	5-chloro-3-phenylbenzo[c]isoxazole	C13 H8 Cl N O	229.0262
<b>49</b>	Levodopa + Cl*	C9 H10 Cl N O4	231.0295
<b>50</b>	Ethychlorzate	C11 H11 Cl N2 O2	238.0507
<b>51</b>	6-Chlorotryptophan <sup>§</sup>	C11 H11 Cl N2 O2	238.0508
<b>52</b>	bupropion	C13 H18 Cl N O	239.1088
<b>53</b>	2,4-DB <sup>§</sup>	C10 H10 Cl2 O3	248.0005
<b>54</b>	Val-Pro + Cl*	C10 H17 Cl N2 O3	248.0925
<b>55</b>	3,5-Dichlorotyrosine	C9 H9 Cl2 N O3	248.9957
<b>56</b>	Dopamine + 3Cl*	C8 H8 Cl3 N O2	254.9618
<b>57</b>	Lamotrigine	C9 H7 Cl2 N5	255.0062
<b>58</b>	Arecoline + 3Cl*	C8 H10 Cl3 N O2	256.9773
<b>59</b>	Traumatic Acid + Cl*	C12 H19 Cl O4	262.0968
<b>60</b>	Leu-Pro + Cl*	C11 H19 Cl N2 O3	262.1082
<b>61</b>	Moclobemide <sup>§</sup>	C13 H17 Cl N2 O2	268.0978
<b>62</b>	1-Hydroperoxy-L-tryptophan + Cl*	C11 H11 Cl N2 O4	270.0406
<b>63</b>	Medazepam	C16 H15 Cl N2	270.0888
<b>64</b>	Bupranolol	C14 H22 Cl N O2	271.1342
<b>65</b>	N2-(4-chlorophenyl)thiophene-2-carboxamide	C11 H8 Cl N O S	274.9519
<b>66</b>	N'-{6-[(5-chloro-3-pyridyl)oxy]-3-pyridyl}-N,N-dimethyliminoformamide	C13 H13 Cl N4 O	276.0815
<b>67</b>	Dibutyl malate + Cl*	C12 H21 Cl O5	280.1075
<b>68</b>	AE1300200	C14 H16 Cl N O3	281.0815
<b>69</b>	Val-Phe + Cl*	C14 H19 Cl N2 O3	298.1082
<b>70</b>	3-(3,4-dichlorobenzyl)-4H-1-benzothiin-4-one <sup>§</sup>	C16 H10 Cl2 O S	319.9826
<b>71</b>	2-chloro-1,3,8-trihydroxy-6-(hydroxymethyl)-9,10-dihydroanthracene-9,10-dione	C15 H9 Cl O6	320.0083
<b>72</b>	12-oxo-phytodienoic acid + Cl*	C18 H27 Cl O3	326.1644
<b>73</b>	A-12(13)-EpODE + Cl*	C18 H29 Cl O3	328.1801
<b>74</b>	2-[(2-chlorobenzyl)sulfanyl]-4,6-dimethylnicotinonitrile	C15 H13 Cl N2 S	343.0264
<b>75</b>	13(S)-HpOTrE + Cl*	C18 H29 Cl O4	344.1749
<b>76</b>	4-{3-[(5-chloro-1,3-benzothiazol-2-yl)oxy]phenyl}morpholine	C17 H15 Cl N2 O2 S	346.0506
<b>77</b>	1-[3-(3,4-dichlorophenoxy)-2-hydroxypropyl]piperidine-4-carboxamide	C15 H20 Cl2 N2 O3	346.0870
<b>78</b>	Val-Trp + 2Cl*	C14 H18 Cl2 N2 O4	348.0638

<b>79</b>	doxefazepam	C17 H14 Cl F N2 O3	348.0663
<b>80</b>	N5-[2-(4-chlorophenyl)-2-oxoethyl]-1-ethyl-3-methyl-4-nitro-1H-pyrazole-5-carboxamide†	C15 H15 Cl N4 O4	350.0784
<b>81</b>	(Z)-4-Chloro-N-(3-ethoxy-1-hydroxy-3-oxopropylidene)tryptophan	C16 H17 Cl N2 O5	352.0829
<b>82</b>	9,12,13-Trihydroxy-10,15-octadecadienoic acid + Cl*	C18 H31 Cl O5	362.1854
<b>83</b>	N1-(1-benzyl-4-piperidyl)-4-chlorobenzene-1-sulfonamide	C18 H21 Cl N2 O2 S	364.0974
<b>84</b>	Metolazone§	C16 H16 Cl N3 O3 S	365.0589
<b>85</b>	(4-chlorophenyl)[4,6-dimethyl-3-(1H-pyrrol-1-yl)thieno[2,3-b]pyridin-2-yl]methanone	C20 H15 Cl N2 O S	366.0582
<b>86</b>	4-{5-[(3S)-1-(4-Chlorobenzyl)-3-pyrrolidinyl]-1,3,4-oxadiazol-2-yl}-N,N-dimethylaniline‡	C21 H23 Cl N4 O	382.1514
<b>87</b>	Dibutyl sebacate + 2Cl*	C18 H32 Cl2 O4	382.1671
<b>88</b>	13S-hydroxyoctadecadienoic acid + 3Cl*	C18 H29 Cl3 O3	398.1175
<b>89</b>	Pinellic acid + 2Cl*	C18 H32 Cl2 O5	398.1620
<b>90</b>	N-{6-[(7-chloro-4-quinazolinyl)oxy]-3-pyridinyl}-4-methoxybenzamide	C21 H15 Cl N4 O3	406.0879
<b>91</b>	N2-({(1S,3S,4R,5R)-3-[(3-chloro-4-fluorobenzoyl)amino]-1,4,5-trihydroxycyclohexyl}carbonyl)-D-leucinamide†	C20 H27 Cl F N3 O6	419.1644
<b>92</b>	Phloionolic acid + 3Cl*	C18 H33 Cl3 O5	434.1387
<b>93</b>	(1S,2R,3S,5S,6S,16E,18E,20R,21S)-11-Chloro-21-hydroxy-12,20-dimethoxy-2,5,16-trimethyl-8,23-dioxo-4,24-dioxa-9,22-diazatetracyclo[19.3.1.1~10,14~0~3,5~]hexacosa-10(26),11,13,16,18-pentaen-6-yl 2-methylpropanoate	C31 H41 Cl N2 O9	620.2500

\*Chemicals are also identified in unchlorinated form in the blank vegetation samples.

†Chemicals are not present in all plant species

‡Chemical is only detected in bleach samples

§Chemical is only detected in chlorinated samples

### 3. Machine learning analysis

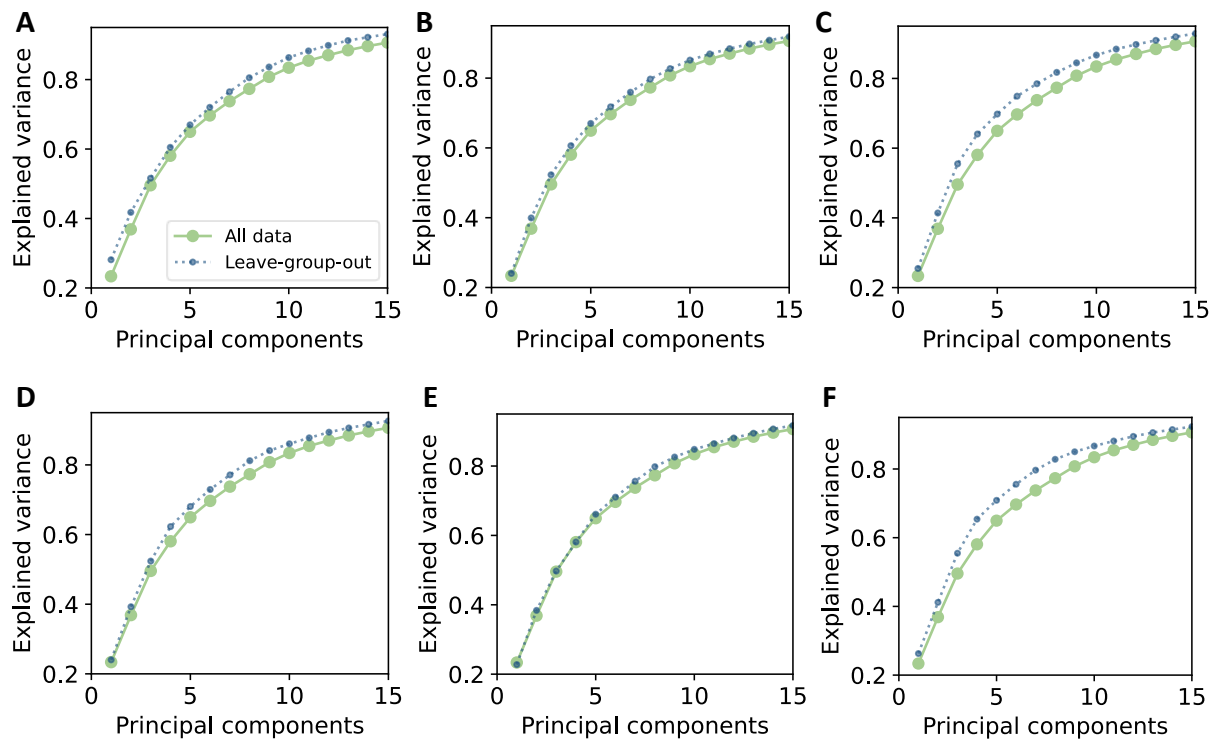


Figure S 1. Explained variance of PCA with effect of leave-one-group-out validation on PCA robustness. Green line: PCA including all samples; blue dashed lines: PCAs with one type of exposure left out: without A) short, B) long, and C) high chlorine exposure, and without D) household, E) pool, and F) concentrated bleach exposure.

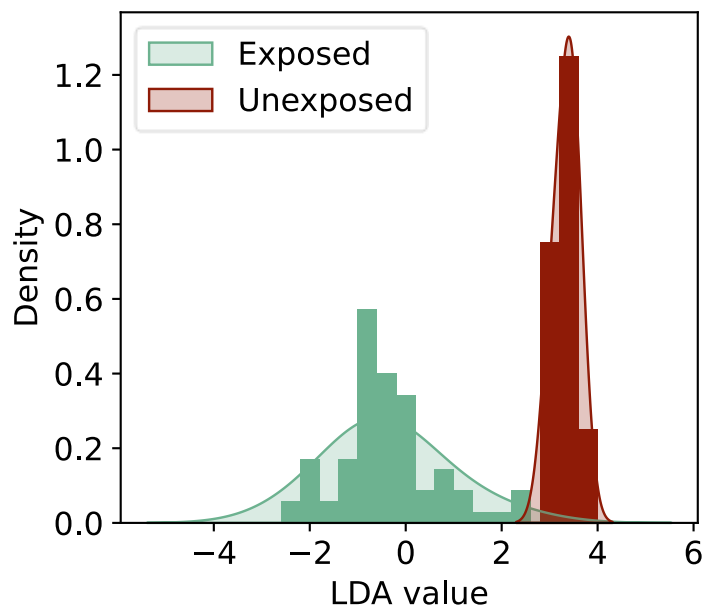


Figure S 2. LDA-score plot for classification of plants exposed to chlorine gas or bleach and unexposed plants ( $n = 12-38$ ). Corresponding LDA scores for the first and second discriminant function are shown. The bars represent the frequency of the individual measurements for a given LDA value adding up to 1. The shaded curve is the kernel density estimation with a bandwidth of 1. Ten principal components (accounting for 97% of the variation) were used to build the LDA model.

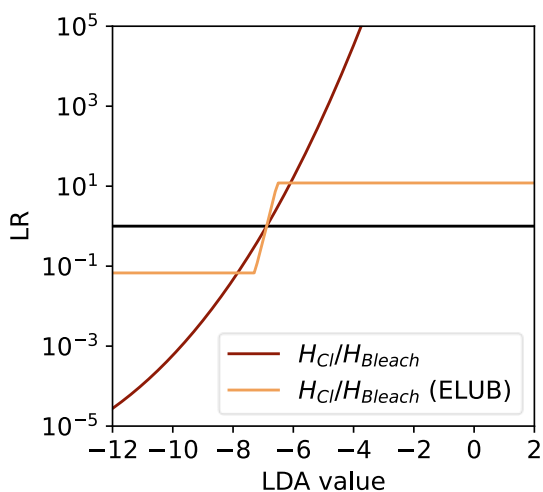


Figure S 3. LDA value to likelihood ratio (LR) plot with and without artificially reducing the empirical upper and lower bound (ELUB) of the LR values. ELUB values are  $6.8 \times 10^{-2}$  to 12. Figure corresponds to Figure 4 of the manuscript.

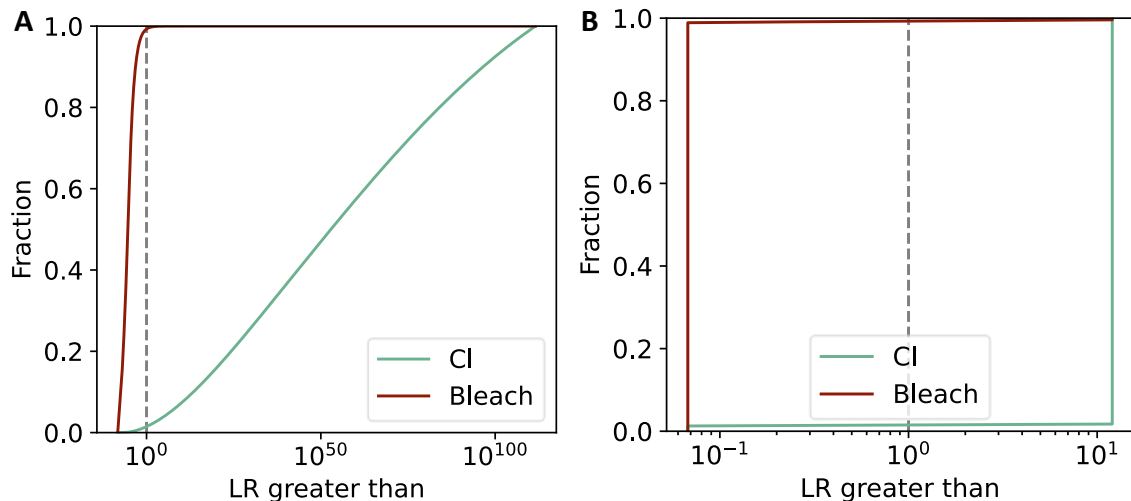


Figure S 4. Tippett plots showing the cumulative likelihood ratio (LR) distributions calculated with LDA for chlorine and bleach exposed samples, measured by LC-HRMS/MS. A) Without correction. B) With ELUB correction. The dashed lines show  $LR = 1$ .

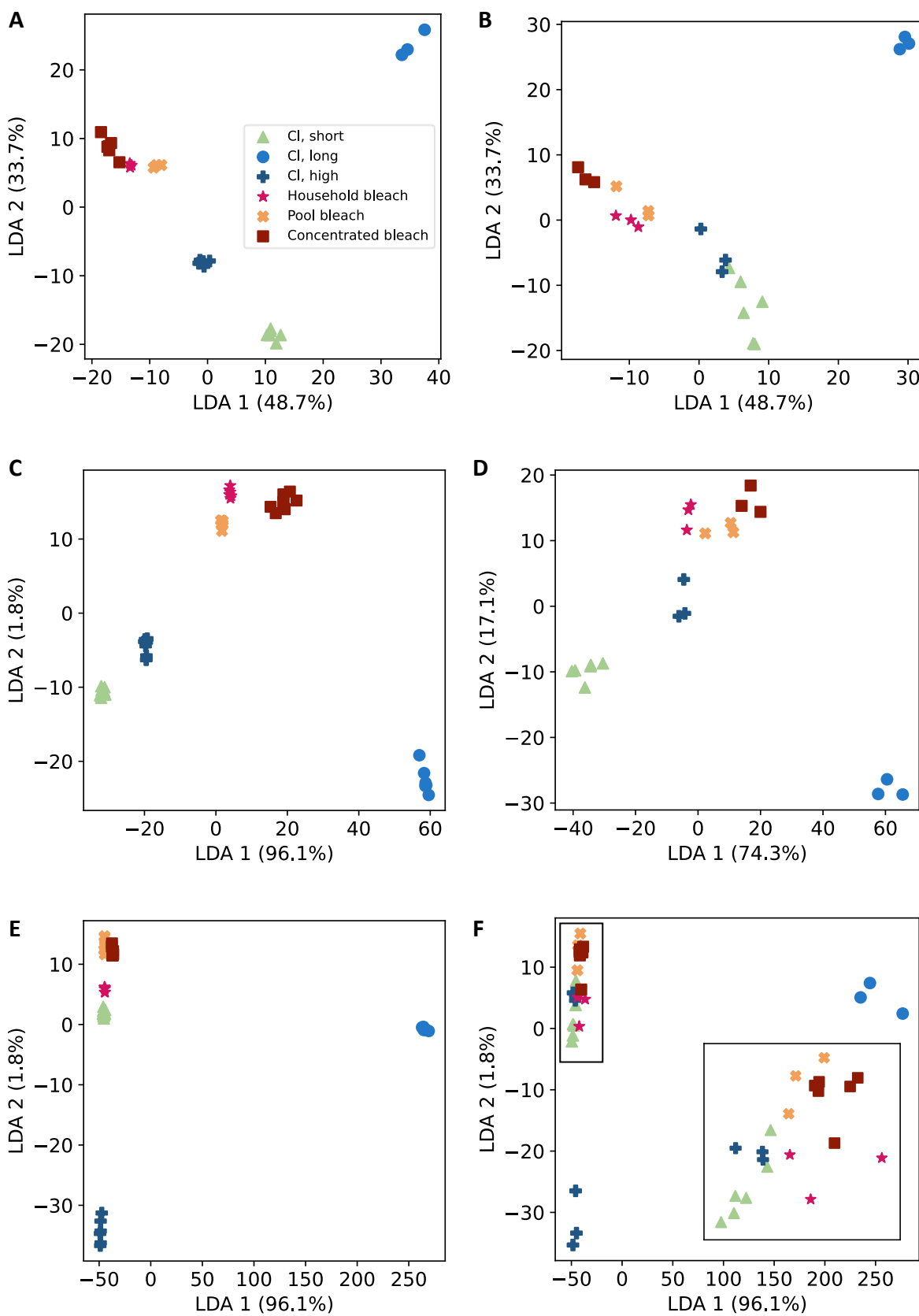


Figure S 5. LDA-score plot for classification of plants exposed to low, mid, or high chlorine gas and household, pool, or concentrated bleach ( $n=9-18$ ). Corresponding LDA scores for the first and second discriminant function are shown. A-C) Training sets, D) test set Euonymus, E) test set grass, F) test set nettle.

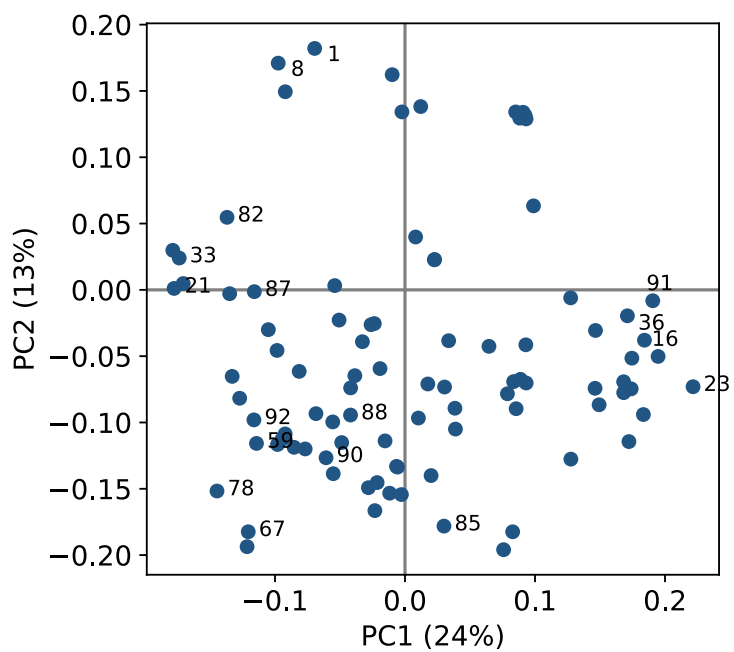


Figure S 6. PCA-loading plot. PC1 represents 23% of the total variance and PC2 accounts for 14% of the variance. Some of the most discriminating compounds are highlighted. 1. Medazepam; 8. 4-(4-chlorophenoxy)-3,5-dimethyl-1H-pyrazole; 16. 2-Chlor-N-(2,6-dimethylphenyl)-N-(2-oxotetrahydro-3-furanyl)acetamid; 21. 2-Chlorobenzoic acid; 23. Valine + 2Cl; 33. 6-Chlorotryptophan; 34. Chlortoluron; 36. Carmustine; 59. 5-chlorocytosine; 67. 2,4-Dichlorophenol; 78. 1-Hydroperoxy-L-tryptophan + Cl; 82. Dopamine + 2Cl; 85. Fenclonine; 87. Dopamine + 3Cl; 88. Dopamine + Cl; 90. 3-Chlorotyrosine; 92. 3,5-Dichlorotyrosine.

#### 4. LC-MS/MS chromatograms

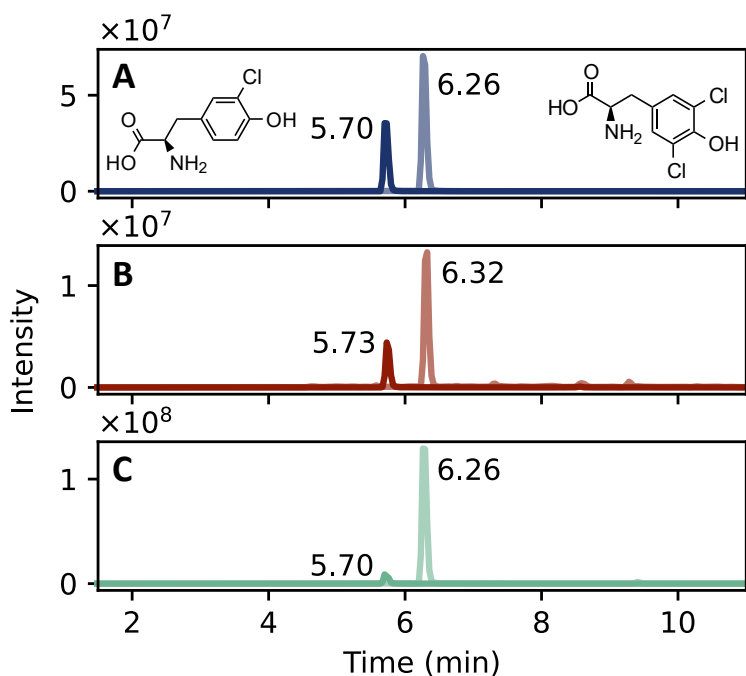


Figure S 7. Extracted ion chromatograms of 3-chlorotyrosine (Cl-Tyr,  $t_R = 5.70$  min,  $m/z 216.2 \rightarrow 170.3$ ) and 3,5-dichlorotyrosine (di-Cl-Tyr,  $t_R = 6.26$  min,  $m/z 250.1 \rightarrow 204.0$ ). A) Commercially available reference standard, B) Nettle exposed to concentrated bleach, C) Nettle exposed to a high concentration chlorine.

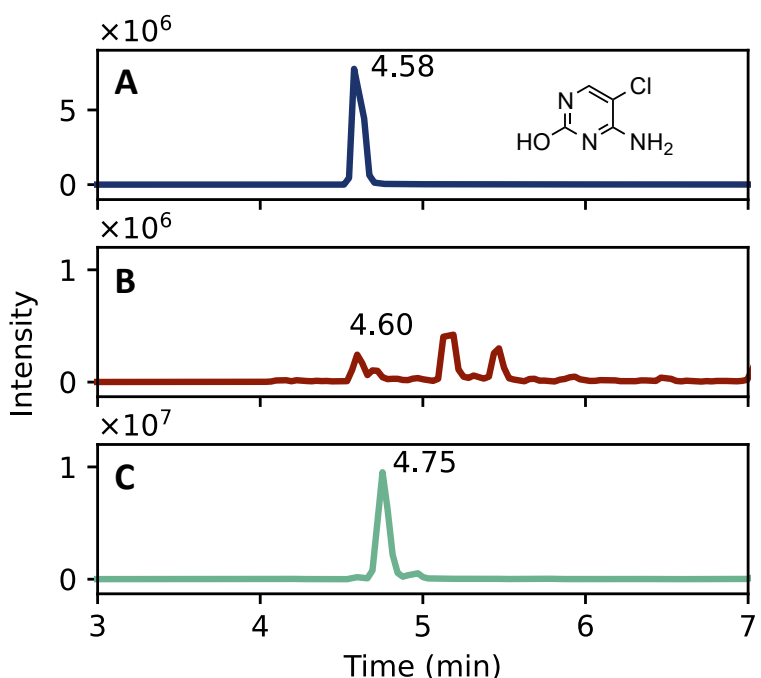


Figure S 8. Extracted ion chromatograms ( $m/z 146.0 \rightarrow 129.0$ ) of 5-chlorocytosine (Cl-Cyt) with  $t_R=4.58$  min. A) Commercially available reference standard, B) Nettle exposed to concentrated bleach, C) Nettle exposed to a high concentration chlorine.

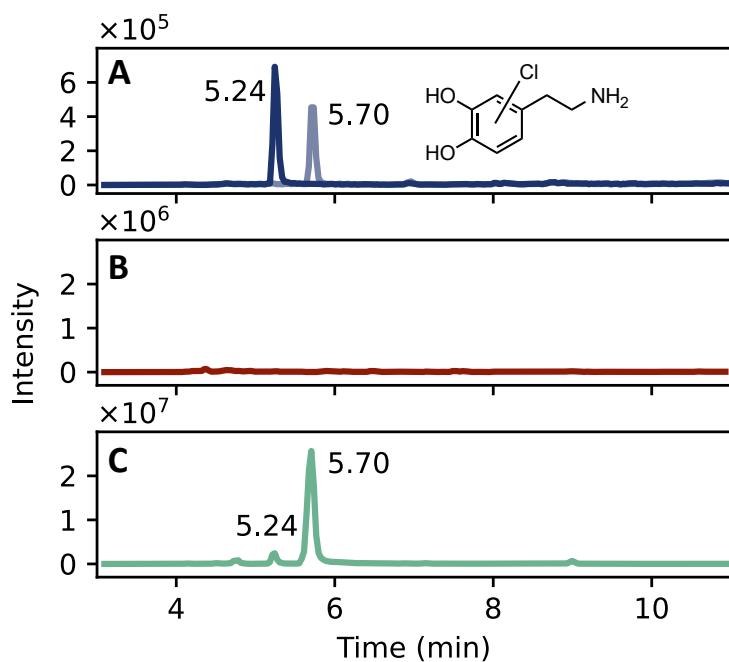


Figure S 9. Extracted ion chromatograms ( $m/z$  188.0 → 171.0) of chlorodopamine (Cl-dopamine) with  $t_R=5.24$  and 5.70 min. A) Synthetic reference standard, B) Nettle exposed to concentrated bleach, C) Nettle exposed to a high concentration chlorine.

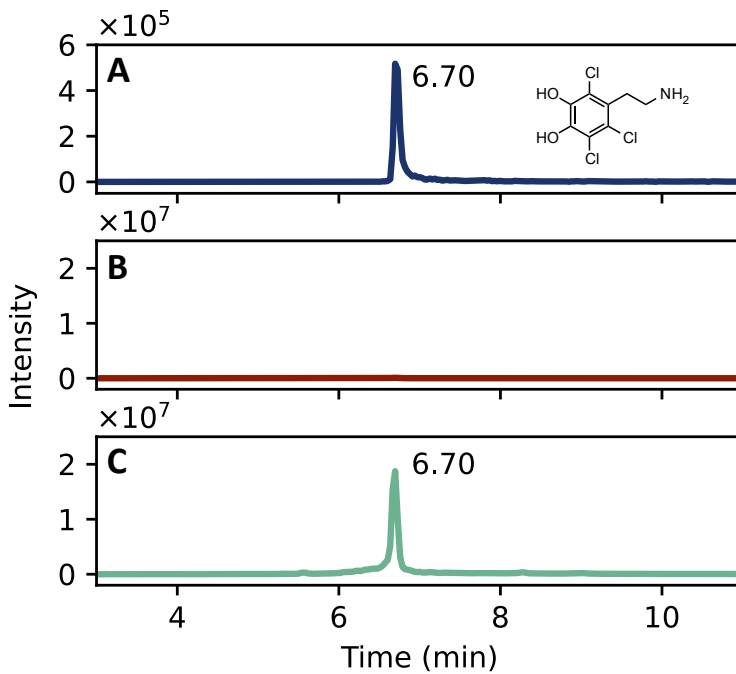


Figure S 10. Extracted ion chromatograms ( $m/z$  239.0 → 204.0) of trichlorodopamine (tri-Cl-dopamine) with  $t_R=6.70$  min. A) Synthetic reference standard, B) Nettle exposed to concentrated bleach, C) Nettle exposed to a high concentration chlorine.

#### 4.1. Stability

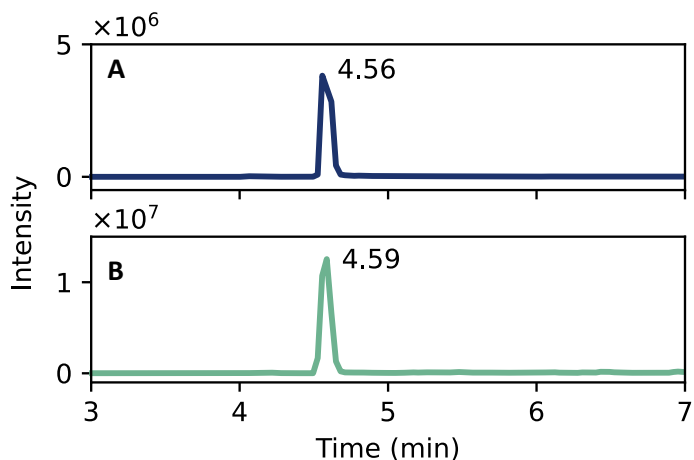


Figure S 11. Extracted ion chromatograms ( $m/z$  146.0 → 129.0) of 5-chlorocytosine (Cl-Cyt) with  $t_R=4.56$  min. A) Commercially available reference standard, B) Nettle, three months after exposure to a high concentration chlorine.

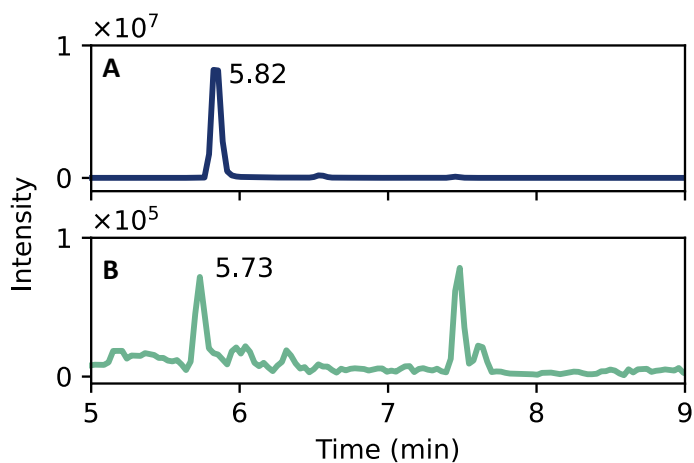


Figure S 12. Extracted ion chromatograms ( $m/z$  170.0 → 107.0) of 2-amino-6-chloropurine (Cl-Ade) at  $t_R=5.82$  min. A) Commercially available reference standard, B) Nettle, three months after exposure to a high concentration chlorine.

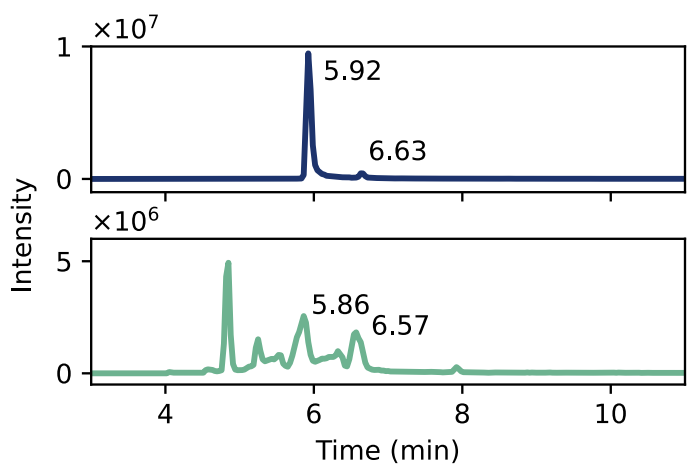


Figure S 13. Extracted ion chromatograms ( $m/z$  222.0 → 205.0) of dichlorodopamine (di-Cl-dopamine) at  $t_R=5.92$  and 6.63 min. A) Synthetic reference standard, B) Nettle, three months after exposure to a high concentration chlorine.

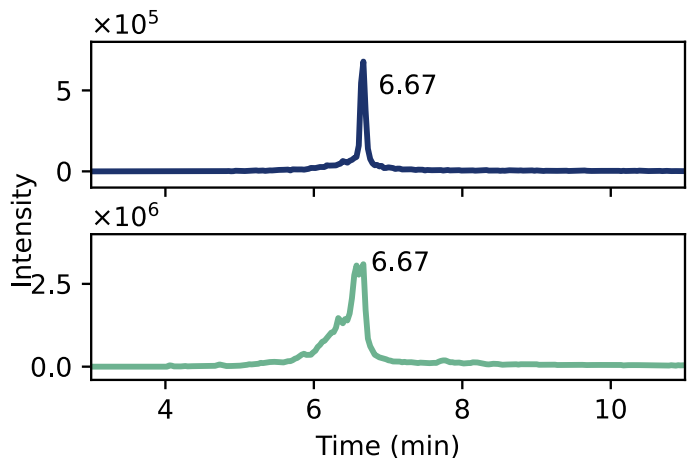


Figure S 14. Extracted ion chromatograms ( $m/z$  239.0 → 204.0) of trichlorodopamine (tri-Cl-dopamine) with  $t_R=6.70$  min. A) Synthetic reference standard, B) Nettle, three months after exposure to a high concentration chlorine.

## 5. NMR spectra

<sup>1</sup>H-NMR spectra were recorded on a Bruker Avance III spectrometer operating at 400 MHz. A concentration of approximately 1 mg/mL was analysed. DMSO-d<sub>6</sub> was used as a solvent (2.5 ppm) and some water was present in the sample (4-3 ppm).

The figures below show the measured NMR spectrum of dopamine, Cl-dopamine, di-Cl-dopamine, and tri-Cl-dopamine. Together with the measured spectrum, the predicted spectrum is also presented. The peaks within a chemical shift of 6 and 7 originate from the aromatic part of the chemical. Two doublets and one doublet of doublets were visible in dopamine, corresponding to three protons in total. After chlorination the number of peaks reduced to two (Cl-dopamine), one (2Cl-dopamine) or zero (3Cl-dopamine) singlets. The responses from the aliphatic part of the chemical were visible around 3 ppm and the peaks around 9 ppm originate from the alcohols. The amine is known to give a broader, but less intense peak that exhibits shifts in the spectrum [1]. Therefore, the peak between 7 and 8 ppm most likely corresponds to the amine. In every spectrum three impurity peaks are visible around 7 ppm. This presumably originates from 3-methoxytyramine [2], a metabolic product of dopamine.

The chemical shifts and ratios of the measured spectra of unchlorinated, mono-, di-, and tri-chlorinated dopamine correspond well to the predicted NMR spectra (Mnova 14.3.3., Mestrelab Research) and published spectra [3–5]. Only, for Cl-dopamine the predicted spectrum was not shown, since it was different compared to the NMR spectrum presented by Garcia-Fernandez et al. [4]. In literature, the isomer 4-(2-aminoethyl)-5-chloro-1,2-benzenediol showed two singlets in the aromatic region, while the other isomers show ortho or meta coupling for the substituted benzene ring [3]. In this study, also two singlets were visible, so Cl-dopamine was most likely identified as 4-(2-aminoethyl)-5-chloro-1,2-benzenediol. Both purified peaks in the LC-MS chromatogram provided a similar NMR spectrum without ortho or meta coupling, so it was not possible to identify the various isomers. Therefore, an unspecific representation of the isomers was provided in this study and future research is needed to unravel the exact structure of the chlorinated dopamines.

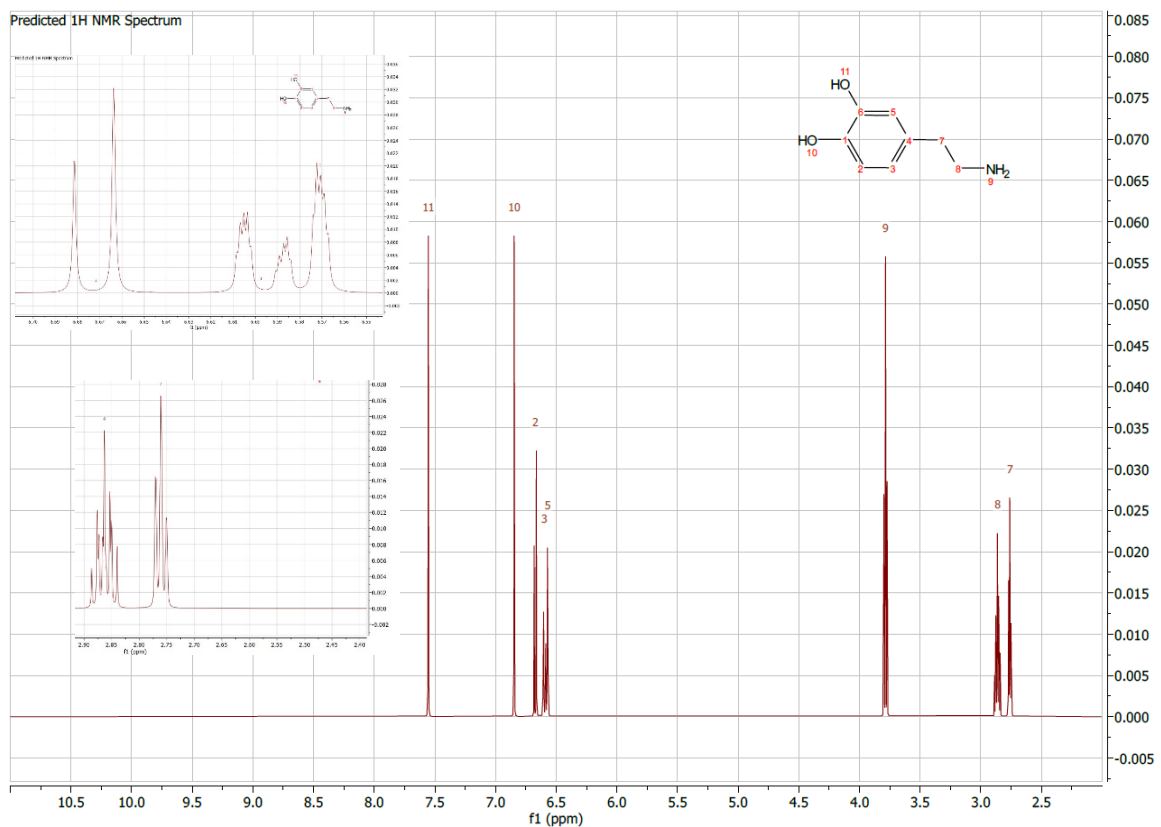
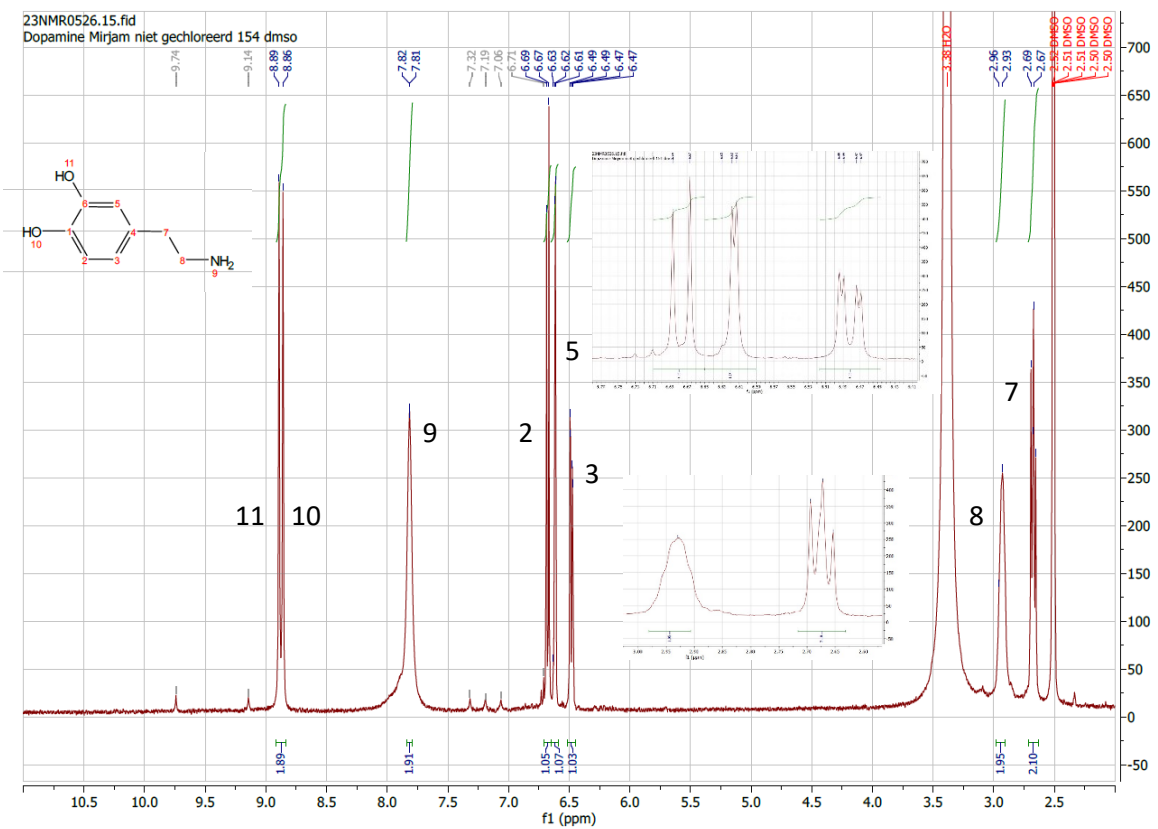


Figure S 15. NMR spectrum of dopamine. A) Measured NMR spectrum. B) Predicted NMR spectrum.

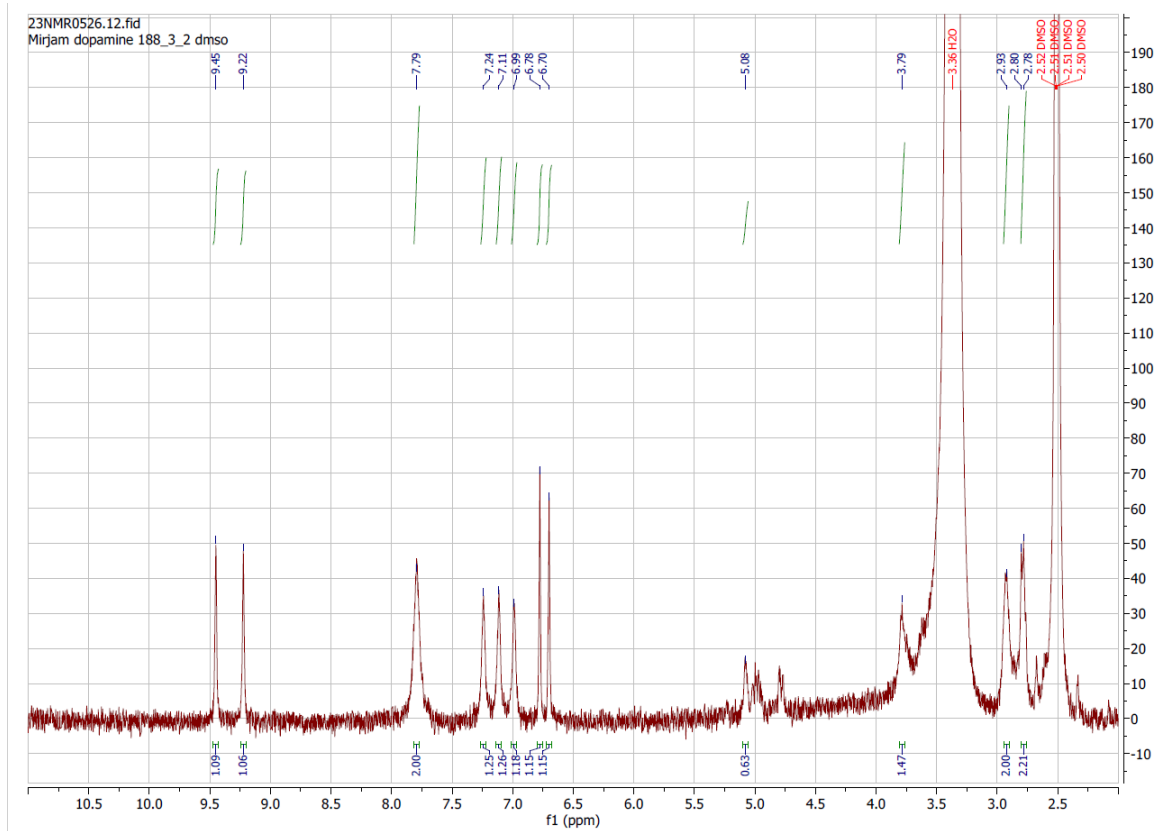


Figure S 16. Measured NMR spectrum of Cl-dopamine (corresponds to LC-MS/MS  $t_R$ : 5.70).

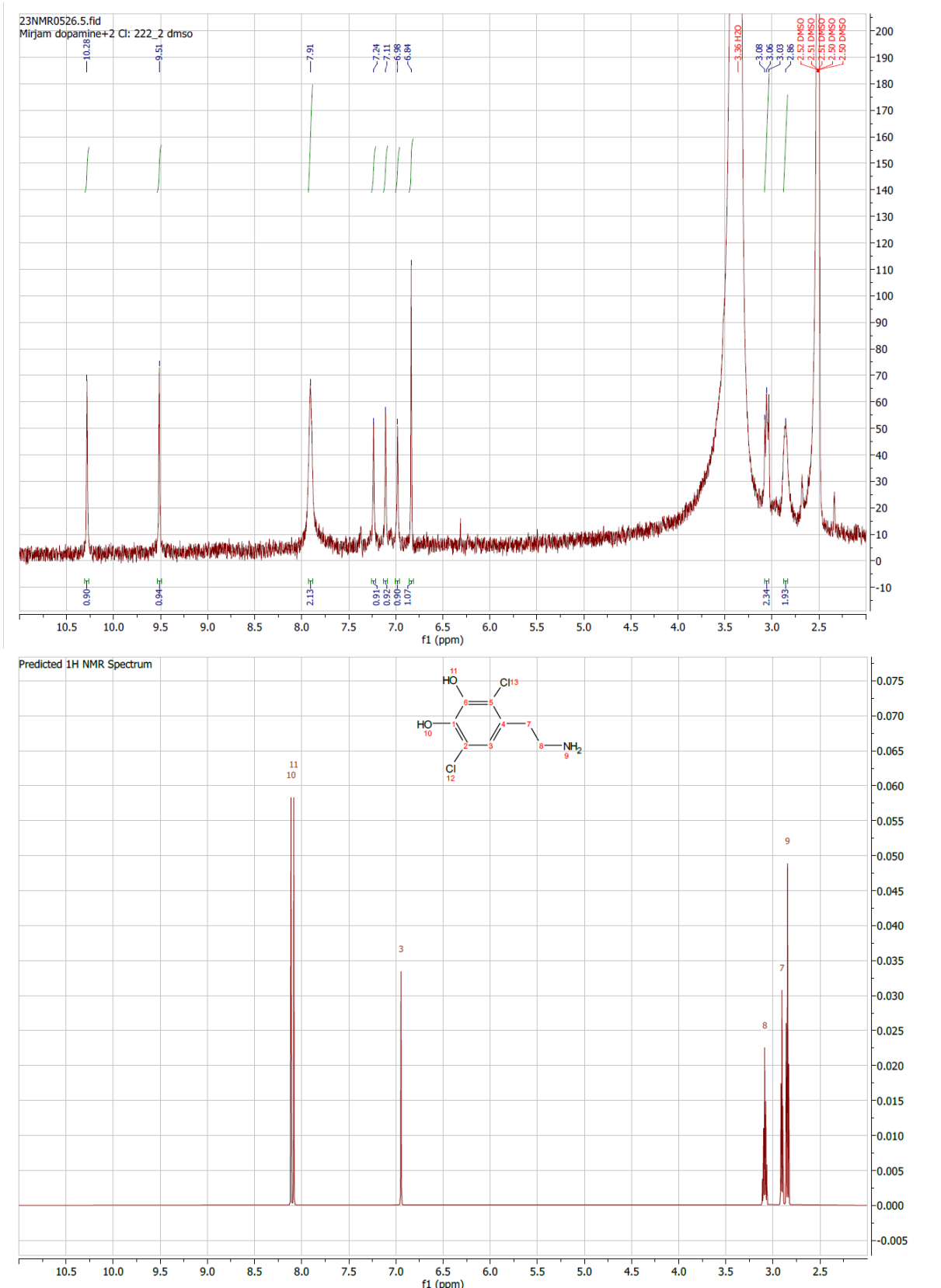


Figure S 17. NMR spectrum of di-Cl-dopamine (corresponds to LC-MS/MS  $t_R$ : 5.96). A) Measured NMR spectrum. B) Predicted NMR spectrum.

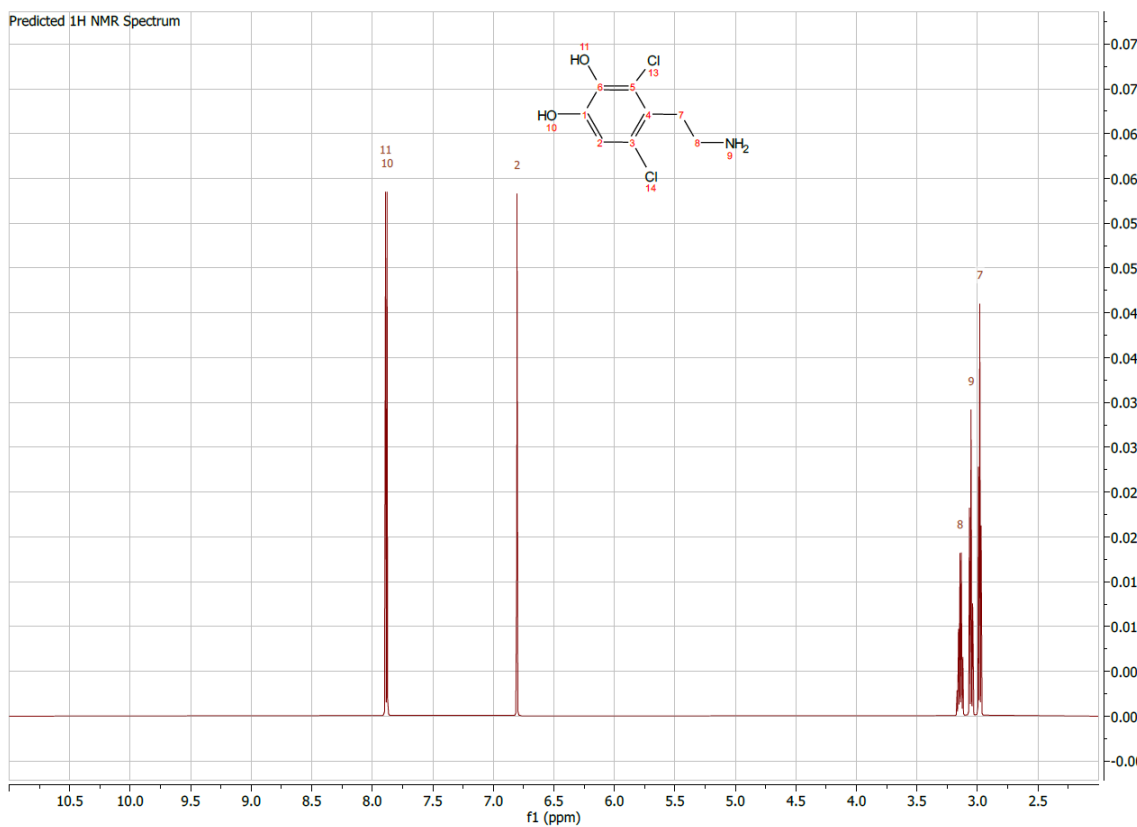
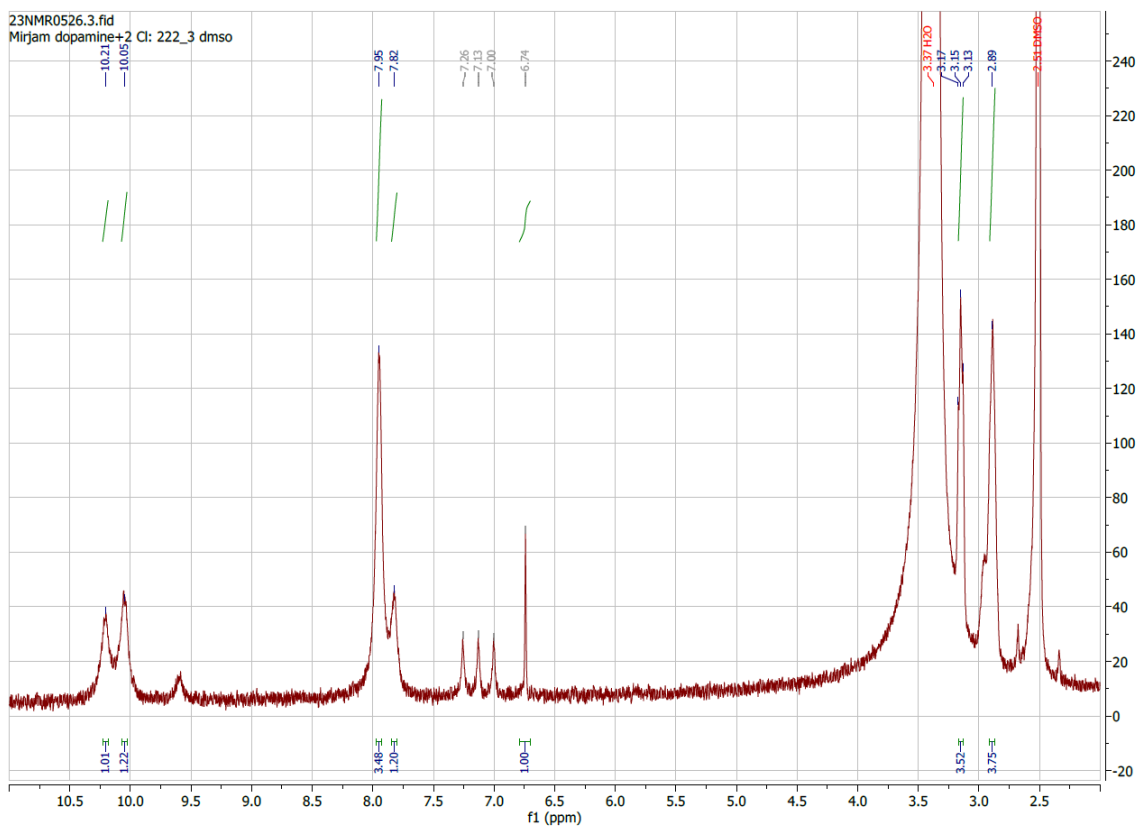


Figure S 18. NMR spectrum of di-Cl-dopamine (corresponds to LC-MS/MS  $t_R$ : 6.66). A) Measured NMR spectrum. B) Predicted NMR spectrum.

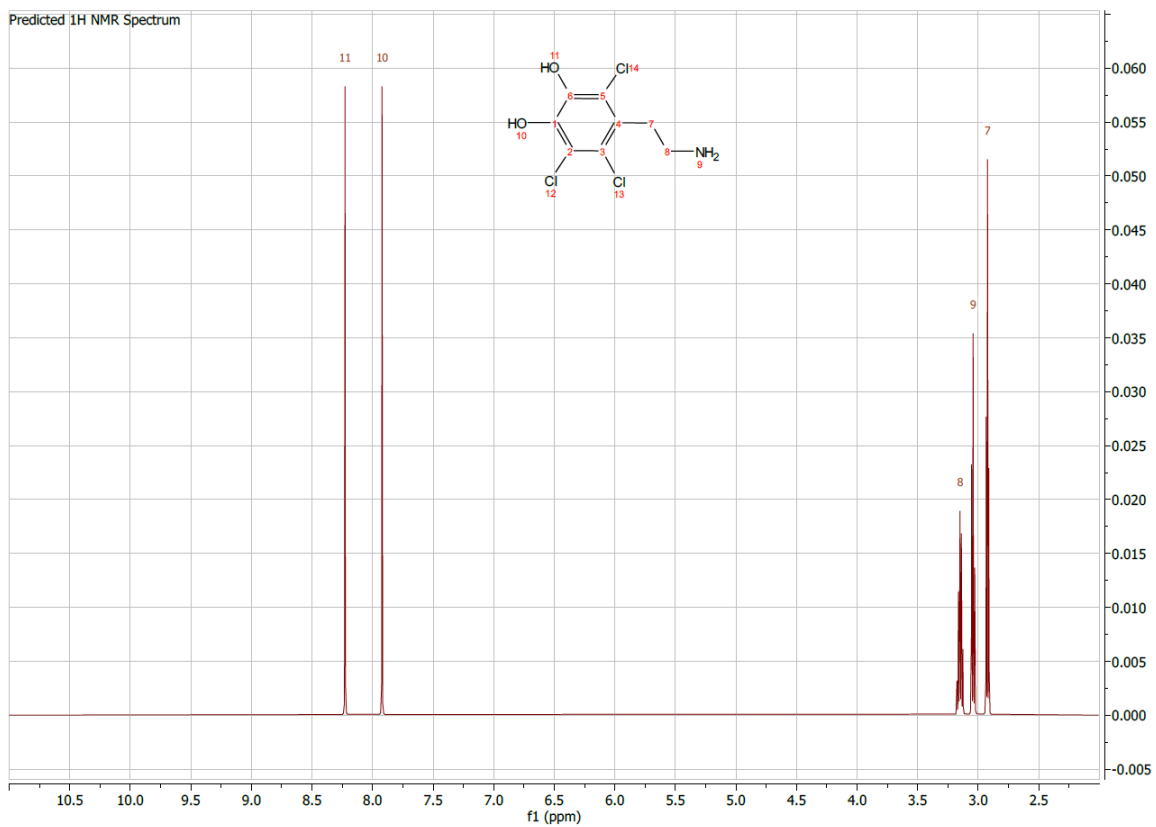
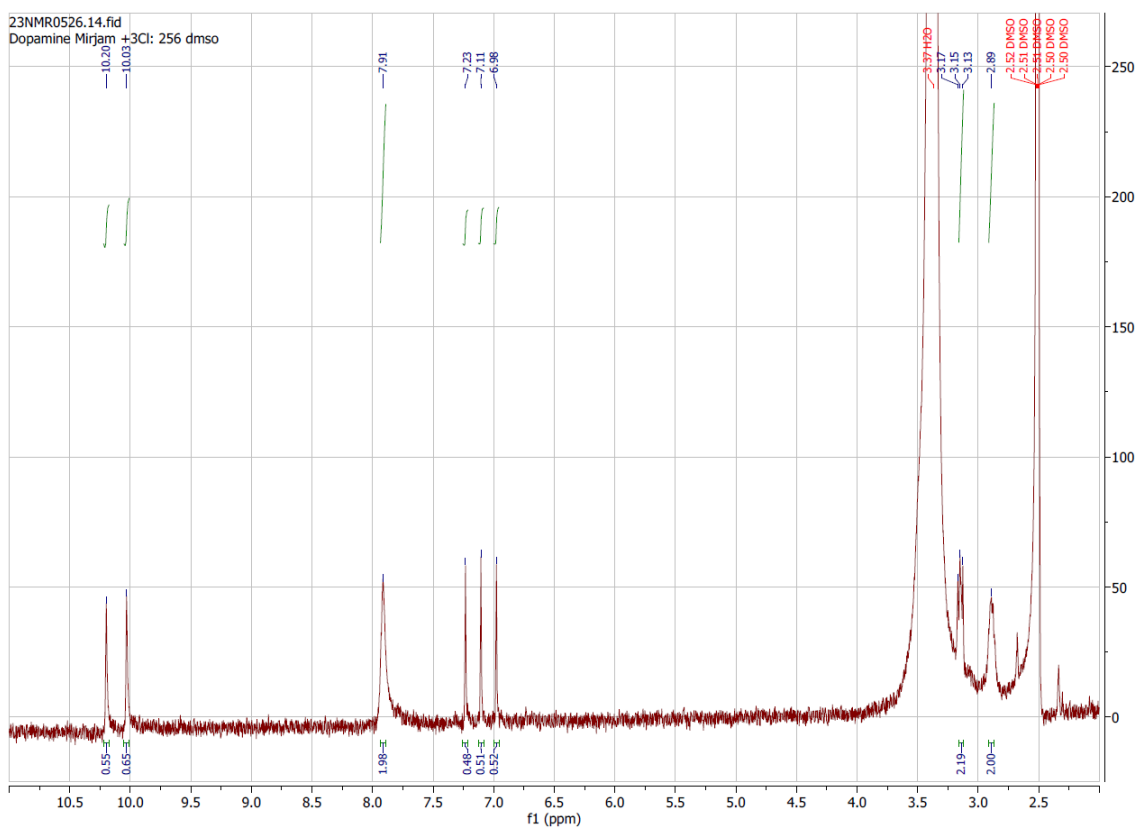


Figure S 19. NMR spectrum of tri-Cl-dopamine (corresponds to LC-MS/MS  $t_R$ : 6.7). A) Measured NMR spectrum. B) Predicted NMR spectrum.

## 6. LC-HRMS/MS isotope ratios

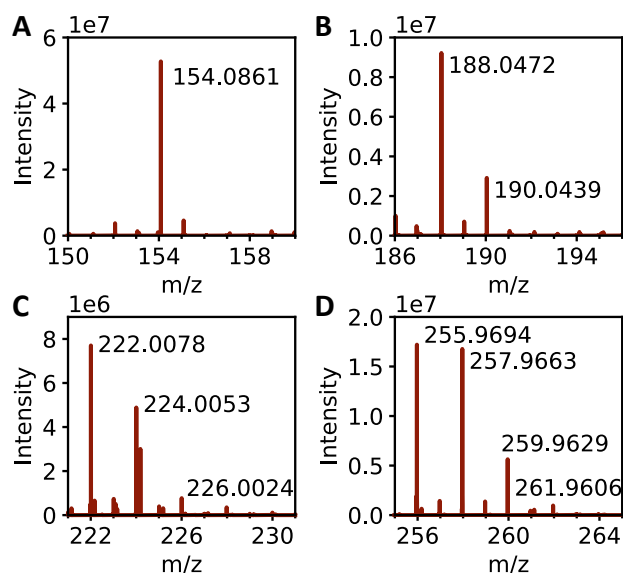


Figure S 20. Full scan MS spectrum analyzed by LC-HRMS/MS of single charged chlorinated dopamine showing the chlorine isotope pattern. A) Dopamine, B) Single chlorination of dopamine with an isotope ratio of 3:1, C) Double chlorination of dopamine with an isotope ratio of 9:6:1, and D) Triple chlorination with an isotope ratio of 27:26:9:1.

Because the  $^{35}\text{Cl}$  isotope has a natural occurrence of 76% and the  $^{37}\text{Cl}$  isotope of 24%, the isotope ratio for the chlorinated compound can be calculated. The isotope value for mono-, di- and tri-chlorinated dopamine is measured including the effect of other isotopes such as  $^{13}\text{C}$ .[6] In Table S3 the theoretical isotope value is compared to the measured isotopes values in the synthetic reference standard and nettle plants exposed to chlorine gas.

Table S 3. Comparison of theoretical versus experimentally observed isotope values in full scan MS spectrum as obtained with LC-HRMS/MS for chlorinated dopamine.

Chlorination	Theoretical isotope value	Measured isotope value in synthetic reference standard	Measured isotope value in nettle
0	1	1	1
1	3:1	3:1	3:1
2	9:6:1	9:6:1	9:6:1
3	27:27:9:1	27:26:9:2	27:27:9:3

Table S 4. Theoretical versus measured monoisotopic mass of chlorinated dopamine isotopes in full scan MS spectrum as obtained with LC-HRMS/MS.

Cl	Isotope	Theoretical monoisotopic mass	Measured monoisotopic mass in synthetic reference standard	Mass error (ppm)	Measured monoisotopic mass in nettle plant	Mass error (ppm)
0	[M+H] <sup>+</sup>	154.0868	154.0861	5	154.0862	4
1	[M+H+35Cl-H] <sup>+</sup>	188.0478	188.0472	3	188.0469	5
1	[M+H+37Cl-H] <sup>+</sup>	190.0449	190.0439	5	190.0442	4
2	[M+H+2*35Cl-2H] <sup>+</sup>	222.0089	222.0078	5	222.0083	2.7
2	[M+H+35Cl+37Cl-2H] <sup>+</sup>	224.0059	224.0053	2.7	224.0050	4
2	[M+H+2*37Cl-2H] <sup>+</sup>	226.0030	226.0024	2.7	226.0022	4
3	[M+H+3*35Cl-2H] <sup>+</sup>	255.9699	255.9694	2.0	255.9695	1.6
3	[M+H+2*35Cl+37Cl-3H] <sup>+</sup>	257.9669	257.9663	2.3	257.9664	1.9
3	[M+H+35Cl+2*37Cl-3H] <sup>+</sup>	259.9640	259.9629	4	259.9639	0.4
3	[M+H+3*37Cl-2H] <sup>+</sup>	261.9610	261.9606	1.5	261.9606	1.5

## 7. LC-HRMS/MS mass spectra

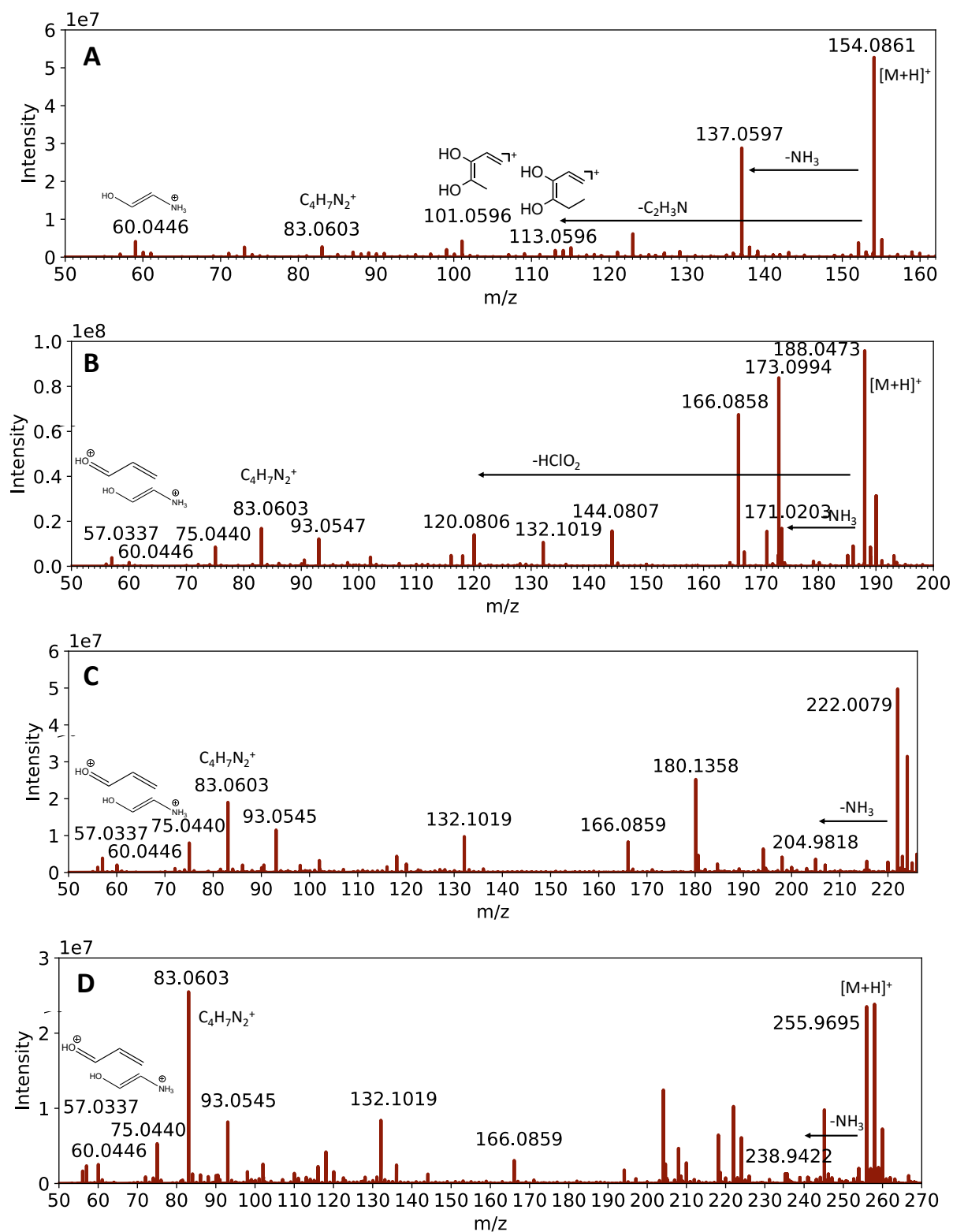


Figure S 21. HRMS/MS spectrum of nettle exposed to chlorine gas with fragmentation pattern of A) Dopamine ( $m/z$  154.0861), B) Cl-dopamine ( $m/z$  188.0472), C) di-Cl-dopamine ( $m/z$  222.0084), and D) tri-Cl-dopamine ( $m/z$  255.9694).

## References

- [1] J. Clayden, N. Greeves, S. Warren, Organic Chemistry, 2nd ed., 2012.  
[www.oxfordtextbooks.co.uk/orc/clayden2e/](http://www.oxfordtextbooks.co.uk/orc/clayden2e/).
- [2] Biological Magnetic Resonance Data Bank, 3-Methoxytyramine (C9H13NO2), n.d.  
[https://bmrb.io/metabolomics/mol\\_summary/show\\_data.php?id=bmse000958](https://bmrb.io/metabolomics/mol_summary/show_data.php?id=bmse000958) (accessed November 15, 2023).
- [3] J.J. Maresh, A.A. Ralko, T.E. Speltz, J.L. Burke, C.M. Murphy, Z. Gaskell, J.K. Girel, E. Terranova, C. Richtscheidt, M. Krzeszowiec, Chemoselective zinc/HCl reduction of halogenated  $\beta$ -nitrostyrenes: Synthesis of halogenated dopamine analogues, *Synlett* 25 (2014) 2891–2894.  
<https://doi.org/10.1055/s-0034-1379481>.
- [4] L. García-Fernández, J. Cui, C. Serrano, Z. Shafiq, R.A. Gropeanu, V.S. Miguel, J.I. Ramos, M. Wang, G.K. Auernhammer, S. Ritz, A.A. Golriz, R. Berger, M. Wagner, A. Del Campo, Antibacterial strategies from the sea: Polymer-bound Cl-catechols for prevention of biofilm formation, *Advanced Materials* 25 (2013) 529–533.  
<https://doi.org/10.1002/adma.201203362>.
- [5] R. Liang, H. Yu, L. Wang, N. Wang, B.U. Amin, NIR Light-Triggered Shape Memory Polymers Based on Mussel-Inspired Iron–Catechol Complexes, *Adv Funct Mater* 31 (2021) 2102621.  
<https://doi.org/10.1002/adfm.202102621>.
- [6] University of California San Francisco, MS-Isotope, (n.d.).  
<https://prospector.ucsf.edu/prospector/cgi-bin/msform.cgi?form=msisotope> (accessed September 18, 2023).

# CHAPTER 8

## SUPPLEMENTARY DATA



## Supplementary Information

# A novel standard for forensic elemental profiling of polymers by LA-ICP-TOF-MS

Mirjam de Bruin-Hoegée<sup>a,b,\*</sup>, Jorien Schoorl<sup>c</sup>, Peter Zoon<sup>c</sup>, Marcel J. van der Schans<sup>b</sup>, Daan Noort<sup>d</sup>, Arian C. van Asten<sup>a, e</sup>

<sup>a</sup>van 't Hoff Institute for Molecular Sciences, Faculty of Science, University of Amsterdam, P.O. Box 94157, 1090GD Amsterdam, The Netherlands

<sup>b</sup>TNO Defence, Safety and Security, Dep. CBRN Protection, Lange Kleiweg 137, 2288GJ Rijswijk, The Netherlands

<sup>c</sup>Netherlands Forensic Institute, PO Box 24044, The Hague, 2490 AA, Netherlands

<sup>d</sup>Organisation for the Prohibition of Chemical Weapons, Johan de Wittlaan 32, 2517 JR The Hague, The Netherlands

<sup>e</sup>CLHC, Amsterdam Center for Forensic Science and Medicine, University of Amsterdam, P.O. Box 94157, 1090GD Amsterdam, The Netherlands

\*Corresponding author. Email address: [mirjam.debruin@tno.nl](mailto:mirjam.debruin@tno.nl) (M. de Bruin-Hoegée)

## Contents

1.	Forensically relevant polymer objects.....	2
2.	Detailed production method of polymer standards .....	3
3.	Design of experiments.....	5
4.	Produced standards and forensic objects .....	6
5.	LA-ICP-TOF-MS line scans .....	9
6.	Linearity.....	10
7.	XRF analysis .....	11
8.	Classification with overlap criteria .....	12

## 1. Forensically relevant polymer objects

Table S 1. Information of wires, tubing, jerrycans and tapes analyzed by LA-ICP-MS and FT-IR.

#	Type	Supplier	Brand	Color	Details	Production date	Polymer type*
86	Wire	Wholesale	Draka	Black	Vinyl (VD)	n.a.	PVC-P
87	Wire	Wholesale	Eldra	Blue	0.75 mm2, Eca fire class.	n.a.	PVC-P
88	Wire	Wholesale	LTC	Brown	0.75 mm2, Lead free label	n.a.	PVC-P-NBR
89_y**	Wire	Gamma	Handson	Yellow-green	2.5 mm2, Yellow part	n.a.	PVC-P
89_g**	Wire	Gamma	Handson	Yellow-green	2.5 mm2, Green part	n.a.	PVC-P
90	Wire	Hornbach	Q-link	Grey	0.35 mm2	n.a.	PVC-U-GF
91_f***	Tubing	Wholesale	Pipelife	Grey	3/4 inch", polvalit, Front side	15-7-2013, 06:37	PVC-U
91_b***	Tubing	Wholesale	Pipelife	Red	3/4 inch", polvalit, Back side	15-7-2013, 06:37	Bunatek K71
92_f***	Tubing	Wholesale	Pipelife	Yellow	5/8", 'polivolt, Front side	18-10-2013, 17:11	PVC-U
92_b**	Tubing	Wholesale	Pipelife	Yellow-orange	5/8", 'polivolt, Back side	18-10-2013, 17:11	PVC-U
93	Tubing	wholesale	Wavin	Grey	3/4", Low Friction	28-3-2013, 11:16	PVC-U-GF/PVC-U-ABS
94	Tubing	Praxis	Martens	White	3/4"	25-8-2020, 23:12	PVC-Hard
95	Tubing	Hornbach	Pipelife, Akonyl	Grey	5/8"	20-9-2021, 23:54	PVC-U
96	Jerrycan	Hornbach	Hünersdorff	Red	811400, Tube	n.a.	LDPE
97	Jerrycan	ANWB	ANWB	Black	10802598, Can	n.a.	HDPE
98	Jerrycan	Bol	Splashbox Product Support B.V.	Blue	970700, Can	n.a.	HDPE
99	Jerrycan	Bol	All Ride, Meno Berlin	Yellow	2514278, Tube	n.a.	HDPE
100	Jerrycan	Bol	Claudius Cosmetics B.V.	White	B042, Can	n.a.	HDPE/LDPE
101	Tape	Hornbach	Hornbach	Blue	n.a.	n.a.	PVC-P
102	Tape	Karwei	Karwei	Red	n.a.	n.a.	PVC-P-NBR
103	Tape	Hornbach	Coroplast	Brown	n.a.	n.a.	PVC-P
104_y**	Tape	Gamma	Handson	Yellow-Green	Yellow part	n.a.	PVC-P-NBR/PVC-P
104_g**	Tape	Gamma	Handson	Yellow-Green	Green part	n.a.	PVC-P-NBR/PVC-P
105	Tape	Praxis	Heinrich Kopp	Black	Label Coroplast	n.a.	PVC-P

\*Identified by FT-IR

\*\*The object consisted of two colors yellow (y) and green (g)

\*\*\* The tube had a different inner layer, so the front (f) and the back (b) were measured

## 2. Detailed production method of polymer standards

Table S 2. Added chemicals to polymer standards with correction for total molecular weight.

Element	Chemical	M (g/mol)	M <sub>element</sub> (g/mol)	M% Element	ρ (g/mL)	Stock 5 mg/mL*
<b>23 Na</b>	Sodium ethanolate	68.05	22.99	0.34		14.8
<b>24 Mg</b>	Magnesium chloride	95.21	54.94	0.58		8.7
<b>27 Al</b>	Aluminium triisopropylate	204.24	26.98	0.13		37.8
<b>29 Si</b>	Tetraethyl orthosilicate	208.33	28.09	0.13	0.93	37.1
<b>39 K</b>	Potassium permanganate	158.03	39.10	0.25		20.2
<b>44 Ca</b>	Calcium chloride dihydrate	147.01	40.08	0.27		18.3
<b>49 Ti</b>	Titanium(IV)isopropoxide	284.22	47.87	0.17	0.96	29.7
<b>52 Cr</b>	Chromium(III)chloride hexahydrate	266.45	52.00	0.20		25.6
<b>55 Mn</b>	Potassium permanganate	158.03	54.94	0.35		14.4
<b>57 Fe</b>	Iron(III)nitrate nonahydrate	404.00	55.85	0.14		36.2
<b>59 Co</b>	Cobalt(II)chloride, hexahydrate	237.93	58.93	0.25		20.2
<b>60 Ni</b>	Nickel(II)acetate tetrahydrate**	248.84	58.69	0.24		21.2
<b>63 Cu</b>	Copper(II)acetate	181.63	63.55	0.35		14.3
<b>69 Ga</b>	Gallium(III) acetylacetone	367.05	69.72	0.19		26.3
<b>75 As</b>	Arsenic (III) chloride	181.28	74.92	0.41	2.16	12.1
<b>88 Sr</b>	Strontium tetramethylheptanedionate	454.15	87.62	0.19		25.9
<b>90 Zr</b>	Zirconium(IV) butoxide solution 80 wt	383.68	91.22	0.30	1.05	16.8
<b>93 Nb</b>	Tetrachlorobis(tetrahydrofuran)niobium	378.93	92.91	0.25		20.4
<b>105 Pd</b>	(bis(triphenylphosphine)Pd(II)dichloride	701.90	106.42	0.15		33.0
<b>118 Sn</b>	Tin(II) 2-ethylhexanoate	405.12	118.71	0.29	1.25	17.1
<b>121 Sb</b>	Antimony pentafluoride	216.75	121.76	0.56	2.99	8.9
<b>137 Ba</b>	Barium bis(2-ethylhexanoate)	423.73	137.32	0.32		15.4
<b>208 Pb</b>	Lead tetra acetate	443.36	207.20	0.47		10.7

\*This column shows the total concentration of the chemical consisting of multiple atoms which is needed to obtain a concentration of 5 mg/mL for the element of interest.

Various volumes of the stock solution presented in Table S2 were added to the standard solutions to obtain different elemental concentrations as shown in Table S3. For the middle and low concentration standards, lower stock solutions of 0.5 and 0.05 mg/mL were made.

Table S 3. Applied elemental concentrations in the low, middle, and high concentration PE, PS and PVC standard.

Element	PE (mg/kg)			PS (mg/kg)			PVC (mg/kg)		
	Low	Mid	High	Low	Mid	High	Low	Mid	High
<b>Na23</b>	2	20	200	1	10	100	5	50	500
<b>Mg24</b>	40	200	1000	5	50	500	5	50	500
<b>Al27</b>	200	400	1000	5	50	500	5	50	500
<b>Si28</b>	100	200	2000	50	100	1000	50	100	1000
<b>K39</b>	2	20	200	1	10	100	1	10	100
<b>Ca44</b>	1000	1500	2000	50	200	1000	10	100	1000
<b>Ti47</b>	20	20	2000	500	5	500	10	100	1000
<b>Cr53</b>	20	100	200	10	50	200	5	50	500
<b>Mn55</b>	2.8	28	280	1.4	14	140	1.4	14	140
<b>Fe56</b>	2	20	200	5	50	500	2	20	200
<b>Co59</b>	1	10	100	0.1	1	10	0.2	2	20
<b>Ni60</b>	1	10	100	0.5	5	50	0.2	2	20
<b>Cu63</b>	2	20	200	1	10	100	5	50	500
<b>Ga71</b>	2	20	200	1	10	100	1	10	100
<b>As75</b>	2	20	200	0.5	5	50	5	50	500
<b>Sr88</b>	4	40	400	1	10	100	1	10	100
<b>Zr90</b>	0.04	0.4	40	0.02	0.2	20	0.02	0.2	20
<b>Nb93</b>	2	20	200	1	10	100	1	10	100
<b>Pd105</b>	2	20	200	1	10	100	1	10	100
<b>Sn118</b>	2	20	200	1	10	100	2	20	200
<b>Sb121</b>	10	100	1000	5	50	500	20	200	1000
<b>Ba137</b>	10	100	1000	5	50	500	5	50	500
<b>Pb208</b>	2	20	200	1	10	100	5	50	500

### 3. Design of experiments

Table S 4. Design of experiments used for method optimization to limit the number of measurements.

RunOrder	Mixing time (hours)	Drying temperature (°C)	Polymer
1	48	50	PS
2	24	20-22	PVC
3	18	50	PS
4	24	20-22	PS
5	18	2-8	PE
6	18	20-22	PS
7	18	50	PE
8	18	20-22	PE
9	24	50	PVC
10	4	2-8	PVC
11	24	50	PE
12	4	20-22	PVC
13	48	20-22	PS
14	24	20-22	PE
15	6	50	PVC
16	6	2-8	PVC
17	48	20-22	PE
18	24	2-8	PE

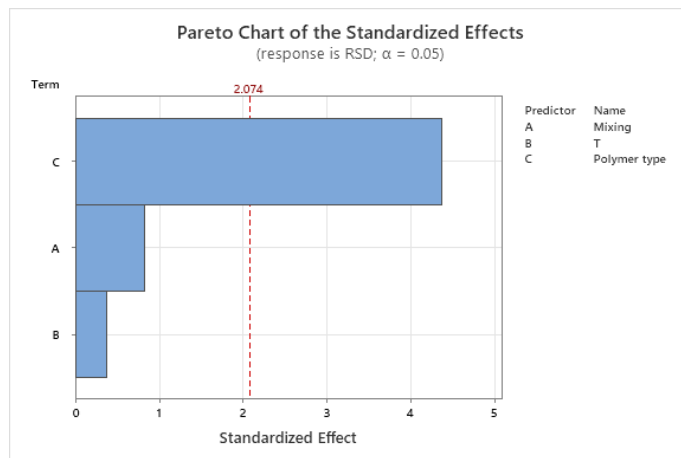


Figure S 1. Pareto Chart of Standardized Effects. The factors mixing time (A), temperature (B) and polymer type (C) were included. The red reference line indicates statistically significant effects with  $\alpha=0.05$ .

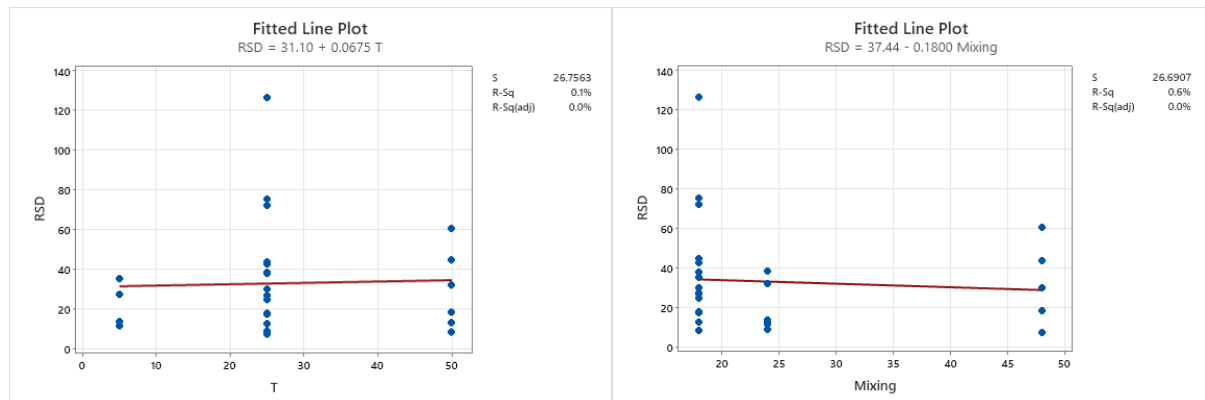
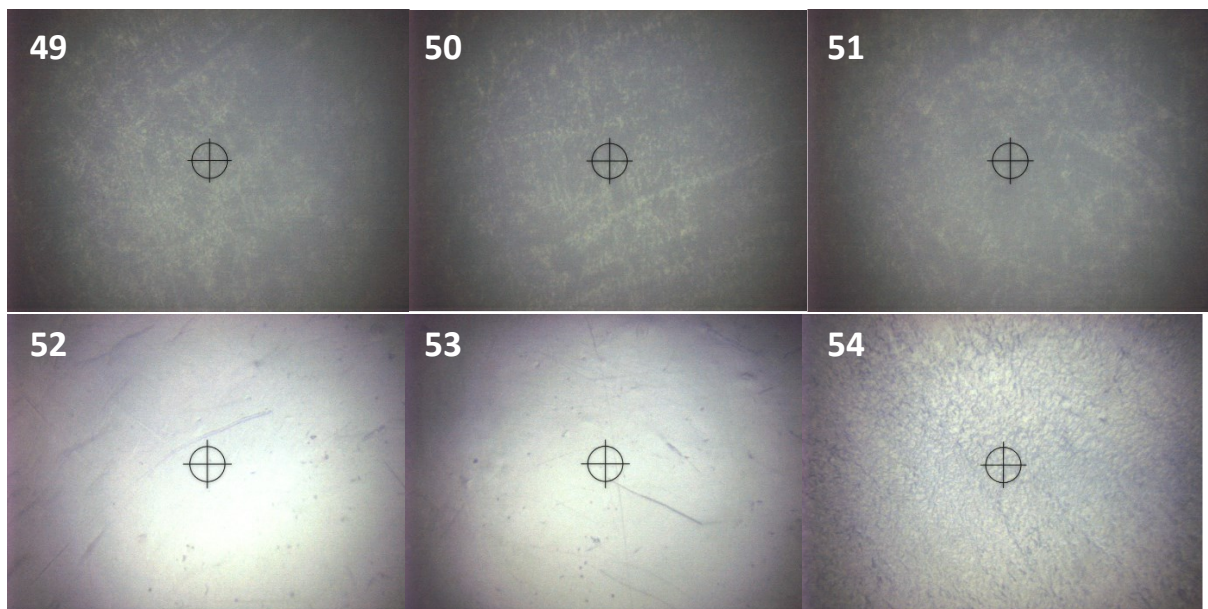


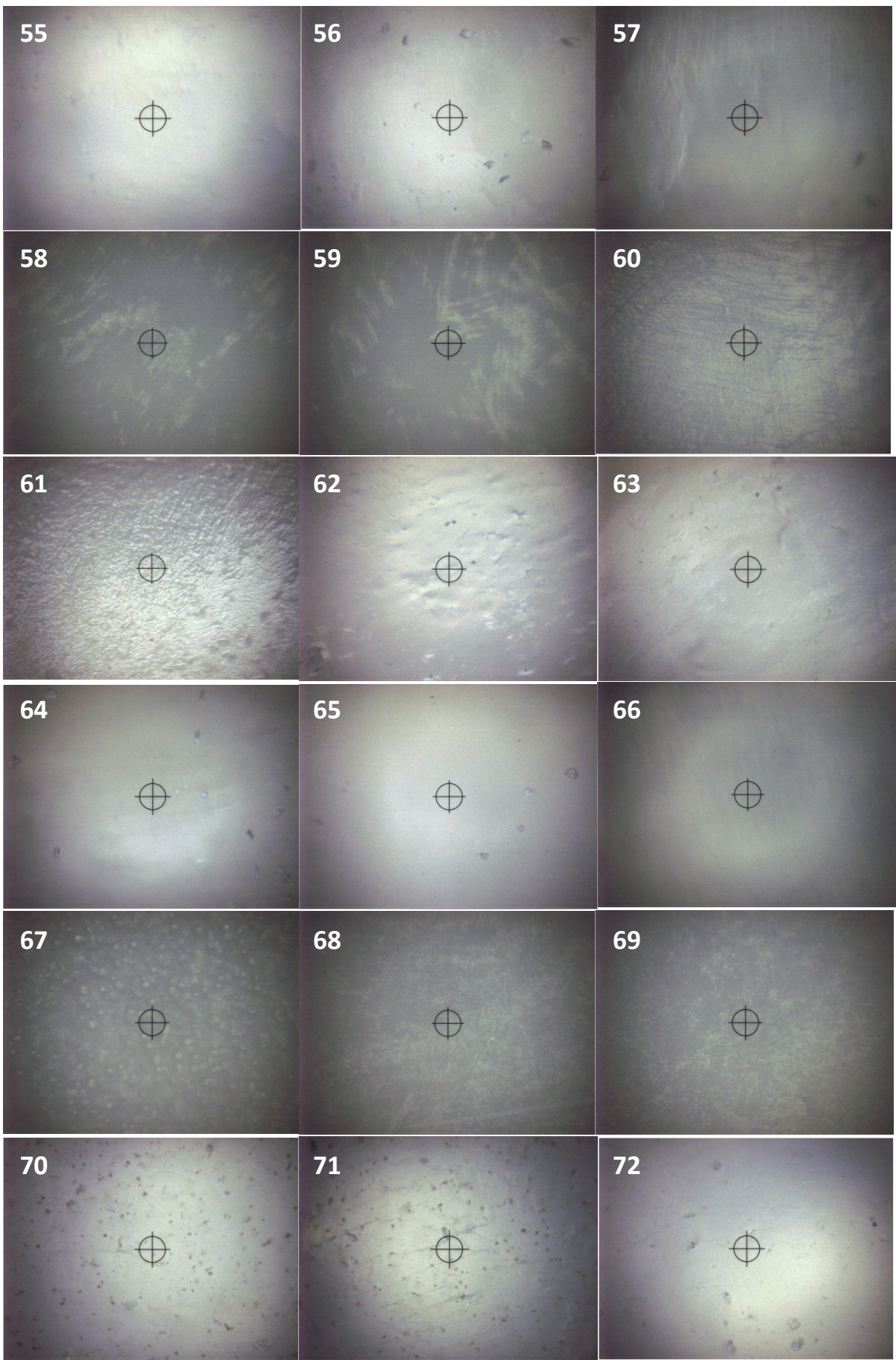
Figure S 2. Fitted line plot of the effect of A) Temperature and B) Mixing time on the homogeneity (%RSD). No significant correlation was observed.

#### 4. Produced standards and forensic objects



Figure S 3. Small pieces of blanks, standards and forensic polymer objects of approximately 5x5 mm for LA-ICP-TOF-MS analysis. 49-51: PE Blank, 52-54: PS blank, 55-57: PVC blank, 58-60: PE low, 61-63: PS low, 64-66: PVC low, 67-69: PE mid, 70-72: PS mid, 73-75: PVC mid, 76-79: PE high, 80-82: PS high, 83-85: PVC high, 86-90 wires, 91-95: tubing, 96-100: jerrycans, 101-105: tapes.





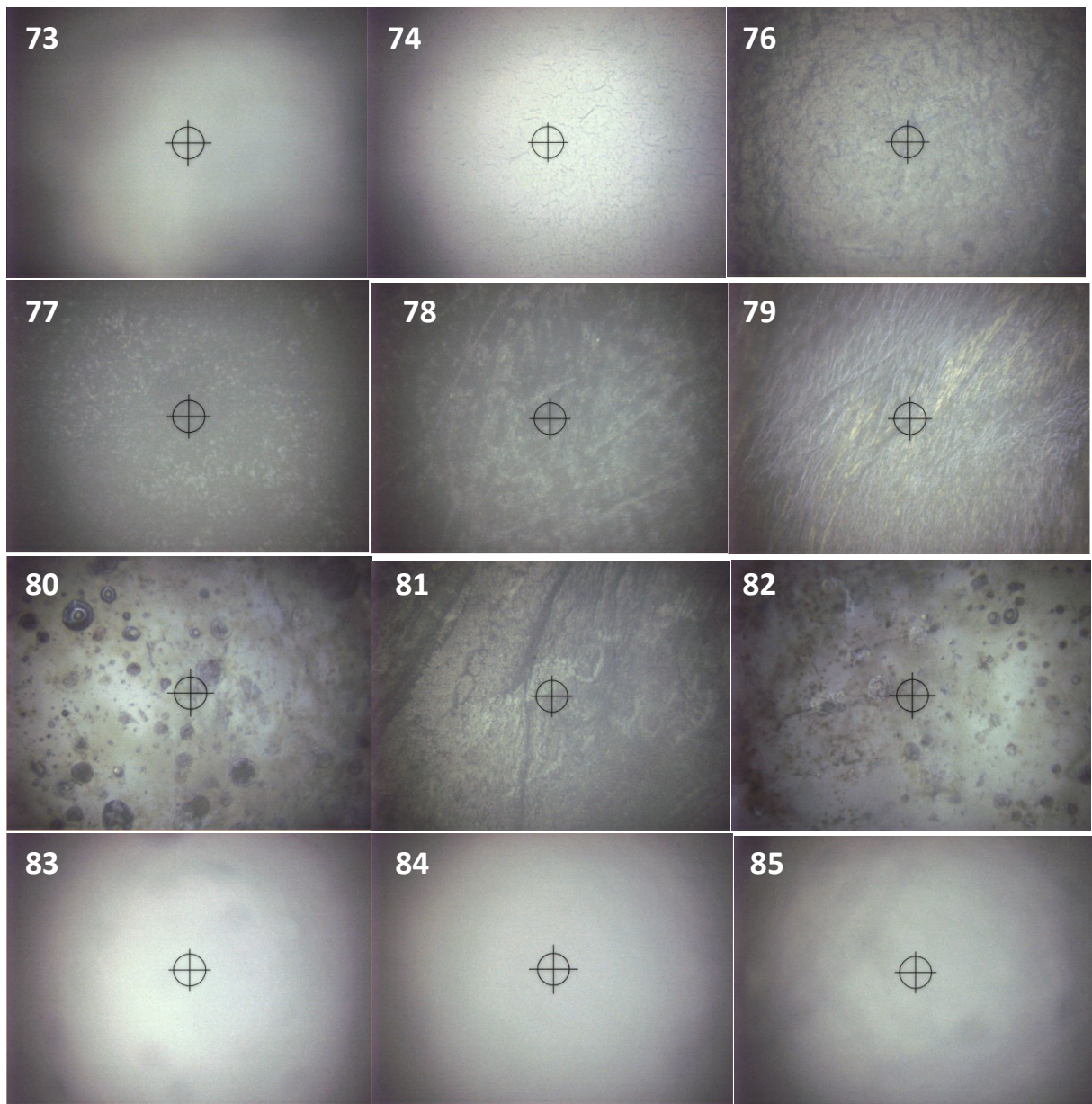


Figure S 4. Magnification with a diameter of approximately 500  $\mu\text{m}$  of new polymer standards. 49-51: PE Blank, 52-54: PS blank, 55-57: PVC blank, 58-60: PE low, 61-63: PS low, 64-66: PVC low, 67-69: PE mid, 70-72: PS mid, 73-75: PVC mid, 76-79: PE high, 80-82: PS high, 83-85: PVC high.

## 5. LA-ICP-TOF-MS line scans

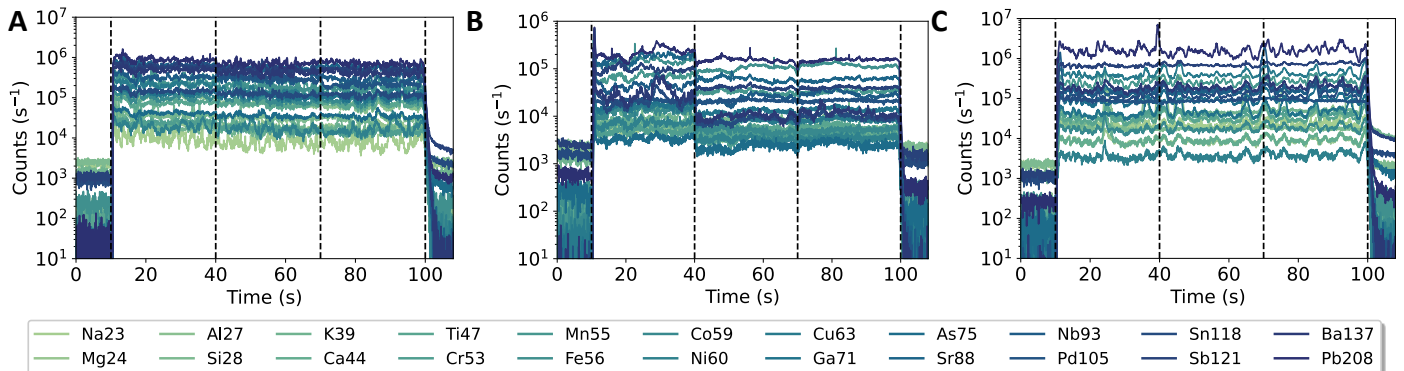


Figure S 5. Three consecutive LA-ICP-TOF-MS line scans over a distance of 1 mm for a) PE, b) PS and c) PVC standards with elements in the concentration range of 10 – 1000 mg/kg polymer. Dashed lines mark the start and end of a line scan.

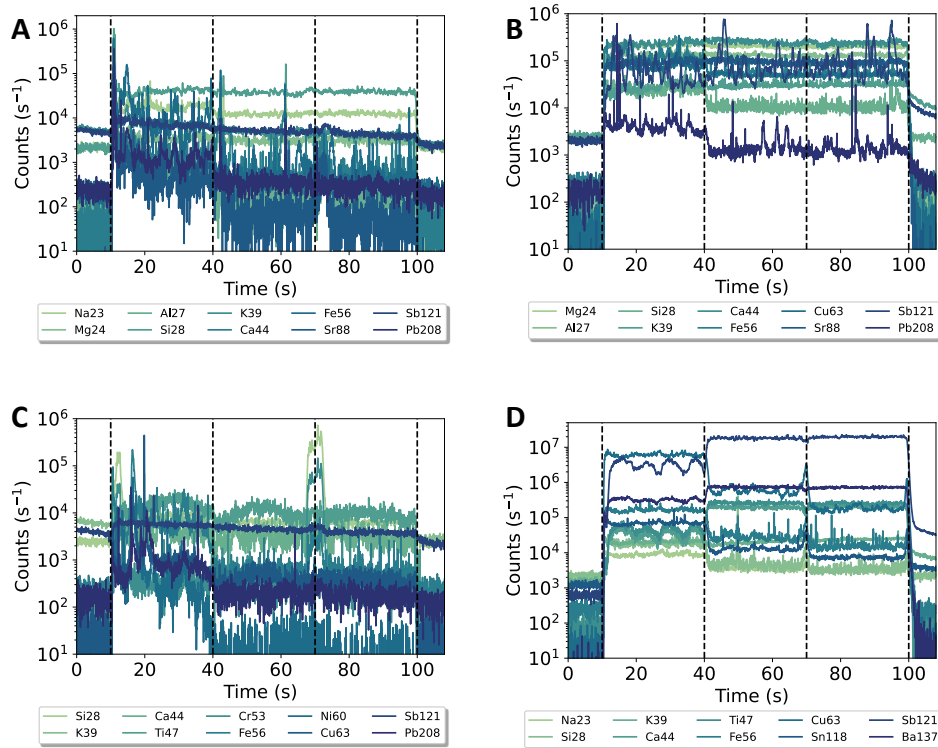


Figure S 6. Three consecutive LA-ICP-TOF-MS line scans over a distance of 1 mm of ten most abundant elements in A) an electrical wire, B) PVC tubing, C) jerrycan and D) tape. Dashed lines mark the start and end of a line scan.

## 6. Linearity

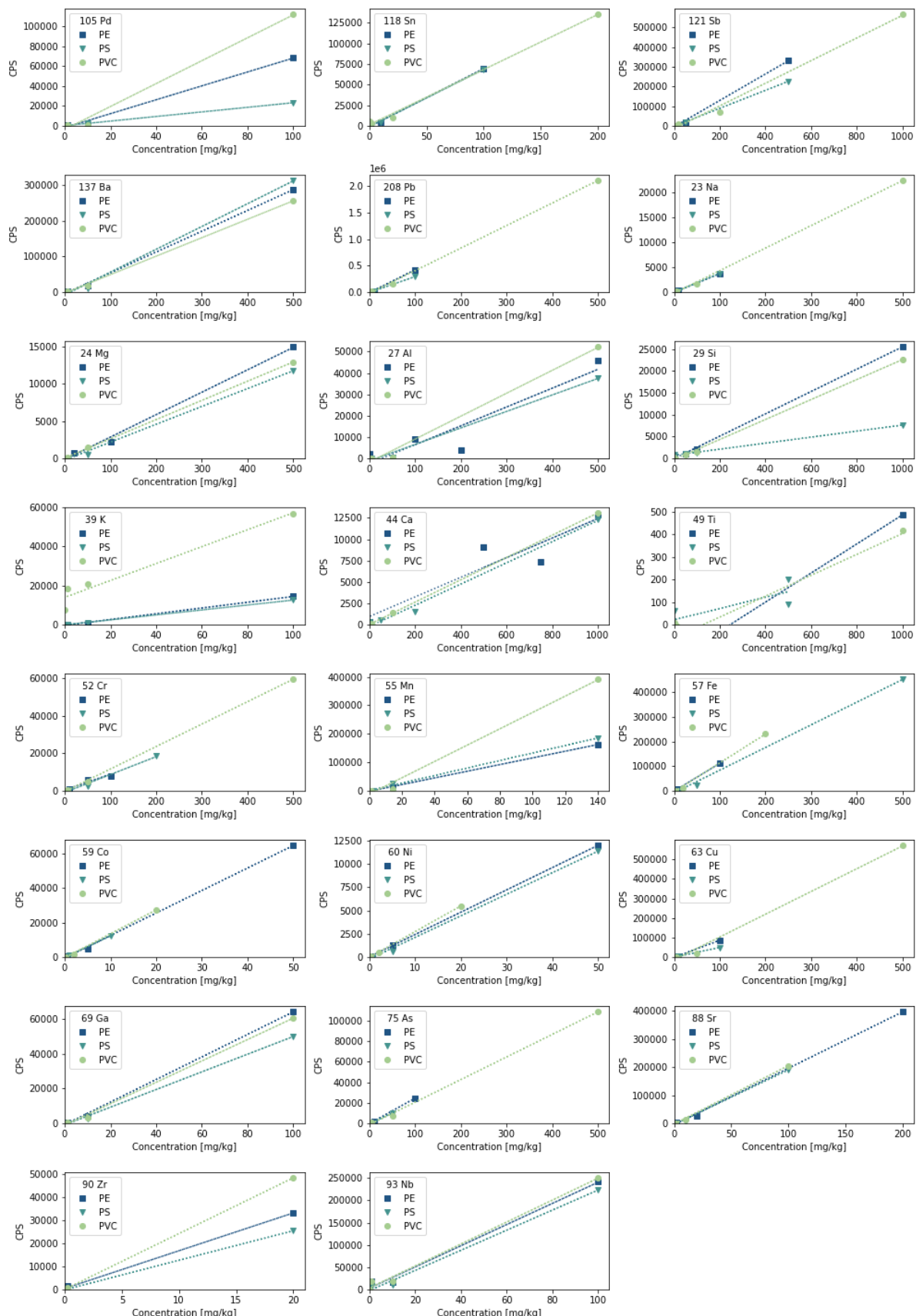


Figure S 7. Calibration curves of responses in counts per seconds (CPS) of PE, PS and PVC with an elemental concentration ranging from 0 to 1000 mg/kg analyzed by LA-ICP-TOF-MS.

## 7. XRF analysis

Table S5 shows the elemental concentrations measured by XRF. Sodium (Na) was not included due to a detection limit of 2000 mg/kg, which exceeded the applied concentrations.

*Table S5. Comparison of applied elemental concentrations in PE, PS and PVC standards with concentrations analyzed by XRF.*

Element	PE			PS			PVC		
	Applied (mg/kg)	Measured (mg/kg)	Deviation (%)	Applied (mg/kg)	Measured (mg/kg)	Deviation (%)	Applied (mg/kg)	Measured (mg/kg)	Deviation (%)
<b>Mg24</b>	1000	405	-63	500	1528	206	500	482	-4
<b>Si28</b>	2000	2104	5	1000	1573	57	1000	798	-20
<b>K39</b>	200	119	-41	100	375	275	100	101	1
<b>Ca44</b>	2000	1632	-18	1000	3891	289	1000	530	-47
<b>Ti47</b>	2000	1466	-27	500	1642	228	1000	441	-56
<b>Cr53</b>	200	191	-4	200	477	138	500	263	-47
<b>Mn55</b>	280	183	-35	140	263	88	140	88	-37
<b>Fe56</b>	200	180	-10	500	937	87	200	102	-49
<b>Co59</b>	100	77	-23	10	17	69	20	14	-30
<b>Ni60</b>	100	65	-35	50	77	53	20	13	-34
<b>Cu63</b>	200	149	-25	100	131	31	500	245	-51
<b>Ga71</b>	200	169	-16	100	128	28	100	34	-66
<b>As75</b>	200	183	-9	50	70	39	500	291	-42
<b>Sr88</b>	400	300	-25	100	105	5	100	59	-41
<b>Nb93</b>	200	169	-16	100	105	5	100	83	-17
<b>Pd105</b>	200	163	-19	100	97	-3	100	88	-12
<b>Sn118</b>	200	151	-25	100	118	18	200	132	-34
<b>Sb121</b>	1000	500	-50	500	280	-44	1000	505	-49
<b>Ba137</b>	1000	1019	2	500	893	79	500	428	-14
<b>Pb208</b>	200	179	-11	100	125	25	500	304	-39

## 8. Classification with overlap criteria

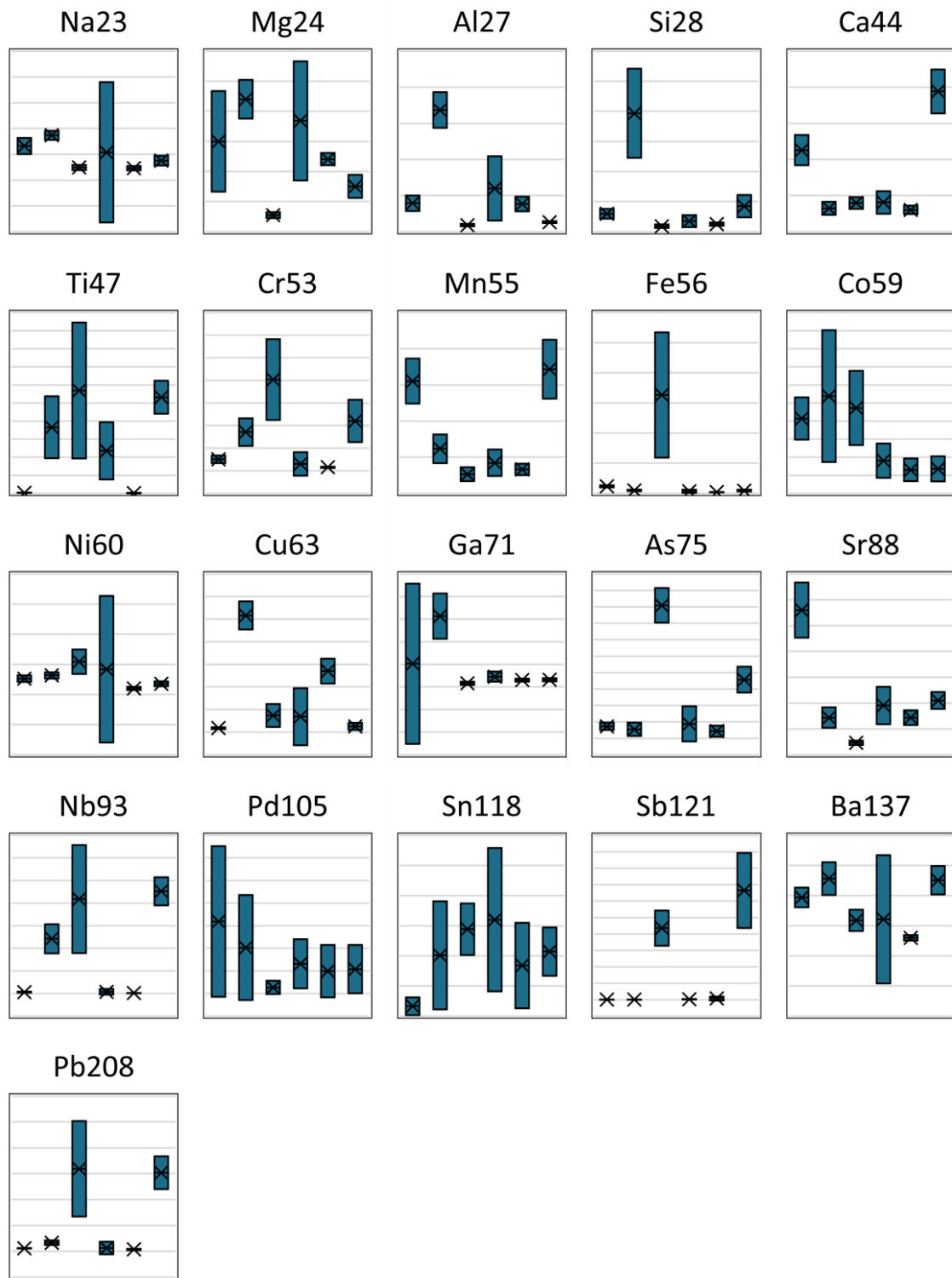


Figure S 8. Box plot of mean elemental responses with correction for new reference standards for wires from seven different suppliers and brands. The minimum and maximum value are  $\pm 2 \times \text{stdv}$ . ( $n=36$ ).

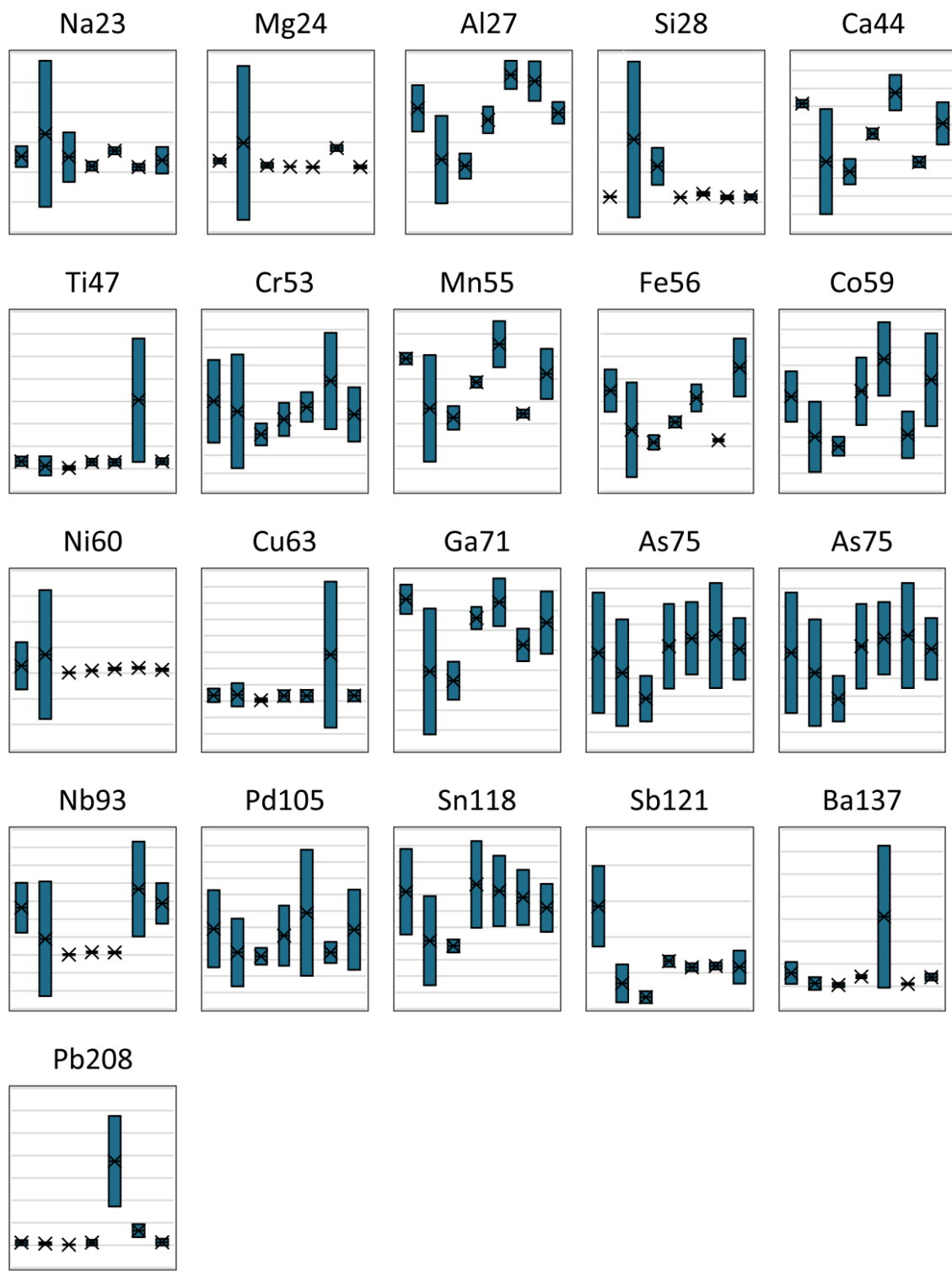
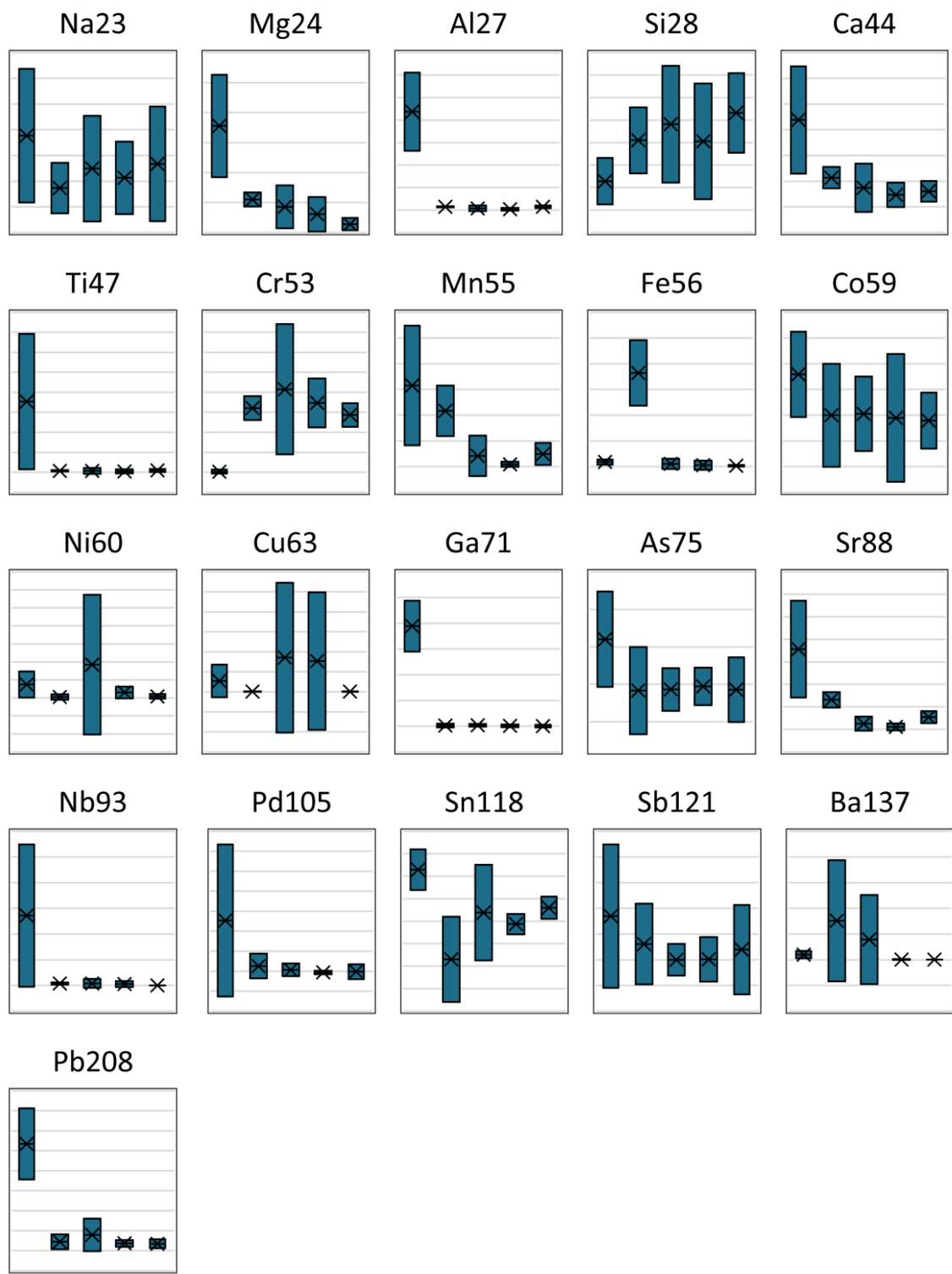


Figure S 9. Box plot of mean elemental responses with correction for new reference standards for tubing from seven different suppliers and brands. The minimum and maximum value are  $\pm 2 \times \text{stdv.}$  ( $n=36$ ).



*Figure S 10. Box plot of mean elemental responses with correction for new reference standards for jerrycans from five different suppliers and brands. The minimum and maximum value are  $\pm 2 \text{ stdv}$ . ( $n=36$ ).*

# CHAPTER 9

## SUPPLEMENTARY DATA



## Supplementary data

# Evaluating the strength of evidence of elemental profiling of polymers with LA-ICP-MS

Mirjam de Bruin-Hoegée<sup>a,b,\*</sup>, Ruthmara Corzo<sup>c</sup>, Peter Zoon<sup>d</sup>, Peter Vergeer<sup>d</sup>, Jorien Schoorl<sup>d</sup>, Marcel J. van der Schans<sup>b</sup>, Daan Noort<sup>b,1</sup>, Arian C. van Asten<sup>a, e</sup>

<sup>a</sup>van 't Hoff Institute for Molecular Sciences, Faculty of Science, University of Amsterdam, P.O. Box 94157, 1090GD Amsterdam, The Netherlands

<sup>b</sup>TNO Defence, Safety and Security, Dep. CBRN Protection, Lange Kleiweg 137, 2288GJ Rijswijk, The Netherlands

<sup>c</sup>National Institute of Standards and Technology, Materials Measurement Science Division, Gaithersburg, MD 20899, the United States of America, ORCID: 0000-0003-1907-3368

<sup>d</sup>Netherlands Forensic Institute, PO Box 24044, The Hague, 2490 AA, Netherlands

<sup>e</sup>CLHC, Amsterdam Center for Forensic Science and Medicine, University of Amsterdam, P.O. Box 94157, 1090GD Amsterdam, The Netherlands

<sup>1</sup>Current address: Organisation for the Prohibition of Chemical Weapons, Johan de Wittlaan 32, 2517 JR The Hague, The Netherlands

\*Corresponding author. Email address: [mirjam.debruin@tno.nl](mailto:mirjam.debruin@tno.nl) (M. de Bruin-Hoegée)

## Contents

1.	Elemental concentrations of polymer standards .....	2
2.	Information forensically relevant polymer objects .....	3
3.	Feature-based MVK model.....	9
4.	LA-ICP-MS method optimization .....	18
5.	Performance of the polymer standard.....	24
6.	Correlation plots.....	27
7.	Leave-one-out validation PCA .....	28
8.	Leave one-out validation LDA.....	29
9.	Boxplot of concentrations for each element.....	30
10.	False inclusions/exclusions comparison models .....	32
11.	Tippett plots feature-based LR model.....	34
12.	Performance measures feature-based LR model.....	36
13.	Tippett plots score-based LR model.....	38
14.	Performance measures score-based LR model.....	40
	Disclaimer .....	44
	References.....	44

## 1. Elemental concentrations of polymer standards

*Table S1.* Applied elemental concentrations in the low, middle, and high concentration PE, PS, and PVC standard.

Element	PE (mg/kg)			PS (mg/kg)			PVC (mg/kg)		
	Low	Mid	High	Low	Mid	High	Low	Mid	High
<b>Na23</b>	2	20	200	1	10	100	5	50	500
<b>Mg24</b>	40	200	1000	5	50	500	5	50	500
<b>Al27</b>	200	400	1000	5	50	500	5	50	500
<b>Si28</b>	100	200	2000	50	100	1000	50	100	1000
<b>K39</b>	2	20	200	1	10	100	1	10	100
<b>Ca44</b>	1000	1500	2000	50	200	1000	10	100	1000
<b>Ti47</b>	20	20	2000	500	5	500	10	100	1000
<b>Cr53</b>	20	100	200	10	50	200	5	50	500
<b>Mn55</b>	2.8	28	280	1.4	14	140	1.4	14	140
<b>Fe56</b>	2	20	200	5	50	500	2	20	200
<b>Co59</b>	1	10	100	0.1	1	10	0.2	2	20
<b>Ni60</b>	1	10	100	0.5	5	50	0.2	2	20
<b>Cu63</b>	2	20	200	1	10	100	5	50	500
<b>Ga71</b>	2	20	200	1	10	100	1	10	100
<b>As75</b>	2	20	200	0.5	5	50	5	50	500
<b>Sr88</b>	4	40	400	1	10	100	1	10	100
<b>Zr90</b>	0.04	0.4	40	0.02	0.2	20	0.02	0.2	20
<b>Nb93</b>	2	20	200	1	10	100	1	10	100
<b>Pd105</b>	2	20	200	1	10	100	1	10	100
<b>Sn118</b>	2	20	200	1	10	100	2	20	200
<b>Sb121</b>	10	100	1000	5	50	500	20	200	1000
<b>Ba137</b>	10	100	1000	5	50	500	5	50	500
<b>Pb208</b>	2	20	200	1	10	100	5	50	500

## 2. Information forensically relevant polymer objects

Tapes from 82 different brands/suppliers (referred to as: 'Source') were evaluated. For three tapes three batches (A, B, C) of the same Source were investigated (64, 72, 82). In addition, five tapes consisted of two colors. To make the data analysis more convenient, the original number was kept for the green colored part of the tapes. The yellow parts were numbered 83-87 instead of 7, 25, 29, 39, and 45. The tapes mainly consisted of plasticized PVC (PVC-P).

*Table S1. Information of tapes analyzed by LA-ICP-MS and FT-IR, obtained from various suppliers.*

#	Supplier/country	Brand	Color	Details	Polymer type*
1	Hornbach	Hornbach	Yellow		PVC-P
2	Hornbach	Hornbach	Red		PVC-P
3	Hornbach	Hornbach	Green		PVC-P
4	Hornbach	Hornbach	Blue		PVC-P
5	Hornbach	Hornbach	Black		PVC-P
6	Hornbach	Hornbach	White		PVC-P
7	Karwei	Karwei	Yellow-Green		PVC-P-NBR
8	Karwei	Karwei	Blue		PVC-P-NBR
9	Karwei	Karwei	Black		PVC-P-NBR
10	Karwei	Karwei	White		PVC-P-NBR
11	Karwei	Karwei	Red		PVC-P-NBR
12	Hornbach	Coroplast	Purple		PVC-P
13	Hornbach	Coroplast	Yellow		PVC-P
14	Hornbach	Coroplast	Brown		PVC-P
15	Hornbach	Coroplast	Grey		PVC-P
16	Hornbach	Coroplast	Red		PVC-P
17	Hornbach	Coroplast	Blue		PVC-P
18	Hornbach	Coroplast	Orange		PVC-P
19	Hornbach	Coroplast	Black		PVC-P
20	Hornbach	Coroplast	White		PVC-P
21	Hornbach	Coroplast	Green		PVC-P
22	Gamma	Handson	Brown		PVC-P-NBR
23	Gamma	Handson	Black		PVC-P-NBR
24	Gamma	Handson	Blue		PVC-P-NBR
25	Gamma	Handson	Yellow-Green		PVC-P
26	Gamma	Handson	Red		PVC-P-NBR
27	Gamma	Handson	Black		PVC-P-NBR
28	Gamma	Handson	White		PVC-P-NBR
29	Gamma	Handson	Yellow-Green		PVC-P-NBR/PVC-P
30	Gamma	Tesa	Black	5mx50mm	PVC-P-NBR
31	Gamma	Tesa	Red	10mx15mm	PVC-U
32	Gamma	Tesa	Black	10mx15mm	PVC-U
33	Praxis	GS International	Green	10mx18mm	PVC-P-NBR
34	Praxis	GS International	White	10mx18mm	PVC-P-NBR
35	Praxis	GS International	Black	10mx18mm	PVC-P-NBR
36	Praxis	GS International	Blue	10mx18mm	PVC-P-NBR
37	Praxis	GS International	Yellow	10mx18mm	PVC-P-NBR
38	Praxis	GS International	Red	10mx18mm	PVC-P-NBR
39	Praxis	Tesa	Yellow-Green	10mx15mm	PVC-P-NBR
40	Praxis	Tesa	White	20mx50mm	PVC-P
41	Praxis	Tesa	Red	20mx50mm	PVC-P
42	Praxis	Heinrich Kopp	Black	20mx19mm	PVC-P
43	Praxis	Heinrich Kopp	Green	10mx15mm, Coroplast imprint	PVC-P
44	Praxis	Heinrich Kopp	Black	10mx15mm, Coroplast imprint	PVC-P
45	Praxis	Heinrich Kopp	Yellow-Green	10mx15mm, Coroplast imprint	PVC-P
46	Praxis	Heinrich Kopp	Grey	10mx15mm, Coroplast imprint	PVC-P
47	Praxis	Heinrich Kopp	Blue	10mx15mm, Coroplast imprint	PVC-P
48	Praxis	Heinrich Kopp	Brown	10mx15mm, Coroplast imprint	PVC-P
49	Praxis	Heinrich Kopp	Yellow	10mx15mm, Coroplast imprint	PVC-P
50	Praxis	Heinrich Kopp	Orange	10mx15mm, Coroplast imprint	PVC-P
51	Praxis	Heinrich Kopp	Red	10mx15mm, Coroplast imprint	PVC-P

52	Praxis	Heinrich Kopp	White	10mx15mm, Coroplast imprint	PVC-P
53	Lowe	Utilitech	Black	1/2inx10ftx7mil	-
54	Lowe	Utilitech	White	1/2inx10ftx7mil	-
55	Lowe	Utilitech	Green	1/2inx10ftx7mil	-
56	Lowe	Utilitech	Blue	1/2inx10ftx7mil	-
57	Lowe	Utilitech	Yellow	1/2inx10ftx7mil	-
58	Lowe	Utilitech	Red	1/2inx10ftx7mil	-
59	USA	3M	Black	Scotch 700 Vinyl Electrical Tape	-
60	USA	3M	Black	Scotch Heavy Duty Vinyl Electrical Tape 22	-
61	USA	3M	Black	Scotch Super 33+ Vinyl Electrical Tape	-
62	USA	3M	Black	Scotch Super 88 Professional Grade Vinyl Electrical Tape	-
63	Poland	3M	Black	Temflex 165 General Use Vinyl Electrical Tape	-
65	Poland	3M	Black	Temflex 175 General Use Vinyl Electrical Tape	-
66	USA	3M	Black	Temflex General Use Vinyl Electrical Tape 1776	-
67	Taiwan	Amazon	Black	Amazon Commercial Vinyl Electrical Tape	-
68	China	DiversiTech	Black	Morris General Purpose Vinyl Electrical Tape 60000	-
69	China	DiversiTech	Black	Morris Premium + Vinyl Electrical Splicing Tape 60110	-
70	China	DiversiTech	Black	Morris Premium Vinyl Electrical Splicing Tape 60100	-
71	Taiwan	Intertape Polymer Group	Black	Economy Grade Vinyl Electrical Tape	-
73	Taiwan	NSI	Black	WarriorWrap Black General Electrical Tape WW-716	-
74	Taiwan	NSI	Black	WarriorWrap Premium Vinyl Electrical Tape WW-732	-
75	Taiwan	NSI	Black	WarriorWrap Select Vinyl Electrical Tape WW-722	-
76	China	Shurtape	Black	Duck Brand Economy Electrical Tape 282289	-
77	China	Shurtape	Black	Duck Brand Professional Electrical Tape 393119	-
78	China	Shurtape	Black	Duck Heavy Duty Electrical Tape 393120	-
79	China	Shurtape	Black	EV 097 Premium Grade Vinyl Electrical Tape 104697	-
80	China	Shurtape	Black	EV 57 General Purpose Electrical Tape	-
81	China	Shurtape	Black	EV 77 Professional Grade Vinyl Electrical Tape 104706	-
64_A	USA	3M	Black	Temflex 1700 Vinyl Electrical Tape 5 pk	-
64_B	USA	3M	Black	Temflex 1700 Vinyl Electrical Tape 5 pk	-
64_C	USA	3M	Black	Temflex 1700 Vinyl Electrical Tape 5 pk	-
72_A	Taiwan	NSI	Black	Easy-Wrap Electrical Tape EWG7060 10 pk	-
72_B	Taiwan	NSI	Black	Easy-Wrap Electrical Tape EWG7060 10 pk	-
72_C	Taiwan	NSI	Black	Easy-Wrap Electrical Tape EWG7060 10 pk	-
82_A	China	Utilitech	Black	10 CT Vinyl Electrical Tape	-
82_B	China	Utilitech	Black	10 CT Vinyl Electrical Tape	-
82_C	China	Utilitech	Black	10 CT Vinyl Electrical Tape	-

Tubing from 36 different brands/suppliers (referred to as: 'Source') were evaluated. For source 1-3 also the inner part with a red coating was analyzed and numbered 37-39.

*Table S2. Information of tubing analyzed by LA-ICP-MS and FT-IR, obtained from various suppliers.*

#	Supplier	Brand	Color	Details	Polymer type*
<b>1</b>	wholesale	Pipelife	Grey	8712603060146	PVC-U (back: bunatex K71)
<b>2</b>	wholesale	Pipelife	Yellow	8712603054015	PVC-U-ABS (back: bunatex K71)
<b>3</b>	wholesale	Pipelife	Yellow	8712603054008	PVC-U
<b>4</b>	wholesale	Wavin	Grey	1 1/4	PVC-U
<b>5</b>	wholesale	Wavin	Grey	8712148067884	PVC-U
<b>6</b>	wholesale	Wavin	Yellow	1 1/4	PVC-U
<b>7</b>	wholesale	Univolt	White	3/4	PP
<b>8</b>	wholesale	Wavin	Grey	8712148067945	PVC-U
<b>9</b>	wholesale	Wavin	Creme	12X1	PVC-U
<b>10</b>	wholesale	Wavin	Grey	8712148067976	PVC-U
<b>11</b>	wholesale	Wavin	Grey	8712148512353	PVC-U-GF/ PVC-U-ABS (graphite fibril)
<b>12</b>	wholesale	-	Yellow		PVC-U-ABS
<b>13</b>	wholesale	-	White	1 1/4	PVC-U-GF
<b>14</b>	Praxis	Martens	Grey	32mm	PVC-Hard
<b>15</b>	Praxis	Martens, ecomar®	Grey	40mm	PVC-U-ABS
<b>16</b>	Praxis	Martens	White	32mm	PVC-Hard
<b>17</b>	Praxis	Martens	White	40mm	PVC-Hard
<b>18</b>	Praxis	Martens, ecomar®	Grey	50mm	PVC-Hard
<b>19</b>	Praxis	Martens	Yellow	8711422090945	PVC-U
<b>20</b>	Praxis	Martens	Yellow	8711422090969	PVC-Hard
<b>21</b>	Praxis	Martens	Grey	8711422107780	PVC-U
<b>22</b>	Praxis	Martens	Grey	8711422090990	PVC-U
<b>23</b>	Praxis	Martens	White	8711422189809	PVC-Hard
<b>24</b>	Praxis	Martens	White	8711422189779	PVC-Hard
<b>25</b>	Gamma	Pipelife, Akonyl	Grey	8716507000192	PVC-Hard
<b>26</b>	Gamma	Pipelife, Akonyl	Grey	8716507000239	PVC-Hard
<b>27</b>	Gamma/Hornbach	Pipelife, Akonyl	Yellow	871650700024	PVC-U
<b>28</b>	Gamma/Hornbach	Pipelife, Akonyl	Yellow	871650700086	PVC-Hard
<b>29</b>	Gamma/Hornbach	Pipelife, Akonyl	Yellow	871650700024	PVC-U
<b>30</b>	Gamma/Hornbach	Pipelife, Akonyl	Yellow	871650700086	PVC-U-ABS
<b>31</b>	Hornbach	Pipelife, Akonyl	Grey	8716507000147	PVC-U
<b>32</b>	Hornbach	Pipelife, Akonyl	Grey	8716507000161	PVC-U
<b>33</b>	Lowe	Charlotte Pipe	Yellow	PLNC 12005	-
<b>34</b>	Lowe	Silver-Line	White	PVC-1120	-
<b>35</b>	Lowe	Cantex	White	Schedule 40 rigid	-
<b>36</b>	Lowe	Charlotte Pipe	White	TrueFit system	-
<b>37</b>	wholesale	Pipelife	Red	8712603060146	PVC-U (back: bunatex K71)
<b>38</b>	wholesale	Pipelife	Red	8712603054015	PVC-U-ABS (back: bunatex K71)
<b>39</b>	wholesale	Pipelife	Red	8712603054008	PVC-U

Wires from 44 different brands/suppliers (referred to as: 'Source') were evaluated. For five sources the wires were colored with yellow-green stripes. The yellow part was considered as a separate sample and numbered 45-49.

*Table S3. Information of wires analyzed by LA-ICP-MS and FT-IR, obtained from various suppliers.*

#	Supplier	Brand	Color	Details	Polymer type*
1	wholesale	Nexans	Green		PVC-P-NBR
2	wholesale	Draka	Grey		PVC-P-NBR
3	wholesale	Ramcro	Red(-Black)		PVC-U-GF
4	wholesale	Ramcro	(Red-)Black		PVC-U-GF
5	wholesale	Draka	Black		PVC-P
6	wholesale	Draka	Blue		PVC-P
7	wholesale	Eldra	Blue		PVC-P
8	wholesale	Eldra	Brown		PVC-P
9	wholesale	Draka	Black		PVC-P
10	wholesale	Eldra	White		PVC-P
11	wholesale	Eldra	Green		PVC-P
12	wholesale	Draka	Red		PVC-P-NBR
13	wholesale	LTC	Brown	Lead free	PVC-P-NBR
14	wholesale	LTC	Red		PVC-P-NBR
15	wholesale	LTC	Orange	Lead free	PVC-P-NBR
16	Praxis	Sencys	Black		PVC-P
17	Praxis	Sencys	Brown		PVC-P
18	Praxis	Sencys	Blue		PVC-P
19	Praxis	Sencys	Green		PVC-P
20	Gamma	Handson	Black		PVC-P
21	Gamma	Handson	Grey		Ca(OH)2/ Silicone
22	Gamma	Handson	Blue		PVC-P
23	Gamma	Handson	Green		PVC-P
24	Gamma	Handson	White		PVC-U-GF
25	Hornbach	Q-link	Blue		Ca(OH)2/ Silicone
26	Hornbach	Q-link	Black		Ca(OH)2/ Silicone
27	Hornbach	Q-link	Black		PVC-P-NBR
28	Hornbach	Q-link	Brown		PVC-U-GF
29	Hornbach	Q-link	Blue		PVC-U-GF
30	Hornbach	Q-link	Green		PVC-U-GF
31	Hornbach	Q-link	White	HangZhou Xingfra Technology	PVC-P-NBR
32	Hornbach	Q-link	Grey		PVC-U-GF
33	Wholesale	Draka	Blue		PVC-P-NBR
34	Gamma	Handson	Red		PVC-U-ABS
35	Gamma	Handson	Blue		Polybutylene Terephthalate/PVC-U-ABS
36	Hornbach	Q-link	Red	HangZhou Xingfra Technology	HDPE
37	Hornbach	Q-link	Black	HangZhou Xingfra Technology	HDPE
38	Lowe	Southwire	Black		-
39	Lowe	Southwire	Green		-
40	Lowe	Southwire	Red		-
41	Lowe	Southwire	White		-
42	Lowe	Southwire	Transparent		-
43	Lowe	Southwire	Black		-
44	Lowe	Southwire	Brown		-
45	wholesale	Nexans	Yellow	Same wire as 1	PVC-P-NBR
46	wholesale	Eldra	Yellow	Same wire as 11	PVC-P
47	Praxis	Sencys	Yellow	Same wire as 19	PVC-P
48	Gamma	Handson	Yellow	Same wire as 23	PVC-P
49	Hornbach	Q-link	Yellow	Same wire as 30	PVC-U-GF

Jerrycans from 13 different brands/suppliers were evaluated. Most jerrycans consisted of several parts, such as the jerrycan, cap, cap pin, and filling tube. These parts were considered separately resulting in 39 samples.

Table S4. Information of jerrycans analyzed by LA-ICP-MS and FT-IR, obtained from various suppliers.

#	Set	Part	Supplier	Brand	Color	Details	Polymer type*
1	1	Can	Gamma	Carpoint	Black	3H1/Y1.2/150/21/ A/PA-03/200164/PLASTIK	HDPE
2	1	Cap	Gamma	Carpoint	Black	3H1/Y1.2/150/21/ A/PA-03/200164/PLASTIK	HDPE
3	1	Tube	Gamma	Carpoint	Yellow	3H1/Y1.2/150/21/ A/PA-03/200164/PLASTIK	LDPE
4	1	Cap pin	Gamma	Carpoint	Red	3H1/Y1.2/150/21/ A/PA-03/200164/PLASTIK	Polyoxymethylene (acetal) POM
5	2	Can	Hornbach	Hünersdorff	Black	3H1/Y1.0/150/ 21 /D/BAM 14026-huen	HDPE
6	2	Cap	Hornbach	Hünersdorff	Red	3H1/Y1.0/150/ 21 /D/BAM 14026-huen	LDPE
7	2	Tube	Hornbach	Hünersdorff	Red	3H1/Y1.0/150/ 21 /D/BAM 14026-huen	LDPE
8	3	Can	ANWB	ANWB	Black	3H1/Y1.2/150/2020 I/CSI89920DEU05	HDPE
9	3	Cap	ANWB	ANWB	Red	3H1/Y1.2/150/2020 I/CSI89920DEU05	PP (ELTEC P HP-603)
10	3	Tube	ANWB	ANWB	Red	3H1/Y1.2/150/2020 I/CSI89920DEU05	HDPE
11	3	Line	ANWB	ANWB	Black	3H1/Y1.2/150/2020 I/CSI89920DEU05	HDPE
12	4	Can	Bol	Splashbox Product Support B.V.	Blue	3H1/Y1.9/200/21/NL/WIVA 3224	HDPE
13	4	Cap	Bol	Splashbox Product Support B.V.	Black	3H1/Y1.9/200/21/NL/WIVA 3224	HDPE
14	5	Can	Bol	All Ride, RPC Promens Jagtenberg, Heerewaarden (NL)	Black	3H1/Y1.0/200/B/HJP-090122	HDPE
15	5	Cap	Bol	All Ride, Meno Berlin	Yellow	3H1/Y1.0/200/B/HJP-090122	HDPE
16	5	Tube	Bol	All Ride, Meno Berlin	Yellow	3H1/Y1.0/200/B/HJP-090122	HDPE
17	6	Can	Bol	Claudius Cosmetics B.V.	Transparent	P.20.101	HDPE/LDPE
18	6	Cap	Bol	Claudius Cosmetics B.V.	White	P.20.101	HDPE/LDPE
19	7	Can	Bol	All Ride, Jagtenberg Plastics BV (NL)	Red	3H1/Y1.0/200/B/HJP 110199	LDPE/HDPE
20	7	Cap	Bol	All Ride, Meno Berlin	Black	3H1/Y1.0/200/B/HJP 110199	HDPE/LDPE
21	7	Tube	Bol	All Ride, Meno Berlin	Black	3H1/Y1.0/200/B/HJP 110199	LDPE
22	8	Can	Bol	Splashbox Product Support B.V.	Blue	3H1/X1.9/250/B/AST-927805	HDPE
23	8	Cap	Bol	Splashbox Product Support B.V.	Black	3H1/X1.9/250/B/AST-927805	HDPE
24	9	Can	Bol	Splashbox Product Support B.V.	White	7434213316314	HDPE
25	9	Cap	Bol	Splashbox Product Support B.V.	Black	7434213316314	HDPE
26	10	Can	Bol	EDA Plastiques	Blue	19554	HDPE
27	10	Cap	Bol	EDA Plastiques	Red	19554	PP

<b>28</b>	10	Tube	Bol	EDA Plastiques	Yellow	19554	LDPE/HDPE
<b>29</b>	11	Can	Bol	Amacoo B.V.	Red	3H1/Y/160/ 20 D/BAM11486-PDD	HDPE
<b>30</b>	11	Cap	Bol	Amacoo B.V.	Black	3H1/Y/160/ 20 D/BAM11486-PDD	HDPE
<b>31</b>	11	Tube	Bol	Amacoo B.V.	Black	3H1/Y/160/ 20 D/BAM11486-PDD	HDPE/LDPE
<b>32</b>	11	Cap pin	Bol	Amacoo B.V.	Red	3H1/Y/160/ 20 D/BAM11486-PDD	Polyoxymethylene (acetal) POM
<b>33</b>	12	Can	Bol	Moralisto, malmarks Hungary	Red	3H1/X1.2/250/*/H 6YS-01- 01483-1-18	HDPE
<b>34</b>	12	Cap	Bol	Moralisto, malmarks Hungary	Black	3H1/X1.2/250/*/H 6YS-01- 01483-1-18	LDPE/HDPE
<b>35</b>	12	Tube	Bol	Moralisto, malmarks Hungary	Black	3H1/X1.2/250/*/H 6YS-01- 01483-1-18	LDPE/HDPE
<b>36</b>	13	Can	Bol	Hecht, J.P Plast, Werco spol.s r.o.	Black	3H1/Y/120/CZ/JPP-IMET 9031	HDPE
<b>37</b>	13	Cap	Bol	Hecht, J.P Plast, Werco spol.s r.o.	Red	3H1/Y/120/CZ/JPP-IMET 9031	LDPE
<b>38</b>	13	Tube	Bol	Hecht, J.P Plast, Werco spol.s r.o.	Red	3H1/Y/120/CZ/JPP-IMET 9031	LDPE
<b>39</b>	3	Fill Line	ANWB	ANWB	Transparent	3H1/Y1.2/150/21/ A/PA- 03/200164/PLASTIK	HDPE

### 3. Feature-based MVK model

For the evaluation of glass evidence various statistical models can be used. The feature-based multivariate Kernel (MVK) model (or two-level model) is currently in use at the Netherlands Forensic Institute for forensic glass casework and the utility of this method is demonstrated by various research groups in an interlaboratory study [1]. In this model, the elemental profile of a questioned sample will be compared to a control sample and all samples in the background database. The result will be a continuous likelihood ratio (LR), which is defined as the probability of the evidence given  $H_1$  divided by the probability of the evidence given  $H_2$  (equation 1). The prosecutor's hypothesis ( $H_1$ ) for comparison problems is the proposition that two samples originate from the same source, while the defense hypothesis ( $H_2$ ) is expressed as two samples having different sources. When the LR of a variable is considered statistically independent, the LR of variable A can be multiplied by the LR of variable B. When variables might be related, such as various physical characteristics or the elemental composition, the combined LR can be calculated [2].

$$LR = \frac{f(E|H_1)}{f(E|H_2)}$$

Equation 1

The MVK model will now be applied to a database consisting of 87 tapes from different sources with  $n=8$  repetitions, containing the response of  $p = 9$  elements measured by LA-ICP-MS. Table S6 shows how the database looks like. The mean concentration of 8 repetitions is given by  $\bar{x}_i$  where  $i$  represents each source.

Table S5. Part of normalized database of tapes measured by LA-ICP-MS ( $n = 8$ ,  $m=87$ ).

Source (m)	n	Al27	As75	Ca44	Cu63	Fe57	Mg25	Pb208	Si29	Sn118
<b>1</b>	<b>1</b>	0.02	-1.63	1.51	-2.01	-1.31	-0.52	-0.62	-1.67	-2.31
	<b>2</b>	-0.09	-1.71	1.43	-2.04	-1.49	-0.60	-0.71	-1.77	-2.33
	<b>3</b>	0.01	-1.63	1.50	-2.00	-1.31	-0.48	-0.63	-1.77	-2.32
	<b>4</b>	-0.09	-1.70	1.46	-2.03	-1.46	-0.60	-0.70	-1.72	-2.45
	<b>5</b>	0.02	-1.64	1.47	-2.02	-1.32	-0.50	-0.63	-1.63	-2.36
	<b>6</b>	-0.01	-1.61	1.46	-1.97	-1.33	-0.55	-0.62	-1.69	-2.35
	<b>7</b>	-0.11	-1.73	1.45	-2.06	-1.52	-0.62	-0.72	-1.91	-2.41
	<b>8</b>	-0.06	-1.71	1.42	-1.96	-1.53	-0.71	-0.71	-1.68	-2.54
<b>2</b>	<b>1</b>	-0.37	-1.65	1.59	-2.43	-1.25	-0.42	-0.58	-1.62	-2.60
...	...	...	...	...	...	...	...	...	...	...
<b>86</b>	<b>8</b>	2.26	-2.20	0.89	-1.48	-0.89	-0.65	-1.10	0.60	-1.81
<b>87</b>	<b>1</b>	1.93	-1.62	1.52	-1.74	-1.00	1.13	-0.91	-1.00	-2.45
	<b>2</b>	1.94	-1.67	1.54	-1.69	-0.99	1.15	-0.91	-1.02	-2.53
	<b>3</b>	1.91	-1.71	1.51	-1.44	-1.00	1.12	-0.92	-1.01	-2.58
	<b>4</b>	1.87	-1.75	1.43	-1.78	-1.09	1.07	-0.96	-1.07	-2.55
	<b>5</b>	1.90	-1.61	1.44	-1.89	-1.07	1.10	-1.02	-1.03	-2.46
	<b>6</b>	1.93	-1.69	1.50	-1.75	-1.06	1.14	-0.99	-1.03	-2.59
	<b>7</b>	1.89	-1.74	1.46	-1.81	-1.11	1.09	-1.02	-1.07	-2.52
	<b>8</b>	1.87	-1.77	1.44	-1.59	-1.13	1.08	-1.07	-1.09	-2.49

### 3.1. Normalization

Prior to the likelihood ratio calculation, the data was normalized to the elemental response of  $^{13}\text{C}$ . and a logarithmic transformation ( $\log_{10}$ ) was applied to bring the data closer to normality and reduce stochastic measurement fluctuations [3]. Figure S1 shows the effect of the log transformation on the data.

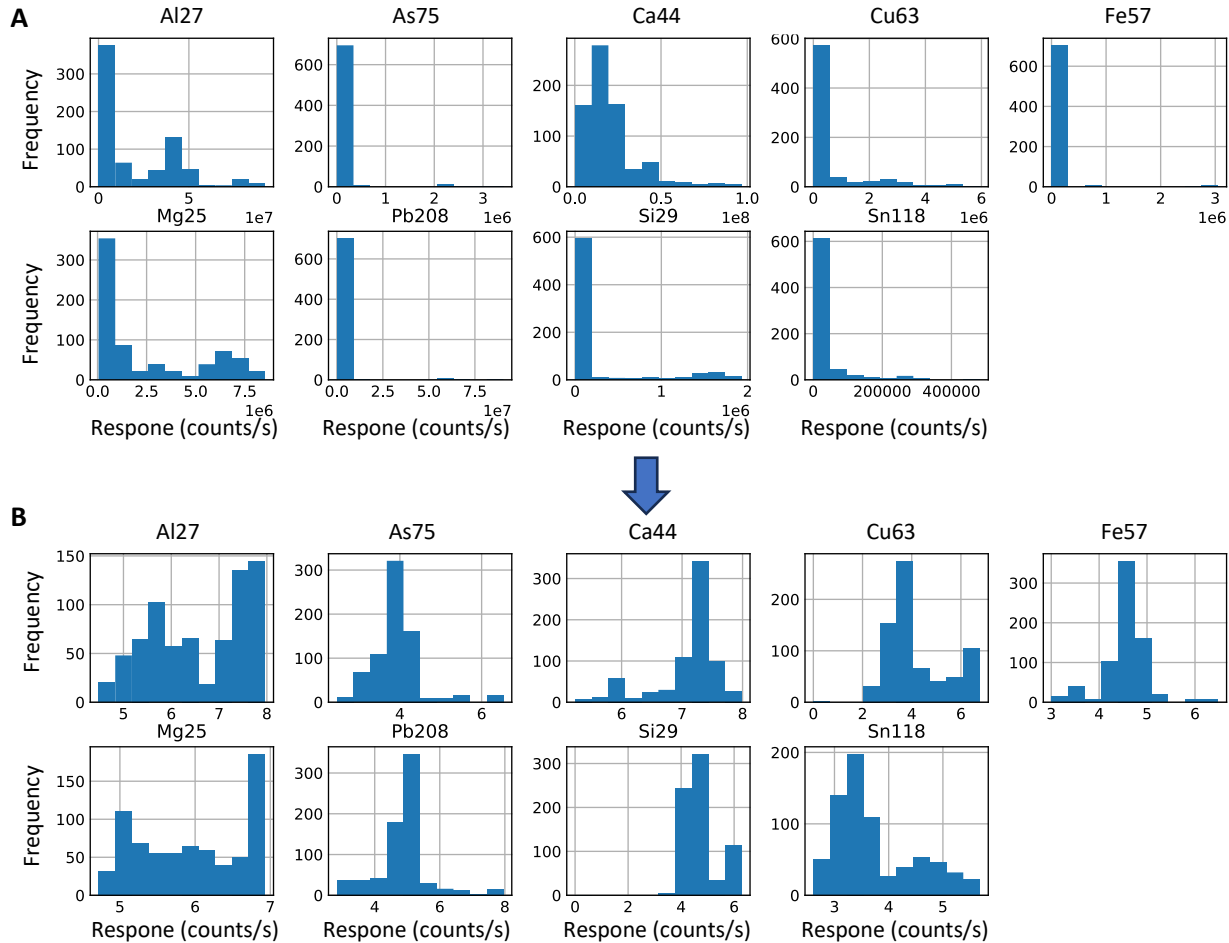


Figure S1. Effect of  $\log_{10}$  transformation on the LA-ICP-MS data of tapes. A) Raw data. B) Data after normalization.

### 3.2. Same-source comparison

Subsequently, we first apply a same-batch comparison, where we select one sample from the database, and we separate it into a control and a recovered sample (ground truth: samples come from the same source). The control has  $n_1 = 4$  repetitions with mean elemental concentrations of  $\bar{y}_1$ . The recovered sample has  $n_2=4$  repetitions with mean elemental concentrations of  $\bar{y}_2$ . The resulting background database will now have 86 (87-1) sources. The mean of four replicates of the control sample ( $\bar{y}_1$ ) is shown in Table S7. and the mean of the recovered sample ( $\bar{y}_2$ ) is shown in Table S8.

Table S6. Mean of four replicates of the control sample.

Source (m)	Al27	As75	Ca44	Cu63	Fe57	Mg25	Pb208	Si29	Sn118
1	-0.04	-1.67	1.48	-2.02	-1.39	-0.55	-0.67	-1.73	-2.35

Table S7. Mean of four replicates of the recovered sample.

Source (m)	Al27	As75	Ca44	Cu63	Fe57	Mg25	Pb208	Si29	Sn118
1	-0.04	-1.67	1.45	-2.00	-1.42	-0.60	-0.67	-1.73	-2.42

### 3.3. Variance-covariance matrix

Since, we are aiming to express the evidential value in a single LR value, the features should be combined in a certain way. To gain knowledge about how the data is distributed, it is important to assess the within-object and between-object variability. For meaningful forensic comparisons it is important that the between-object variability is significantly larger than the within-object variability. One way to express the spread in the data is by calculating the variance (square root of this value is the commonly applied standard deviation). When more than one variable is included, a measure for the joint variability is required. This can be expressed by the covariance, which is a measure of the dependence of two variables. Table S9 and S10 show the variance-covariance matrices for within source distribution (**U**) and between source distribution (**C**). Since the result is symmetric, only the upper right triangle of the matrix is shown. The within source variation was calculated for all 86 samples separately and afterwards the mean matrix was used for the LR calculation. For the between source variation, the mean of each source in the background database was calculated and then the covariance of all the 86 samples was computed. The matrices show that the within source variation is much smaller than the between source variation. A graphical presentation of the correlation between pairs is shown in Figure S2. The diagonal shows the distribution of elemental concentrations found for a single element.

Table S8. Variance-covariance matrix for within source distribution of tape samples in background dataset.

	Al27	As75	Ca44	Cu63	Fe57	Mg25	Pb208	Si29	Sn118
Al27	4.0E-03	7.4E-04	8.1E-04	2.1E-03	5.2E-04	1.0E-03	1.9E-03	3.6E-03	-5.5E-04
As75		1.3E-02	3.0E-06	2.8E-03	1.3E-04	2.5E-04	1.9E-03	7.4E-03	2.4E-03
Ca44			1.3E-03	4.5E-04	8.7E-04	8.5E-04	7.5E-04	1.8E-03	-5.6E-05
Cu63				4.8E-02	8.9E-04	1.9E-04	2.7E-03	5.4E-03	1.6E-03
Fe57					2.6E-03	7.9E-04	7.6E-04	2.0E-03	3.2E-04
Mg25						1.6E-03	6.5E-04	1.6E-03	1.3E-04
Pb208							5.0E-03	3.8E-03	9.8E-04
Si29								4.2E-02	4.1E-03
Sn118									1.7E-02

Table S9. Variance-covariance matrix for between source distribution of tape samples in background dataset.

	Al27	As75	Ca44	Cu63	Fe57	Mg25	Pb208	Si29	Sn118
Al27	5.6E-02	5.1E-03	4.7E-03	5.3E-02	6.6E-03	7.8E-03	2.2E-02	-2.7E-03	-9.0E-02
As75		7.8E-04	9.2E-04	-3.1E-02	1.1E-03	1.1E-03	3.1E-03	-1.8E-04	-1.2E-02
Ca44			1.2E-03	-5.2E-02	1.4E-03	1.2E-03	3.5E-03	-1.2E-04	-1.3E-02
Cu63				4.1E+00	-5.2E-02	-3.2E-02	-1.0E-01	-9.8E-03	3.3E-01
Fe57					1.6E-03	1.5E-03	4.3E-03	-2.2E-04	-1.7E-02
Mg25						1.5E-03	4.2E-03	-3.0E-04	-1.7E-02
Pb208							1.2E-02	-8.2E-04	-4.7E-02
Si29								1.4E-04	3.6E-03
Sn118									1.9E-01

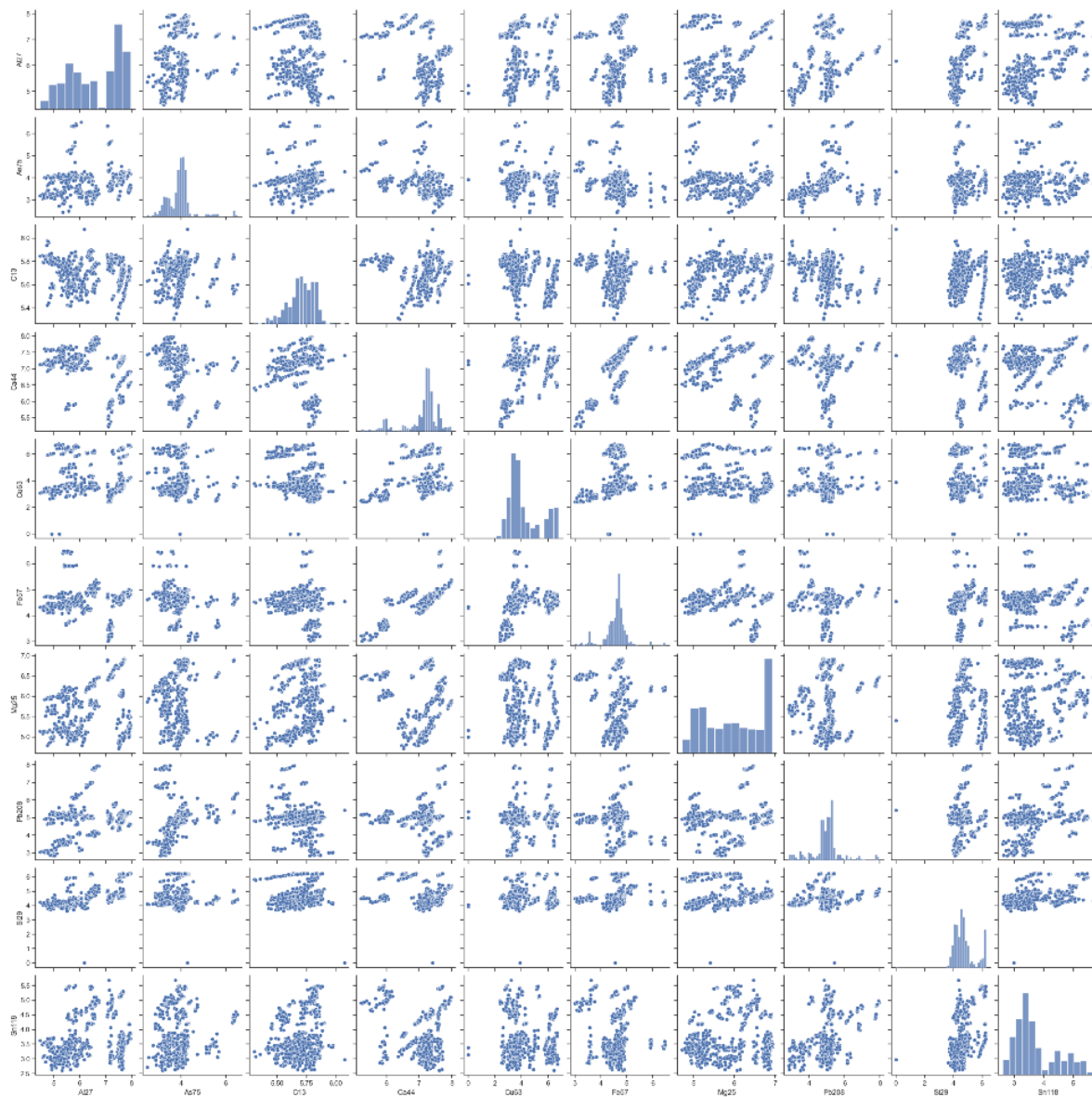


Figure S1. Graphical representation of the correlation between pairs of variables between sources of tape.

### 3.4. Kernel density estimation

It is assumed that the within source sample variation follows a normal distribution. However, the between source variation might not always be normally distributed. Therefore, the between source distribution is fitted by a Kernel density estimation (KDE). This is a method to estimate the probability density function of a variable using individual kernels (or curves) that are combined. The smoothing parameter ( $h$ ) of the KDE can be calculated by equation 2 [4]. The combination of  $h$  with the between covariance is the kernel bandwidth matrix:  $\mathbf{H} = h^2 \mathbf{C}$ .

$$h = \left( \frac{4}{m(2p+1)} \right)^{\frac{1}{p+4}}$$

Equation 2

The general kernel density function for multivariate data ( $\boldsymbol{\theta}$ ) is expressed as follows and can be recognized in the final LR calculation.

$$K(\boldsymbol{\theta} | \bar{\mathbf{x}}_i, \mathbf{H}) = (2\pi)^{-\frac{p}{2}} |\mathbf{H}|^{-\left(\frac{1}{2}\right)} \exp \left\{ -\frac{1}{2} (\boldsymbol{\theta} - \bar{\mathbf{x}}_i)^T \mathbf{H}^{-1} (\boldsymbol{\theta} - \bar{\mathbf{x}}_i) \right\}$$

Equation 3

### 3.5. Likelihood ratio

The numerator of the LR simulates that the control and recovered sample originate from the same source. Therefore, the difference in  $\bar{\mathbf{y}}_1$  and  $\bar{\mathbf{y}}_2$  is expressed by the weighted mean  $\bar{\mathbf{y}}^*$  in equation 4. In addition, the rarity of the data is expressed by the distance from the mean  $\bar{\mathbf{x}}_i$  from the weighted mean  $\bar{\mathbf{y}}^*$  [3].

$$\bar{\mathbf{y}}^* = \frac{n_1 \bar{\mathbf{y}}_1 + n_2 \bar{\mathbf{y}}_2}{n_1 + n_2}$$

Equation 4

For the calculation of the LR it is important to consider specific rules for matrix algebra. All matrices and vector parameters are shown in **bold**. The numerator  $f(E|H_1)$  of the LR for multivariate data is expressed in equation 5 below. The determinant of a matrix function is a scalar value that can be calculated based on the individual entries of a square matrix. In the exponent, the transpose of a vector with length  $1 \times p$  multiplied by a matrix of  $p \times p$  results in a vector of length  $1 \times p$ . This is then multiplied by a vector with length  $p \times 1$ , which gives a final dimension of  $1 \times 1$ , which will be a scalar. Consequently, the result of the numerator will be a single value which consists of the combined data of the features.

$$f(E|H_1) = (2\pi)^{-\frac{p}{2}} \times \det \left( \frac{\mathbf{U}}{n_1} + \frac{\mathbf{U}}{n_2} \right)^{-\frac{1}{2}} \times \exp \left\{ -\frac{1}{2} (\bar{\mathbf{y}}_1 - \bar{\mathbf{y}}_2)^T \left( \frac{\mathbf{U}}{n_1} + \frac{\mathbf{U}}{n_2} \right)^{-1} (\bar{\mathbf{y}}_1 - \bar{\mathbf{y}}_2) \right\} \times \\ \frac{1}{m} \sum_{i=1}^m \left\{ (2\pi)^{-\frac{p}{2}} \times \det \left( \frac{\mathbf{U}}{n_1+n_2} + h^2 \mathbf{C} \right)^{-\frac{1}{2}} \times \exp \left\{ -\frac{1}{2} (\bar{\mathbf{y}}^* - \bar{\mathbf{x}}_i)^T \left( \frac{\mathbf{U}}{n_1+n_2} + h^2 \mathbf{C} \right)^{-1} (\bar{\mathbf{y}}^* - \bar{\mathbf{x}}_i) \right\} \right\}$$

Equation 5

The denominator  $f(E|H_2)$  is calculated by equation 6. The first part describes the control ( $n_1$ ,  $\bar{y}_1$ ) characteristics and the second part shows the same equation for the recovered samples ( $n_2$ ,  $\bar{y}_2$ ). Also in this case, the result is a scalar value.

$$f(E|H_2) = (2\pi)^{-\frac{p}{2}} \times \det\left(\frac{\mathbf{U}}{n_1} + h^2 \mathbf{C}\right)^{-\frac{1}{2}} \times \frac{1}{m} \sum_{i=1}^m \left\{ -\frac{1}{2} (\bar{y}_1 - \bar{x}_i)^T \left(\frac{\mathbf{U}}{n_1} + h^2 \mathbf{C}\right)^{-1} (\bar{y}_1 - \bar{x}_i) \right\}$$

$$\times (2\pi)^{-\frac{p}{2}} \times \det\left(\frac{\mathbf{U}}{n_2} + h^2 \mathbf{C}\right)^{-\frac{1}{2}} \times \frac{1}{m} \sum_{i=1}^m \left\{ -\frac{1}{2} (\bar{y}_2 - \bar{x}_i)^T \left(\frac{\mathbf{U}}{n_2} + h^2 \mathbf{C}\right)^{-1} (\bar{y}_2 - \bar{x}_i) \right\}$$

Equation 6

For our specific example, the numerator is  $6.2 \times 10^4$  and the denominator is  $3.7 \times 10^{-6}$ . This results in an LR of  $1.7 \times 10^{10}$ . Therefore, the evidence is extremely more probable if the samples originate from the same source than when the samples originate from different sources. The calculation can be performed for the entire database, to evaluate the rate of misleading evidence. If an LR smaller than one was calculated, this would have been a false negative result. The total number of same source pairs equals the database size with  $m$  number of groups. It should be noted that more comparisons can be made if all  $n$  repetitions are considered separately instead of using mean  $\bar{y}_1$  and  $\bar{y}_2$ .

### 3.6. Different-source comparison

A similar calculation can be performed for different-source comparisons. Sample 1 was considered as the control sample with  $n_1=4$  repetitions and mean  $\bar{y}_1$  (Table S11). Sample 2 was the reference sample with  $n_2=4$  repetitions and mean  $\bar{y}_2$  (Table S12). The resulting background database will now have 85 (87-2) sources.

Table S10. Mean of eight replicates of the control sample.

Source (m)	Al27	As75	Ca44	Cu63	Fe57	Mg25	Pb208	Si29	Sn118
<b>1</b>	-0.04	-1.67	1.48	-2.02	-1.39	-0.55	-0.67	-1.73	-2.35

Table S11. Mean of eight replicates of the recovered sample.

Source (m)	Al27	As75	Ca44	Cu63	Fe57	Mg25	Pb208	Si29	Sn118
<b>2</b>	-0.34	-1.70	1.55	-2.49	-1.31	-0.55	-0.65	-1.72	-2.53

The numerator of the LR is calculated to be  $8.5 \times 10^{-72}$  and the denominator is  $2.1 \times 10^{-6}$ . This results in an LR of  $4.0 \times 10^{-66}$ . Therefore, the evidence is extremely more probable if the samples originate from different sources than when the samples originate from the same source. This calculation can be performed for the entire database, to evaluate the rate of misleading evidence. If an LR larger than one was calculated, this would have been a false positive result. The total number of different source pairs can be calculated by equation 7 for background data with  $m$  groups. Because the comparison of source 1 with source 2 equals the comparison of source 2 with source 1, the total number of comparisons can be divided by 2. In this specific example 3741 different source pairs can be compared. It should be noted that a lot more comparisons can be made if not the average value of 4 repetitions of the sources is used.

$$\frac{1}{2} m(m - 1)$$

Equation 7

### 3.7. Example with limited dataset

Since the calculation of the LR iterates over each background sample, it is a lengthy task to calculate it without programming. To get a feeling how the calculation is performed, the normalized database was reduced to four sources and two variables with four repetitions (Table S13). The elements Al and Pb were selected. Each step of the LR calculation is shown in the following sections.

Table S12. Limited dataset of tapes measured by LA-ICP-MS ( $n = 8, m=4$ ).

Source (m)	n	Al27	Pb208
1 (control)	1	0.02	-0.62
	2	0.01	-0.63
	3	-0.09	-0.71
	4	-0.09	-0.70
1 (recovered)	5	0.02	-0.63
	6	-0.01	-0.62
	7	-0.11	-0.72
	8	-0.06	-0.71
2	1	-0.37	-0.58
	2	-0.38	-0.58
	3	-0.46	-0.70
	4	-0.45	-0.70
3	1	-0.10	-0.59
	2	-0.06	-0.57
	3	-0.15	-0.72
	4	-0.14	-0.72
4	1	-0.69	-0.80
	2	-0.64	-0.76
	3	-0.63	-0.89
	4	-0.26	-0.89

We apply a same-batch comparison, where we select sample 1 from the database, and we separate it into a control and a recovered sample (ground truth: samples come from the same source). The control has  $n_1 = 4$  repetitions with mean elemental concentrations of  $\bar{y}_1$ . The recovered sample has  $n_2=4$  repetitions with mean elemental concentrations of  $\bar{y}_2$ . The resulting background database will now have 3 (4-1) sources. The mean of four replicates of the control sample ( $\bar{y}_1$ ), the mean of the recovered sample ( $\bar{y}_2$ ), the weighted mean ( $\bar{y}^*$ ) and the means of background samples  $\bar{x}_1$  (source 2),  $\bar{x}_2$  (source 3) , and  $\bar{x}_3$  (source 4) are shown in Table S14. For the background samples the mean of the first four replicates was calculated.

Table S13. Means of 4-8 replicates of sample analyzed by LA-ICP-MS.

Sample	Variable	Al27	Pb208
Control	$\bar{y}_1$	-0.04	-0.67
Recovered	$\bar{y}_2$	-0.04	-0.67
Weighted mean	$\bar{y}^*$	-0.04	-0.67
Background	$\bar{x}_1$	-0.42	-0.64
Background	$\bar{x}_2$	-0.11	-0.65
Background	$\bar{x}_3$	-0.56	-0.84

Subsequently, the within (co)variance matrix can be calculated for each background sample. The mean value of these matrices (**U**) is used for further calculations (Table S15). Also, the between (co)variance matrix (**C**) can be calculated (Table S16) based on the mean concentrations for each background sample from Table S14.

*Table S14. Variance-covariance matrices for within source distribution of tape samples in background dataset.*

		AI27	Pb208
2	AI27	0.0022	0.0032
	Pb208		0.0046
3	AI27	0.0018	0.0034
	Pb208		0.0069
4	AI27	0.0383	-0.0077
	Pb208		0.0042
average	AI27	0.0141	-0.0004
	Pb208		0.0052

*Table S15. Variance-covariance matrix for between source distribution of tape samples in background dataset*

		AI27	Pb208
2	AI27	0.0512	0.0180
	Pb208		0.0123

The following variables depicted in Table S17 are required for the LR calculation. The smoothing parameter is calculated based on Equation 2.

*Table S16. Variables for LR calculation with limited dataset.*

Variable	Value	Information
n	4	Number of repetitions background
n <sub>1</sub>	4	Number of repetitions control
n <sub>2</sub>	4	Number of repetitions recovered
m	3	Number of sources
p	2	Number of elements
h	0.802	Smoothing parameter KDE

All values can now be implemented in equations 5 and 6 to calculate the LR of equation 1. Each term of equation 5 is shown below.

$$A = (2\pi)^{-\left(\frac{p}{2}\right)} = 0.1592$$

$$B = \left( \frac{\mathbf{U}}{n_1} + \frac{\mathbf{U}}{n_2} \right) = \begin{pmatrix} 0.0071 & -0.0002 \\ -0.0002 & 0.0026 \end{pmatrix}$$

$$D = (\bar{\mathbf{y}}_1 - \bar{\mathbf{y}}_2) = (0.0022 \quad 0.0055)$$

$$E = \left( \frac{\mathbf{U}}{n_1 + n_2} + h^2 C \right) = \begin{pmatrix} 0.0347 & 0.0116 \\ 0.0116 & 0.0086 \end{pmatrix}$$

$$F = \left( -\frac{1}{2} (\bar{\mathbf{y}}^* - \bar{\mathbf{x}}_1)^T (E)^{-1} (\bar{\mathbf{y}}^* - \bar{\mathbf{x}}_1) \right) = -4.63$$

$$G = \left( -\frac{1}{2} (\bar{\mathbf{y}}^* - \bar{\mathbf{x}}_2)^T (E)^{-1} (\bar{\mathbf{y}}^* - \bar{\mathbf{x}}_2) \right) = -0.317$$

$$H = \left( -\frac{1}{2} (\bar{\mathbf{y}}^* - \bar{\mathbf{x}}_3)^T (E)^{-1} (\bar{\mathbf{y}}^* - \bar{\mathbf{x}}_3) \right) = -3.86$$

$$I = \det(B)^{-\left(\frac{1}{2}\right)} = (1.84 \times 10^{-5})^{-\left(\frac{1}{2}\right)} = 233$$

$$J = \det(E)^{-\left(\frac{1}{2}\right)} = (1.63 \times 10^{-4})^{-\left(\frac{1}{2}\right)} = 78.2$$

$$K = \exp \left\{ -\frac{1}{2} (D)^T (B)^{-1} (D) \right\} = 0.9937$$

### Result numerator:

$$\begin{aligned} f(E|H_1) &= A \times I \times K \times \frac{1}{m} \times \sum_{i=1}^m \{A \times J \times (\exp\{F\} + \exp\{G\} + \exp\{H\})\} \\ &= 0.1592 \times 233 \times 0.9937 \times \frac{1}{3} \\ &\quad \times \sum_{i=1}^3 \{0.1592 \times 78.2 \times (\exp\{F\} + \exp\{G\} + \exp\{H\})\} \\ &= 12.3 \times (12.4 \times (9.72 \times 10^{-3} + 7.28 \times 10^{-1} + 2.10 \times 10^{-2}) = 116 \end{aligned}$$

Equation 8

For the limited dataset, this will result in a numerator of 116 and a denominator of 10.5 which is calculated using equation 6 in a similar way as shown above. The uncalibrated LR will then be 11. Therefore, the evidence is more probable if the samples originate from the same source than when the samples originate from different sources.

## 4. LA-ICP-MS method optimization

### 4.1. Spot ablations of mid concentration samples

Figure S3 shows the effect of the laser energy on the counts and RSD for various spot sizes. As expected, an increasing spot size and laser energy resulted in a higher response. The variation was higher for a laser energy below 70%. The variation in the integrated range of the laser signal was also evaluated, but this did not vary a lot. Figure S4 shows the combined results. The combination of a 100% laser with a 100 µm spot gives the highest counts for a relatively good RSD. The application of a 100% laser with an 80 µm spot gives the best RSD with relatively good counts. Settings combining 90% laser and 90 µm spot or 80% laser with 100 µm spot are in between those values. The within RSD is shown, but a similar trend was visible for the between RSD.

Figures S5 and S6 show the same results for the PE standards. The combination of a 100% energy laser with a spot size of either 70 µm, 80 µm, or 100 µm gives the best RSD and counts. The results for the PS standards are shown in Figure S7 and S8. The combination of an 85% energy laser with a spot size of 100 µm resulted in the best counts and RSD. The second-best option is using a laser energy of 100% and spot of 80 µm. Overall, the three best options are applying an 85% laser energy with a 100 µm spot or using 100% laser energy with an 80 µm or 100 µm spot.

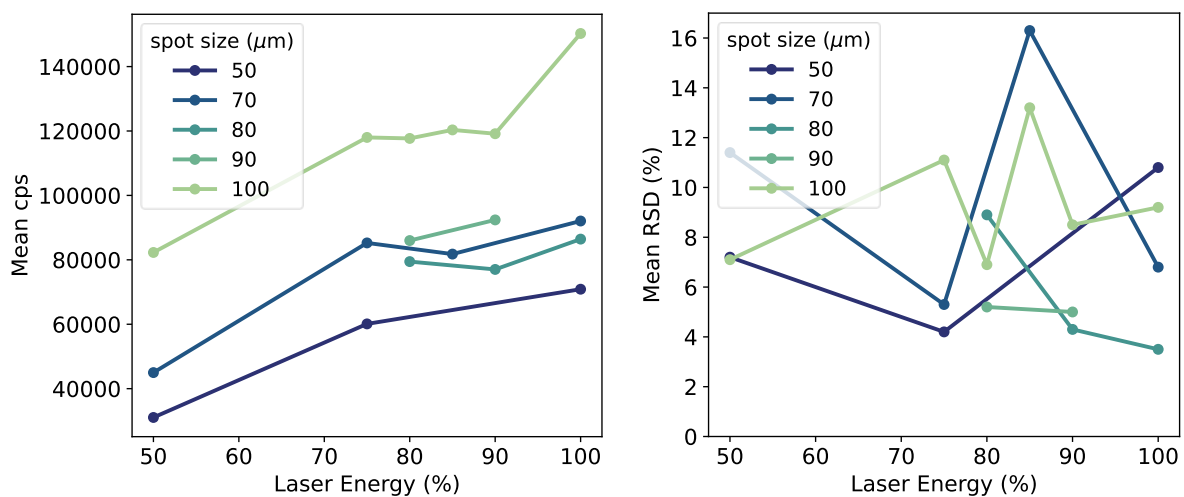


Figure S2. LA-ICP-MS analysis of mid concentration PVC sample for various spot sizes and laser energies. A) Mean cps, B) Mean RSD (%).

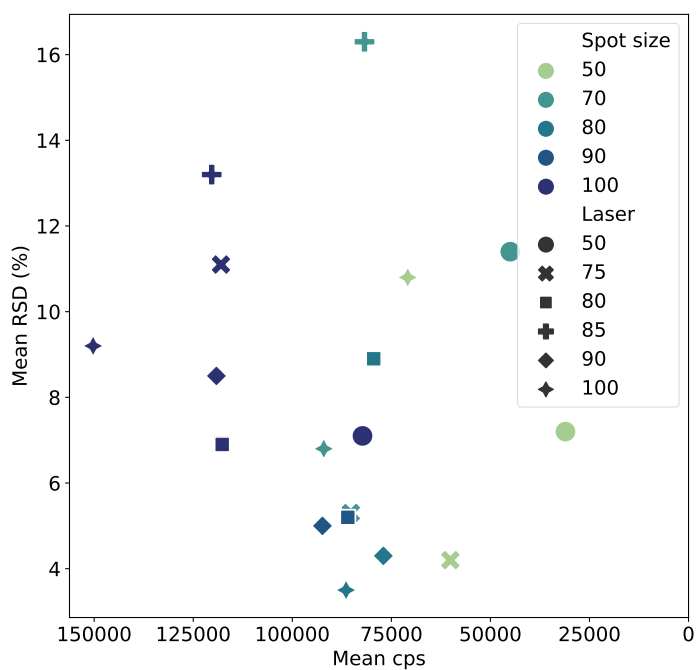


Figure S3. Combination of spot size and laser energy settings on the mean RSD (%) and cps (reverse axis is shown) of mid concentration PVC samples. Ideally, the data points should be positioned in the lower left corner.

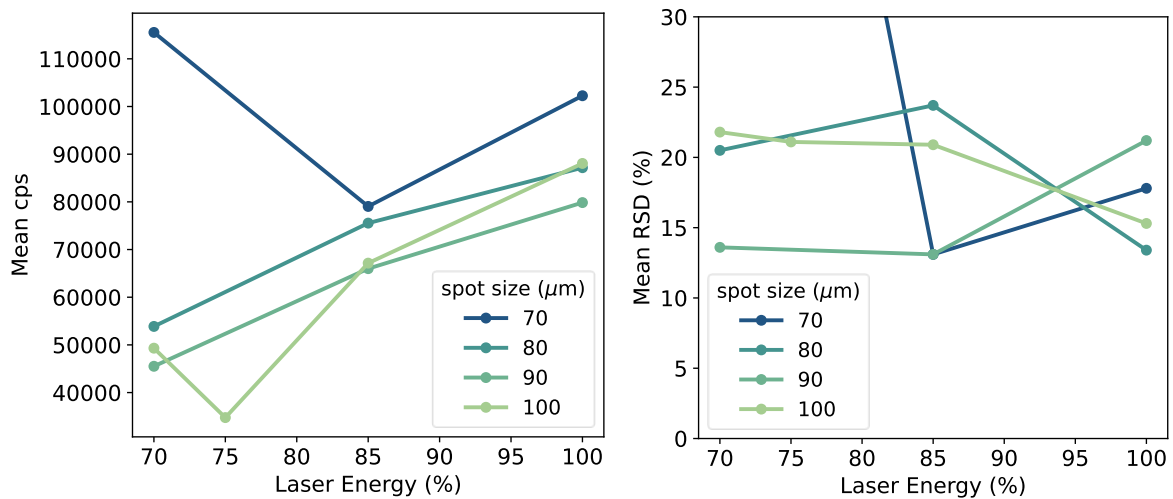


Figure S4. LA-ICP-MS analysis of mid concentration PE sample for various spot sizes and laser energies. A) Mean cps, B) Mean RSD (%).

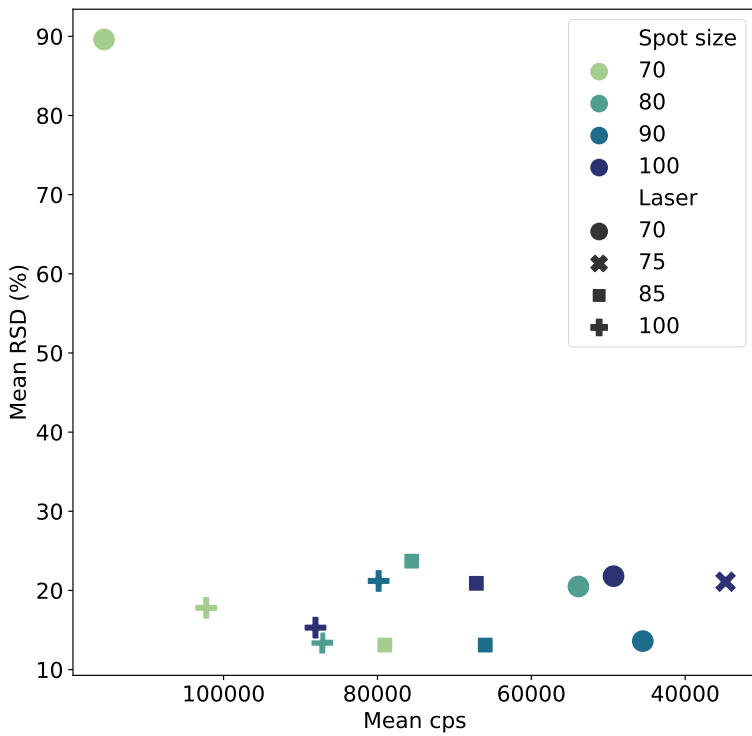


Figure S5. Combination of spot size and laser energy settings on the mean RSD (%) and cps (reverse axis is shown) of mid concentration PE samples. Ideally, the data points should be positioned in the lower left corner.

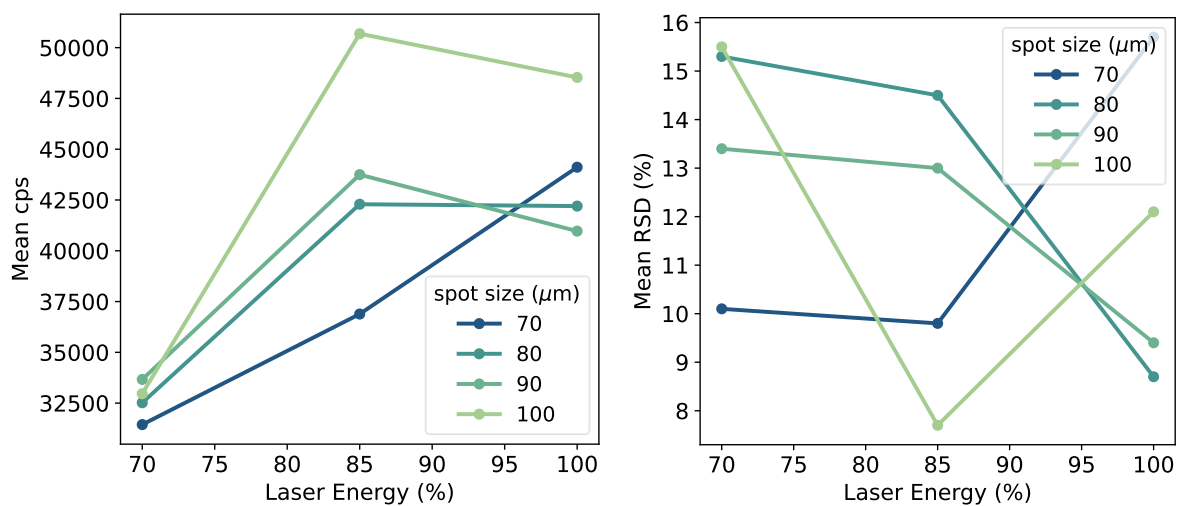


Figure S6. LA-ICP-MS analysis of mid concentration PS sample for various spot sizes and laser energies. A) Mean cps, B) Mean RSD (%).

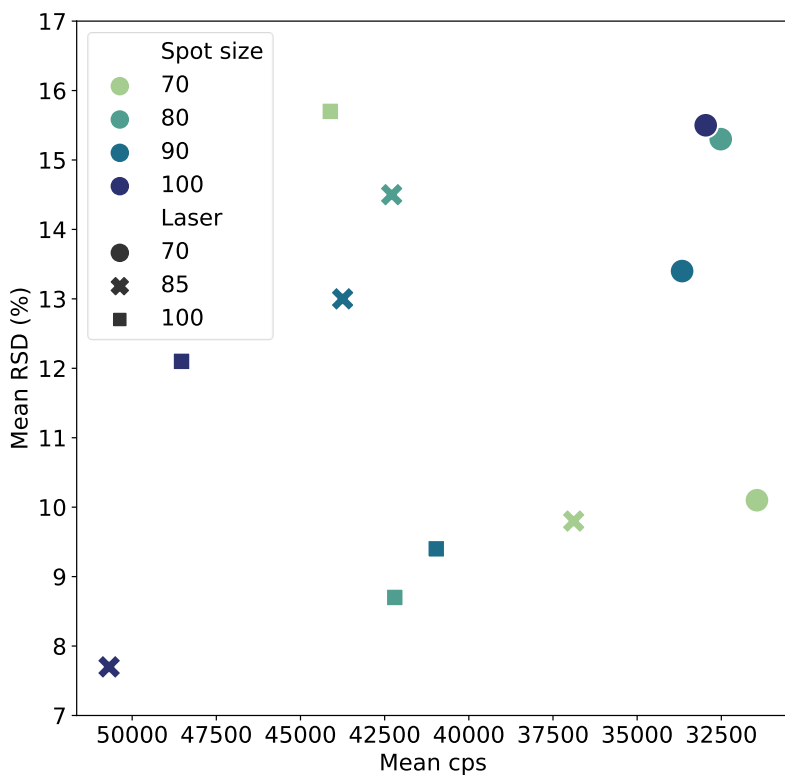


Figure S7. Combination of spot size and laser energy settings on the mean RSD (%) and cps (reverse axis is shown) of mid concentration PS samples. Ideally, the data points should be positioned in the lower left corner.

#### 4.2. Line ablations of mid concentration samples

The three best spot settings were applied to lines as well, but in this case the length and the laser speed were also varied. Figure S9 shows the results for mid concentrations samples of PVC, PE, and PS. Overall, a low speed of 0.015 mm/s with a line length of 0.7 mm was better than a speed of 0.1 mm/s with 3-line ablations over a length of 1.4 mm. Although a spot size of 100  $\mu\text{m}$  with a laser energy of 80% was the best for PVC, this was the worst for PE. The setting of 85% laser energy and 100  $\mu\text{m}$  line width was relatively good for all polymers, followed by a combination of 100% laser energy and a line width of 100  $\mu\text{m}$ .

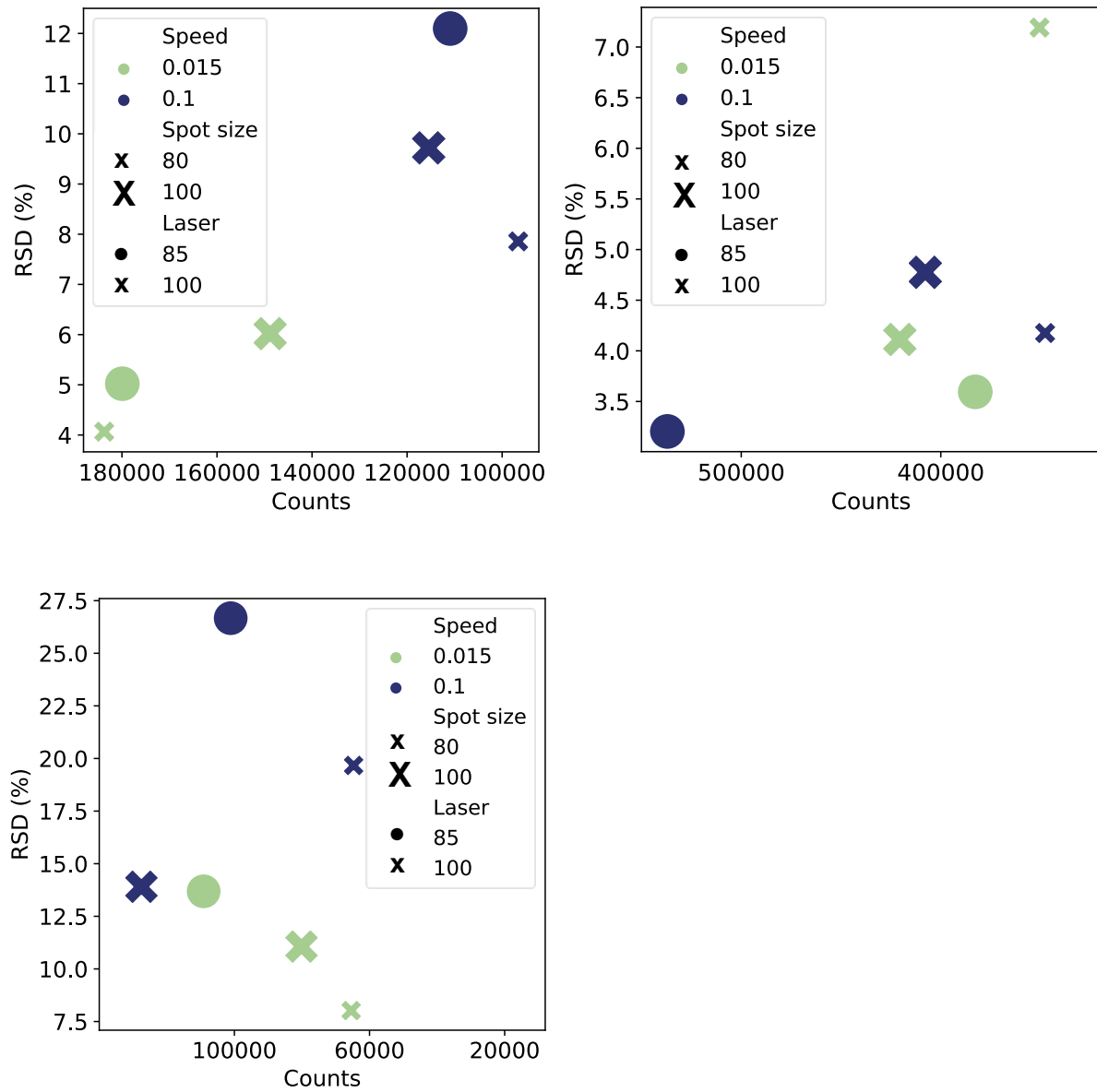


Figure S8. Combination of spot size and laser energy settings on the mean RSD (%) and cps (reverse axis is shown) of mid concentration samples measured in line mode (0.7 mm, 0.015 mm/s). Ideally, the data points should be positioned in the lower left corner. A) PVC, B) PE, C) PS.

#### 4.3. Spot and lines for various concentration standards

Based on the previous results, a limited number of preferred settings were selected that were applied to all concentration standards. Spots were measured with either 100 µm spot size with 85% laser energy or 80 µm spot size with 100% laser energy. In addition, lines were measured with 100 µm spot size and 85% or 100% laser energy over a line of 0.7 mm sampled at 0.015 mm/s. Two different ways of integration were evaluated: a small range of 40 s to 60 s and a wider range of 30 s to 60 s. Table S18 shows the performance with the RSD within-sample, RSD within-batch, signal RSD, mean of the maximum values of the elemental concentrations, the abundance of the minimum value compared to the blank, and the number of samples that were below a signal-to-noise (S/N) ratio of 3.

Overall, the best performance was found for 0.7 mm (0.015 mm/s) line ablations with 100 µm spot size, 85% laser energy and an integration range of 30 s to 60 s. This was in accordance with previous results based on a small selection of standards. The described method was selected for further analysis of the samples.

*Table S17. Average characteristics of low, medium and high concentration standards analyzed with various settings.*

Polymer	Type	Spot (µm)	Laser (%)	Range (s)	RSD within- sample (%)	RSD within- batch (%)	Signal RSD (%)	Max signal (mean)	Min signal/ blank (%)	N (S/N<3)
PVC	Line	100	85	40-60	8	21	15	2.2E+06	170	25
PVC	Line	100	85	30-60	7	21	20	1.9E+06	165	25
PVC	Line	100	100	30-60	11	22	18	2.7E+06	116	15
PVC	Spot	80	100	40-60	18	23	25	1.9E+07	23	25
PVC	Spot	100	85	40-60	15	30	22	3.8E+06	906	14
PE	Line	100	85	40-60	13	31	21	4.8E+06	137	14
PE	Line	100	85	30-60	14	33	24	4.7E+06	105	13
PE	Spot	80	100	40-60	20	43	47	3.8E+06	444	12
PE	Spot	100	85	40-60	19	34	32	2.5E+06	468	12
PS	Line	100	85	40-60	29	41	23	4.4E+06	274	24
PS	Line	100	85	30-60	26	39	26	3.5E+06	242	24
PS	Spot	80	100	40-60	44	44	35	4.5E+06	141	25
PS	Spot	100	85	40-60	35	48	29	5.8E+06	293	16

## 5. Performance of the polymer standard

### 5.1. Homogeneity

Table S19 compares the mean relative standard deviations for within-sample, between-batch, and between-run variation of the PVC, PE, and PS standards. The within-sample variation was measured based on four replicates within one batch of polymer standard. Additionally, three batches of PE, PS, and PVC standards at three concentrations were analyzed and evaluated for between-batch variation and linearity. The between-run variation of the standards was based on measurements repeated on 17 days. Especially,  $\mu$ -XRF analysis provides a good indication of the homogeneity, since the  $\mu$ -XRF samples a larger volume. The PS standard shows poor homogeneity which is presumably due to higher background concentrations for multiple elements [5]. For these standards, the  $\mu$ -XRF results were comparable to the LA-ICP-(TOF-)MS findings.

*Table S18. Average relative standard deviation (RSD, 18-160 repetitions) as indicator for within-sample ( $n=4$ , 68 repetitions), within-batch ( $n=3$ , 17 repetitions), and between-run variation ( $n=14$ ), for high concentration PE, PS, and PVC standards, analyzed by LA-ICP-MS for 21 elements, and  $\mu$ -XRF ( $n=32$ , 3 repetitions) for 12-15 elements. The signals were normalized to the nickel signal and are presented  $\pm$  stdev.*

	Within sample RSD (%)		Within-batch RSD (%)		Between run (%)
	LA-ICP-MS	$\mu$ -XRF	LA-ICP-MS	$\mu$ -XRF	LA-ICP-MS
PVC	$4.0 \pm 1.9$	16	$10 \pm 5$	12	$17 \pm 12$
PE	$7.2 \pm 2.3$	10	$13 \pm 15$	12	$12 \pm 6$
PS	$16 \pm 9$	28	$23 \pm 11$	43	$21 \pm 8$

### 5.2. LA-ICP-MS response

The line ablation signals of four representative elements are shown in Figure S10.

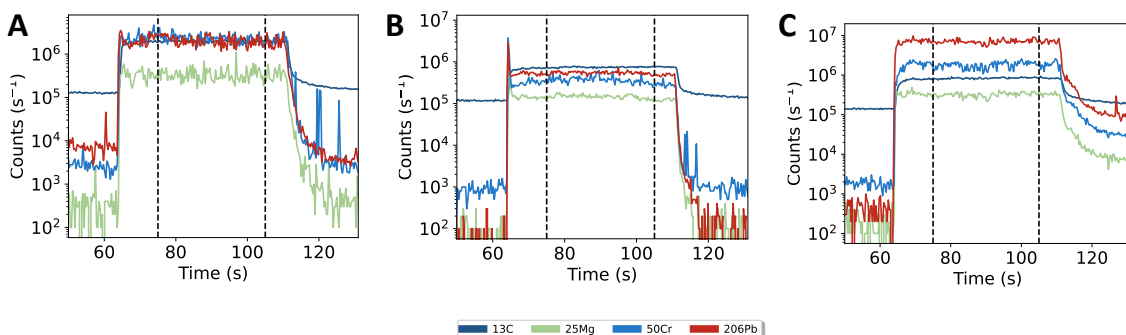


*Figure S9. LA-ICP-MS line scans over a distance of 0.7 mm for A) PE, B) PS, and C) PVC standards with four representative elements. Dashed lines mark the start and end of a line scan.*

### 5.3. Signal drift

To evaluate the signal drift, the standards were measured two times a day, i.e., before and after measuring the forensic objects. A mean decrease in elemental signal of 10, 8, and 19% was observed in respectively the PVC, PE, and PS standards. This was reduced by normalization to the signal of one element. Normalizing to carbon gave a maximum drift of -14% and normalization to the nickel signal resulted in a maximum drift of 5%.

## 5.4. Linearity

To evaluate the linearity, three batches of the blank, low, mid, and high concentration PVC, PE, and PS standards were measured in triplicate. In accordance with previously reported results [5], the LA-ICP-MS analyses showed excellent linear response with  $R^2$  for >0.99 for all elements in the PVC standards (Table S20). For PE, two elements ( $^{27}\text{Al}$  and  $^{44}\text{Ca}$ ) showed an  $R^2$  below 0.99, but still above 0.93. For PS  $^{47}\text{Ti}$  showed worse performance, probably because of the relatively large within-sample variation of the PS samples. The calibration graphs are shown in Figure S11. The response between the different polymer matrices varied considerably. The level of Pd and Si in PE was six orders of magnitude lower than its concentration in PVC and PS. For the other elements the difference was less apparent, where the highest response was on average seven times higher than the lowest response. To be able to correct for this variation, the PVC and PE polymer standards were both included in the analyses in this study.

*Table S19. Linearity of the elemental responses of PVC, PE, and PS reference standards analyzed by LA-ICP-MS.*

Element	$R^2$		
	PVC	PE	PS
<b>Na23</b>	0.9998	0.9999	0.9993
<b>Mg25</b>	0.9999	0.9995	0.9996
<b>Al27</b>	0.9965	0.9354	0.9963
<b>Si29</b>	0.9999	0.9996	0.9975
<b>K39</b>	0.9977	0.9997	1.0000
<b>Ca44</b>	1.0000	0.9886	0.9980
<b>Ti47</b>	1.0000	0.9992	0.5640
<b>Mn55</b>	0.9973	0.9999	1.0000
<b>Fe57</b>	0.9999	0.9999	0.9993
<b>Co59</b>	0.9999	0.9999	0.9994
<b>Ni60</b>	1.0000	0.9998	0.9993
<b>Cu63</b>	1.0000	1.0000	0.9996
<b>Ga69</b>	0.9999	0.9998	0.9991
<b>As75</b>	0.9999	0.9997	0.9990
<b>Sr88</b>	1.0000	0.9999	0.9997
<b>Nb93</b>	0.9961	0.9972	0.9975
<b>Pd106</b>	0.9964	0.9962	0.9995
<b>Sn118</b>	1.0000	0.9999	0.9993
<b>Sb121</b>	0.9934	0.9996	0.9992
<b>Ba138</b>	1.0000	1.0000	0.9998
<b>Pb208</b>	1.0000	0.9994	0.9991

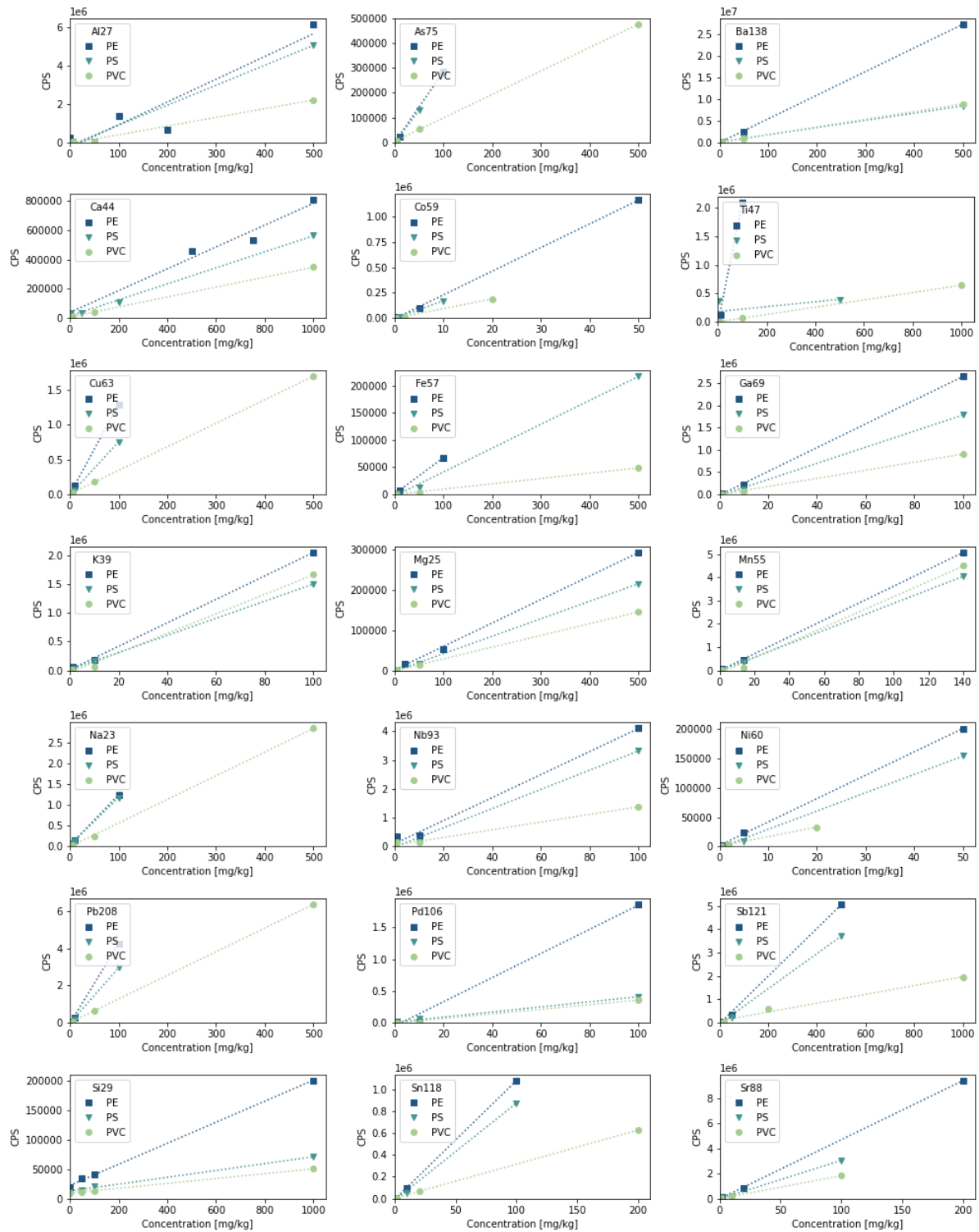


Figure S10. Calibration curves of responses in counts per seconds (CPS) of PE, PS and PVC with an elemental concentration ranging from 0 to 1000 mg/kg analyzed by LA-ICP-MS.

## 6. Correlation plots

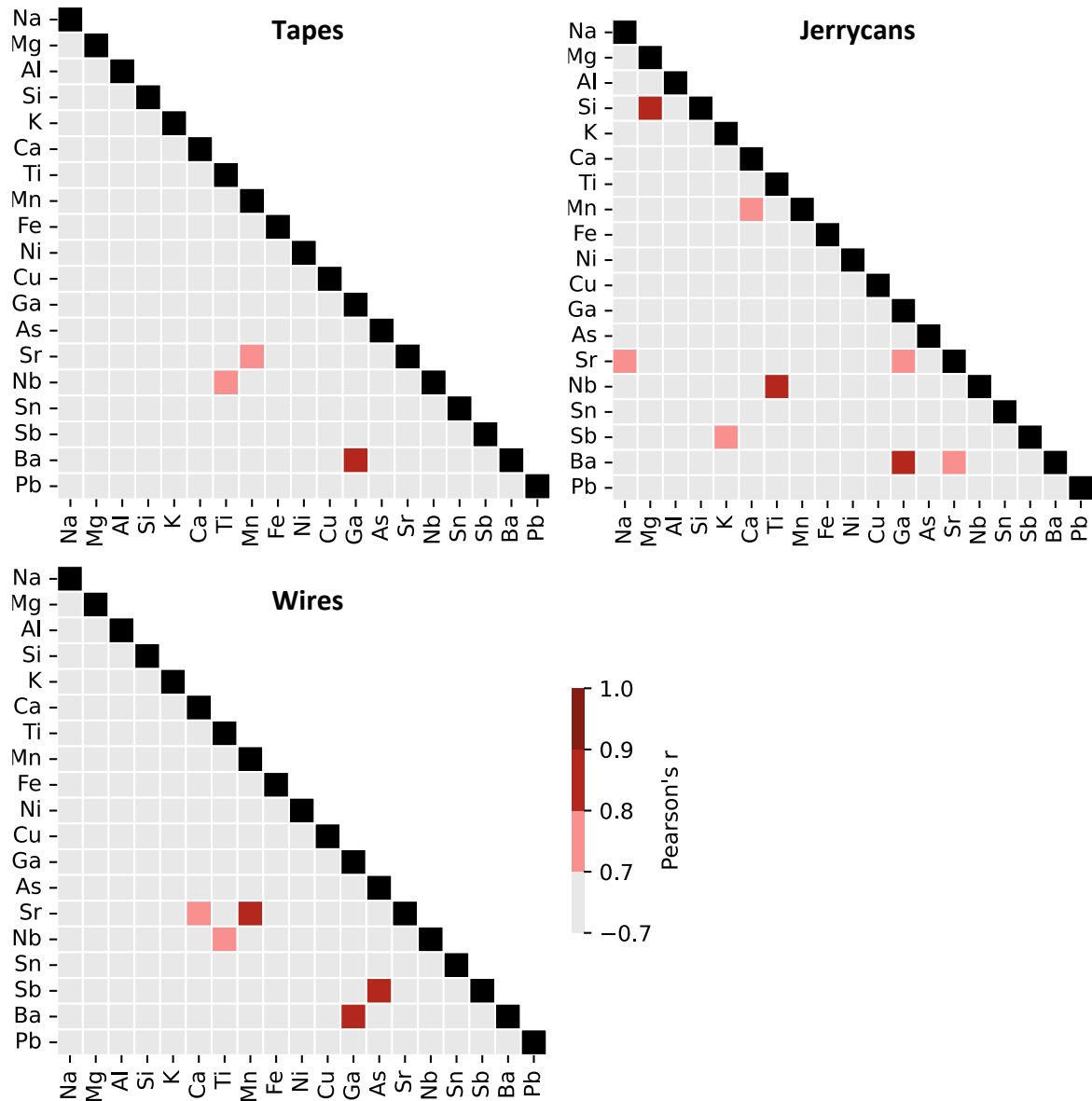


Figure S11. Pearson's correlation coefficients of the elements detected by LA-ICP-MS in tapes, jerrycans, and wires.

## 7. Leave-one-out validation PCA

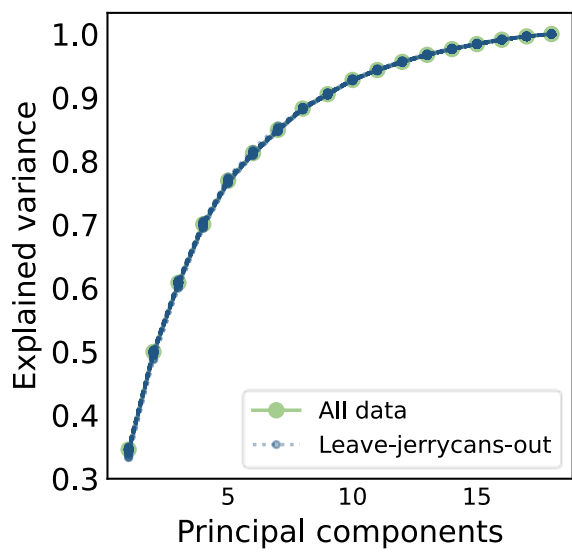


Figure S12. Explained variance of PCA with all data or when leaving out one sample.

## 8. Leave one-out validation LDA

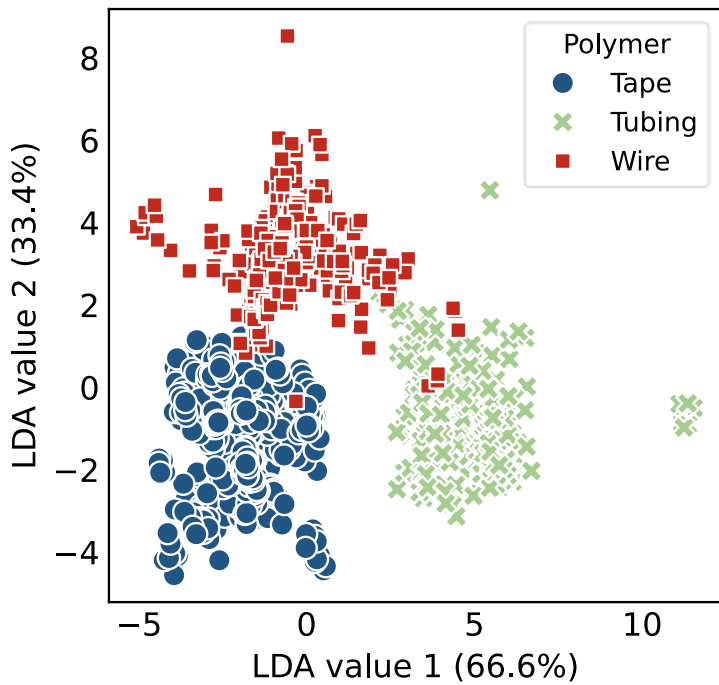


Figure S13. LDA-score plot of predicted values of leave-one-out samples, based on the elemental concentrations of tapes, tubing, and wires measured by LA-ICP-MS. Responses are quantified with the PVC standard and log10 transformed. The figure shows misclassification of eight repetitions of a transparent wire.

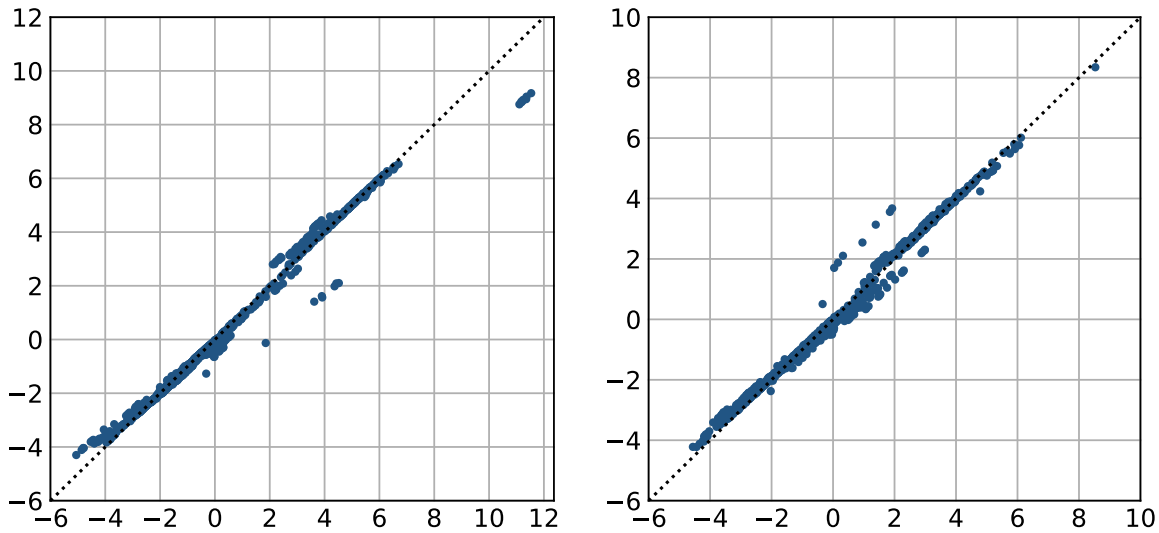


Figure S14. LDA values of training set (black dotted line) compared to predicted values based on test set with leave-one-out observation (blue dots). A) First LDA dimension (mean: 23% RSD, median: 2.6% RSD). B) Second LDA dimension (mean: 34% RSD, median: 5.2% RSD).

## 9. Boxplot of concentrations for each element

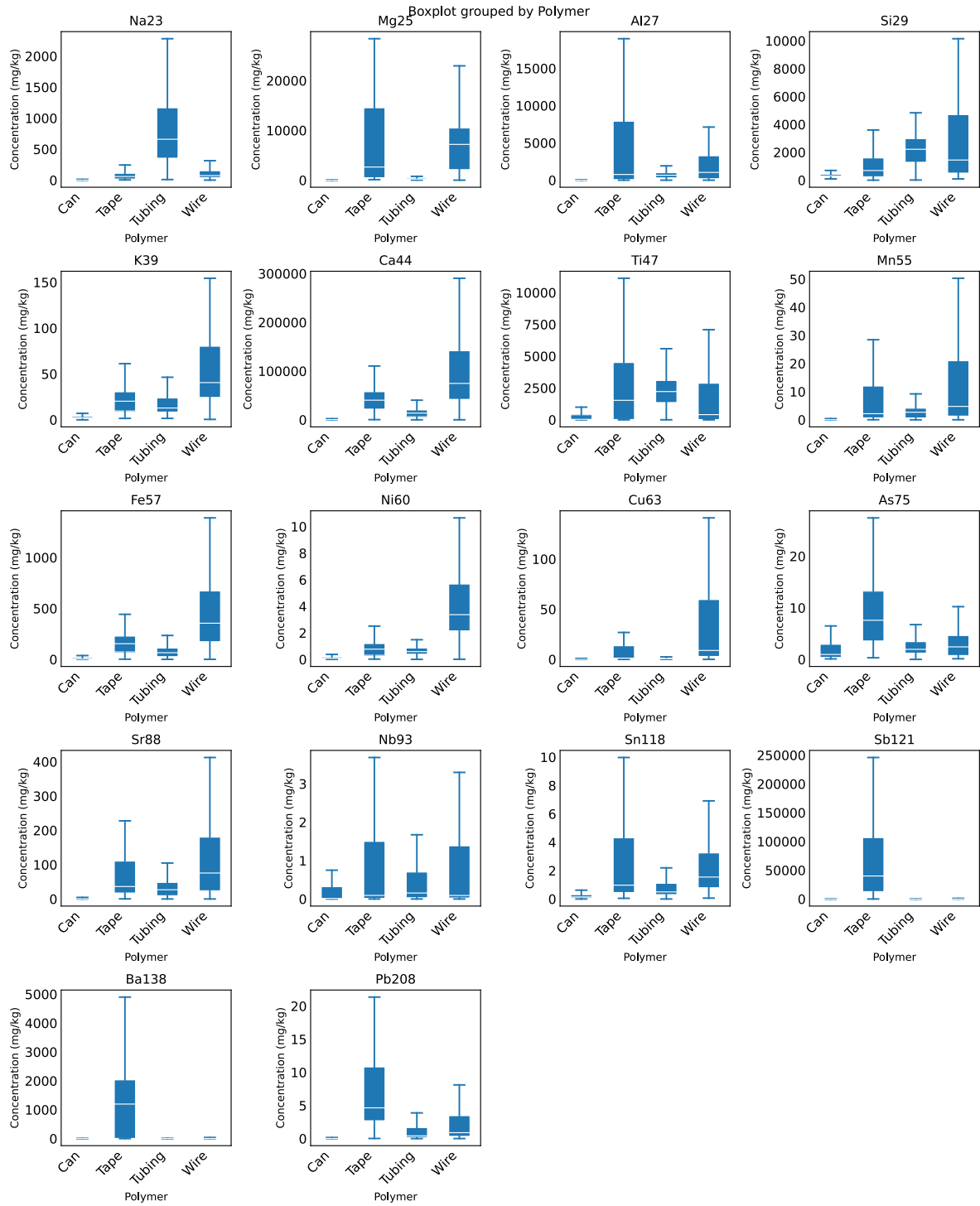


Figure S15. Boxplot with median elemental concentrations grouped by the type of forensic object. Elemental concentrations in mg/kg are shown based on correction with the PVC standard.

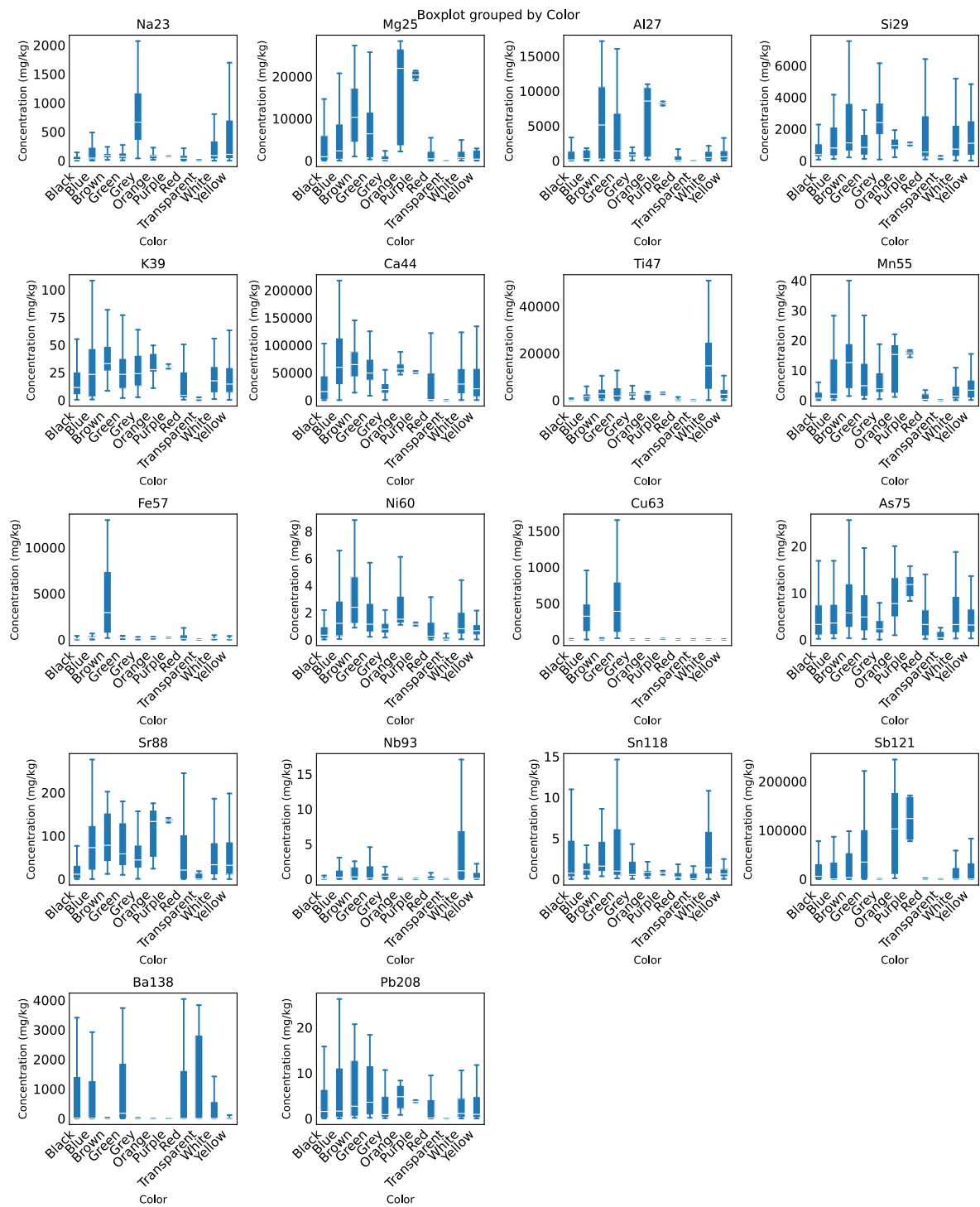


Figure S16. Boxplot median log<sub>10</sub> transformed elemental concentrations of all objects grouped by color. Elemental concentrations are shown based on correction with the PVC standard.

## 10. False inclusions/exclusions comparison models

Table S20. Rates of misleading evidence for the tape database, calculated by 4 sigma criterion, t-test with Bonferroni correction, MKV feature-based model, and score-based model with SVM and KDE.

Normalization	Elements	False exclusion (%)				False inclusion (%)			
		4s	t-test	Feature	Score	4s	t-test	Feature	Score
<b>Without</b>	18	1.1	4.6	4.6	0	1.2	0.080	1.8	0.65
<sup>13</sup> C	18	5.7	2.3	2.3	0	0.16	0.094	4.8	0.65
<b>Glass standard</b>	18	40	2.3	4.6	0	0.040	0.027	5.4	0.65
<b>PVC standard</b>	18	2.3	3.4	4.6	0	0.24	0.013	6.0	0.65
<sup>13</sup> C, PVC standard	18	2.3	1.1	3.4	0	0.24	0	5.1	0.65
<b>Without</b>	9	0	3.4	3.4	11	3.1	0.29	5.4	0.65
<sup>13</sup> C	9	0	0	3.4	5.6	0.84	0.31	7.7	0.65
<b>Glass standard</b>	9	31	1.1	3.4	0	0.13	0.21	3.6	0.65
<b>PVC standard</b>	9	0	1.1	5.7	5.6	0.86	0.16	4.2	0.65
<sup>13</sup> C, PVC standard	9	2.3	0	4.6	11	0.95	0.20	2.7	0.65

Table S21 Rates of misleading evidence for the tubing database, calculated by 4 sigma criterion, t-test with Bonferroni correction, MKV feature-based model, and score-based model with SVM and KDE.

Normalization	Elements	False exclusion (%)				False inclusion (%)			
		4s	t-test	Feature	Score	4s	t-test	Feature	Score
<b>Without</b>	18	5.1	0	17	13	11	0.17	14	7.1
<sup>13</sup> C	18	5.1	5.1	15	0	1.9	0.20	5.3	11
<b>Glass standard*</b>	18	41	2.6	16	0	0.20	0.60	30	7.1
<b>PVC standard</b>	18	2.6	2.6	13	13	8.1	0.34	16	3.6
<sup>13</sup> C, PVC standard	18	2.6	2.6	18	0	2.3	0.20	5.2	11
<b>Without</b>	9	2.6	0	7.7	0	19	1.2	8.8	11
<sup>13</sup> C	9	2.6	0	5.1	0	3.7	1.0	11	14
<b>Glass standard*</b>	9	21	2.6	2.6	0	0.40	1.1	14	11
<b>PVC standard</b>	9	0	0	7.7	0	18	1.1	11	18
<sup>13</sup> C, PVC standard	9	0	0	5.1	0	7.3	1.2	12	11

\*Limited repetitions for data corrected for glass standard.

Table S22. Rates of misleading evidence for the wires database, calculated by 4 sigma criterion, t-test with Bonferroni correction, MKV feature-based model, and score-based model with SVM and logistic regression.

Normalization	Elements	False exclusion (%)				False inclusion (%)			
		4s	t-test	Feature	Score	4s	t-test	Feature	Score
<b>Without</b>	18	2.0	0	6.1	10	0.60	0.17	4.2	0
<sup>13</sup> C	18	16	2.0	2.0	0	0.13	0	2.1	0
<b>Glass standard</b>	18	20	2.0	6.1	0	0.17	0.13	5.2	0
<b>PVC standard</b>	18	6.1	0	4.1	10	2.5	0.085	4.2	0
<sup>13</sup> C, PVC standard	18	10	2.0	2.0	0	0.26	0	2.1	0
<b>Without</b>	9	0	0	2.0	0	4.2	0.30	0	0
<sup>13</sup> C	9	14	0	8.2	0	0.89	0.13	1.0	0
<b>Glass standard</b>	9	14	0	4.1	0	0.85	0.38	0	2.2
<b>PVC standard</b>	9	2.0	0	4.1	0	9.2	0.21	0	2.2
<sup>13</sup> C, PVC standard	9	4.1	0	8.2	0	1.7	0.085	2.1	0

*Table S23. Rates of misleading evidence for the jerrycans database, calculated by 4 sigma criterion, t-test with Bonferroni correction, MKV feature-based model, and score-based model with SVM and logistic regression.*

Normalization	Elements	False exclusion (%)				False inclusion (%)			
		4s	t-test	Feature	Score	4s	t-test	Feature	Score
<b>Without</b>	18	21	2.6	3.2	0	2.0	1.3	4.4	0
<sup>13</sup> C	18	13	5.1	0	0	1.4	2.0	2.2	7.1
<b>Glass standard</b>	18	13	2.6	2.9	0	14	0.88	2.0	3.6
<b>PVC standard</b>	18	15	2.6	3.7	0	1.2	0.61	2.6	7.1
<sup>13</sup> C, PVC standard	18	18	2.6	6.5	13	1.6	2.2	4.4	7.1
<b>Without</b>	9	2.6	0	5.1	0	8.8	4.0	1.8	0
<sup>13</sup> C	9	5.1	2.6	0	13	6.3	4.1	1.8	3.6
<b>Glass standard</b>	9	10	2.6	2.6	0	27	2.8	1.8	0
<b>PVC standard</b>	9	7.7	0	2.6	0	5.0	2.4	1.8	0
<sup>13</sup> C, PVC standard	9	7.7	0	2.6	13	5.2	4.0	1.8	3.6

## 11. Tippett plots feature-based LR model

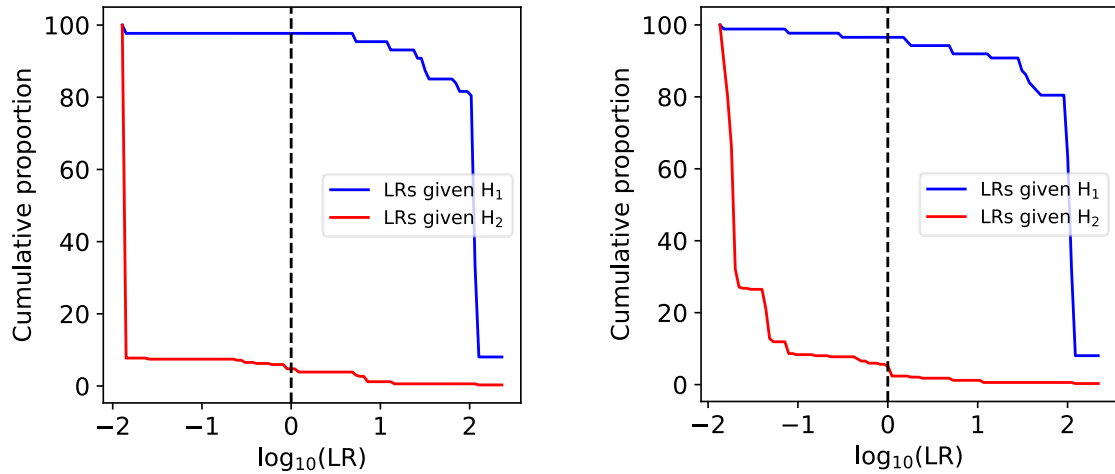


Figure S17. Tippett plots with PAV-calibrated cumulative distributions of  $\log_{10}$  likelihood ratio (LR) values for the tapes dataset, obtained with the feature-based MVK model. A) Elemental concentrations normalized to  $^{13}\text{C}$ . B) Elemental concentrations normalized to  $^{13}\text{C}$  and quantified with the PVC standard.

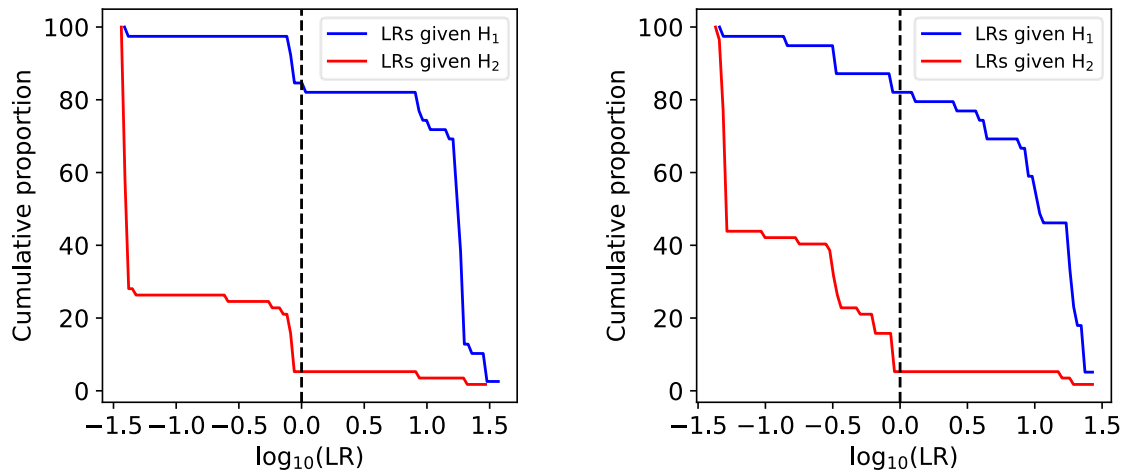


Figure S18. Tippett plots with PAV-calibrated cumulative distributions of  $\log_{10}$  likelihood ratio (LR) values for the tubing dataset, obtained with the feature-based MVK model. A) Elemental concentrations normalized to  $^{13}\text{C}$ . B) Elemental concentrations normalized to  $^{13}\text{C}$  and quantified with the PVC standard.

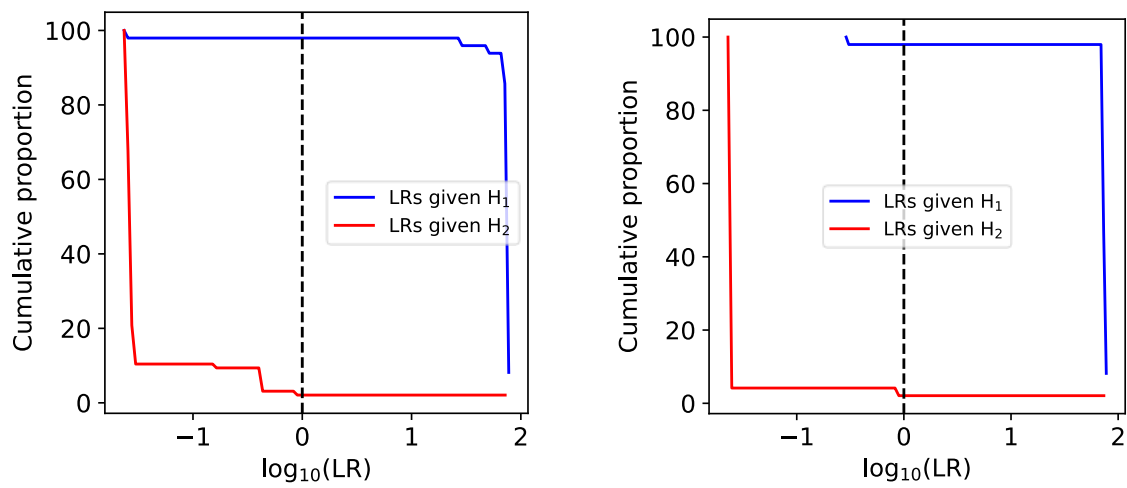


Figure S19. Tippett plots with PAV-calibrated cumulative distributions of  $\log_{10}$  likelihood ratio (LR) values for the wires dataset, obtained with the feature-based MVK model. A) Elemental concentrations normalized to  $^{13}\text{C}$ . B) Elemental concentrations normalized to  $^{13}\text{C}$  and quantified with the PVC standard.

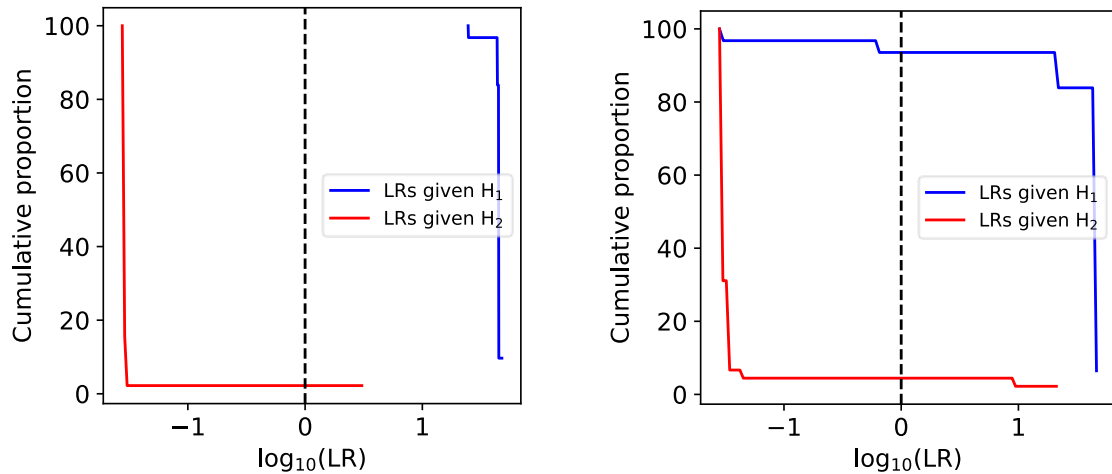


Figure S20. Tippett plots with PAV-calibrated cumulative distributions of  $\log_{10}$  likelihood ratio (LR) values for the jerrycans dataset, obtained with the feature-based MVK model. A) Elemental concentrations normalized to  $^{13}\text{C}$ . B) Elemental concentrations normalized to  $^{13}\text{C}$  and quantified with the PVC standard.

## 12. Performance measures feature-based LR model

Table S24. Performance measures of the feature-based LR model of the tape dataset after calibration and validation with 18 and 9 elements: log-likelihood-ratio cost (Clir), minimum, and maximum  $\log_{10}$  PAV LR value.

Elements	Normalization and quantification	Clir	Min log10 LR	Max log10 LR
<b>9</b>	<b>Without</b>	0.22	-1.81	2.07
	<sup>13</sup> C	0.19	-1.87	2.06
	<b>Glass standard</b>	0.20	-1.84	2.33
	<b>PVC standard</b>	0.23	-1.84	2.00
	<sup>13</sup> C, PVC standard	0.21	-1.85	2.05
<b>18</b>	<b>Without</b>	0.19	-1.83	2.31
	<sup>13</sup> C	0.18	-1.89	2.36
	<b>Glass standard</b>	0.17	-1.88	2.33
	<b>PVC standard</b>	0.20	-1.89	2.33
	<sup>13</sup> C, PVC standard	0.17	-1.87	2.34

Table S25. Performance measures of the feature-based LR model of the tubing dataset after calibration and validation with 18 and 9 elements: log-likelihood-ratio cost (Clir), minimum, and maximum  $\log_{10}$  PAV LR value.

Elements	Normalization and quantification	Clir	Min log10 LR	Max log10 LR
<b>9</b>	<b>Without</b>	0.43	-1.33	1.28
	<sup>13</sup> C	0.41	-1.51	1.32
	<b>Glass standard</b>	0.41	-1.51	1.12
	<b>PVC standard</b>	0.39	-1.51	1.25
	<sup>13</sup> C, PVC standard	0.39	-1.48	1.31
<b>18</b>	<b>Without</b>	0.50	-1.41	1.43
	<sup>13</sup> C	0.40	-1.44	1.57
	<b>Glass standard</b>	0.58	-1.43	1.48
	<b>PVC standard</b>	0.42	-1.46	1.55
	<sup>13</sup> C, PVC standard	0.51	-1.37	1.43

Table S26. Performance measures of the feature-based LR model of the wires dataset after calibration and validation with 18 and 9 elements: log-likelihood-ratio cost (Clir), minimum, and maximum  $\log_{10}$  PAV LR value.

Elements	Normalization and quantification	Clir	Min log10 LR	Max log10 LR
<b>9</b>	<b>Without</b>	0.050	-1.65	1.88
	<sup>13</sup> C	0.21	-1.62	1.87
	<b>Glass standard</b>	0.15	-1.63	1.88
	<b>PVC standard</b>	0.15	-1.61	1.88
	<sup>13</sup> C, PVC standard	0.20	-1.64	1.87
<b>18</b>	<b>Without</b>	0.32	-1.63	1.87
	<sup>13</sup> C	0.17	-1.63	1.89
	<b>Glass standard</b>	0.27	-1.63	1.87
	<b>PVC standard</b>	0.26	-1.63	1.88
	<sup>13</sup> C, PVC standard	0.12	-1.64	1.89

*Table S27. Performance measures of the feature-based LR model of the jerrycans dataset after calibration and validation with 18 and 9 elements: log-likelihood-ratio cost (Cllr), minimum, and maximum log<sub>10</sub> PAV LR value.*

Elements	Normalization and quantification	Cllr	Min log10 LR	Max log10 LR
<b>9</b>	<b>Without</b>	0.22	-1.55	1.67
	<b><sup>13</sup>C</b>	0.049	-1.56	1.68
	<b>Glass standard</b>	0.14	-1.56	1.68
	<b>PVC standard</b>	0.14	-1.56	1.68
	<b><sup>13</sup>C, PVC standard</b>	0.14	-1.56	1.68
<b>18</b>	<b>Without</b>	0.21	-1.55	1.65
	<b><sup>13</sup>C</b>	0.059	-1.56	1.68
	<b>Glass standard</b>	0.17	-1.56	1.68
	<b>PVC standard</b>	0.15	-1.54	1.67
	<b><sup>13</sup>C, PVC standard</b>	0.23	-1.55	1.67

### 13. Tippett plots score-based LR model

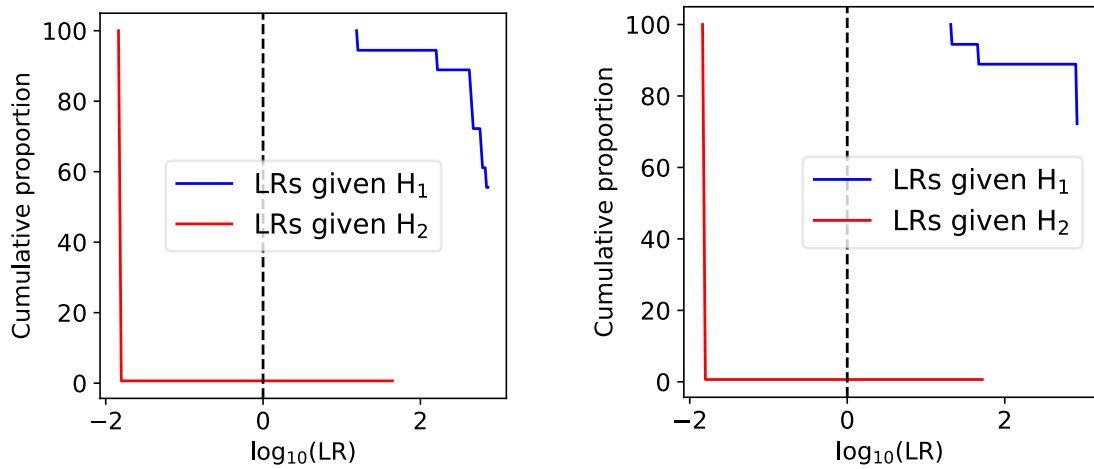


Figure S21. Tippett plots with the validated cumulative distributions of  $\log_{10}$  likelihood ratio (LR) values for the tapes dataset, obtained by the score-based model with SVM scoring system. A) Elemental concentrations normalized to  $^{13}\text{C}$ . B) Elemental concentrations normalized to  $^{13}\text{C}$  and quantified with the PVC standard.

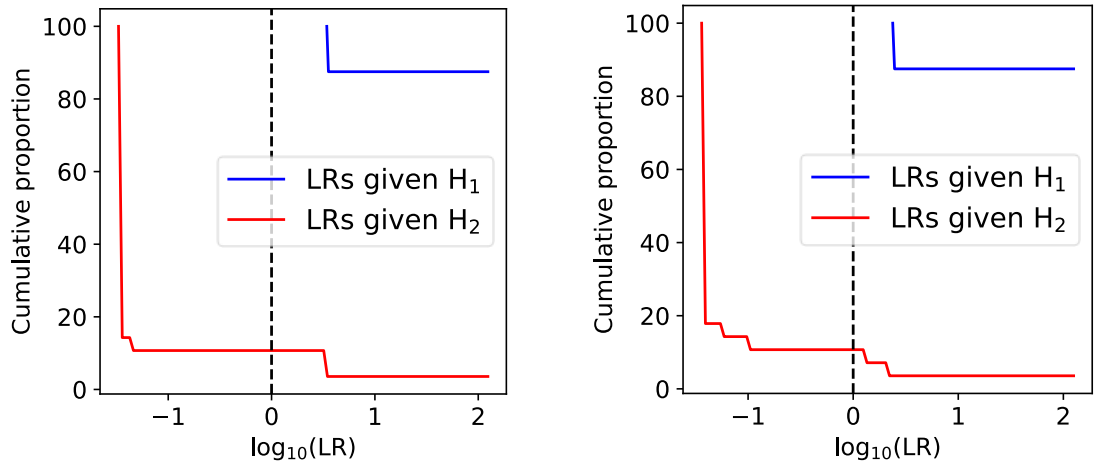


Figure S22. Tippett plots with the validated cumulative distributions of  $\log_{10}$  likelihood ratio (LR) values for the tubing dataset, obtained by the score-based model with SVM scoring system. A) Elemental concentrations normalized to  $^{13}\text{C}$ . B) Elemental concentrations normalized to  $^{13}\text{C}$  and quantified with the PVC standard.

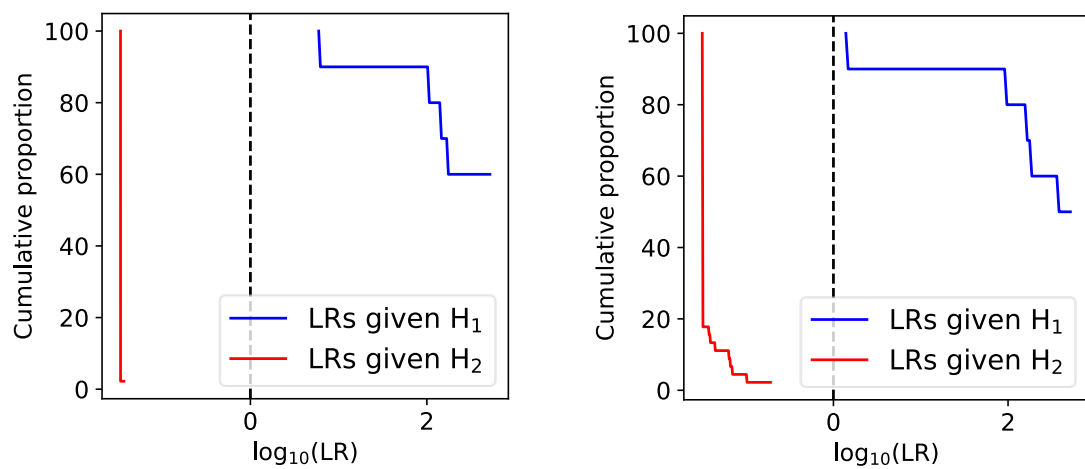


Figure S23. Tippett plots with the validated cumulative distributions of  $\log_{10}$  likelihood ratio (LR) values for the wires dataset, obtained by the score-based model with SVM scoring system. A) Elemental concentrations normalized to  $^{13}\text{C}$ . B) Elemental concentrations normalized to  $^{13}\text{C}$  and quantified with the PVC standard.

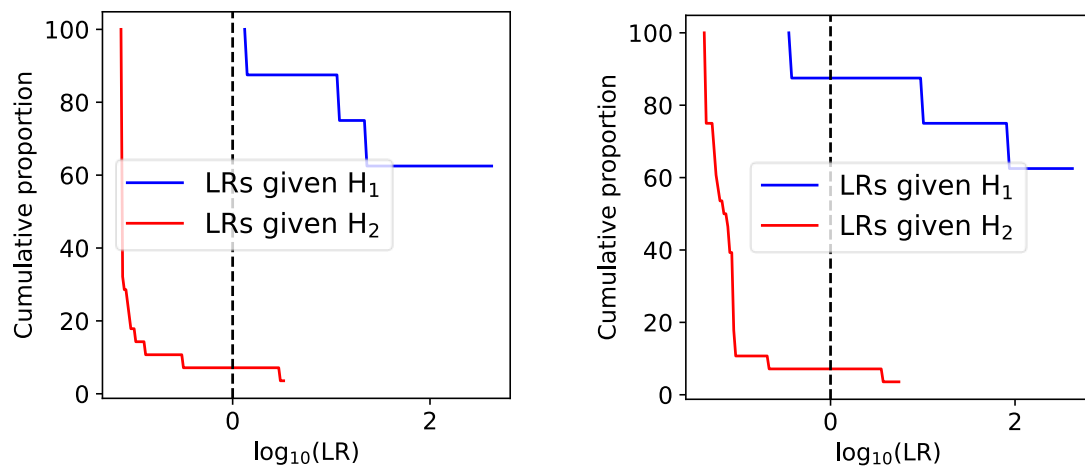


Figure S24. Tippett plots with the validated cumulative distributions of  $\log_{10}$  likelihood ratio (LR) values for the jerrycans dataset, obtained by the score-based model with SVM scoring system. A) Elemental concentrations normalized to  $^{13}\text{C}$ . B) Elemental concentrations normalized to  $^{13}\text{C}$  and quantified with the PVC standard.

## 14. Performance measures score-based LR model

Table S28. Performance measures of the score-based LR model of the tape database with log-likelihood-ratio cost (Clr) and minimum and maximum likelihood ratio values with empirical lower and upper bounds (ELUB) before validation.

Elements	Correction	Measure	LR to score	Clr	Min log <sub>10</sub> LR	Max log <sub>10</sub> LR
9	No correction	<b>Manhattan distance</b>	KDE	0.29	-1.70	2.00
			Logreg	0.30	-1.69	2.04
		SVM	KDE	0.25	-1.65	2.43
			Logreg	0.26	-1.62	2.52
	C	<b>Manhattan distance</b>	KDE	0.16	-1.70	1.97
			Logreg	0.16	-1.69	1.99
		SVM	KDE	0.44	-1.73	2.40
			Logreg	0.31	-1.69	2.20
glass	Manhattan distance	KDE	0.09	-1.72	2.20	
			Logreg	0.10	-1.71	2.42
		SVM	KDE	0.11	-1.67	2.65
			Logreg	0.11	-1.63	2.34
	PVC	KDE	0.30	-1.71	2.09	
			Logreg	0.27	-1.70	2.11
		SVM	KDE	0.47	-1.73	2.38
			Logreg	0.30	-1.68	2.29
C, PVC	Manhattan distance	KDE	0.30	-1.70	2.06	
			Logreg	0.30	-1.69	2.12
		SVM	KDE	0.48	-1.73	2.45
			Logreg	0.34	-1.68	2.32
	18	No correction	KDE	0.18	-1.72	2.28
			Logreg	0.19	-1.71	2.61
		SVM	KDE	0.13	-1.62	3.04
			Logreg	0.11	-1.63	2.85
C	Manhattan distance	KDE	0.10	-1.72	2.18	
			Logreg	0.10	-1.71	2.47
		SVM	KDE	0.08	-1.74	2.95
			Logreg	0.07	-1.73	2.91
	glass	KDE	0.10	-1.74	2.45	
			Logreg	0.11	-1.73	2.52
		SVM	KDE	0.11	-1.74	2.87
			Logreg	0.09	-1.71	2.46
PVC	Manhattan distance	KDE	0.12	-1.72	2.31	
			Logreg	0.14	-1.72	2.68
		SVM	KDE	0.12	-1.74	3.04
			Logreg	0.10	-1.72	3.03
	C, PVC	KDE	0.13	-1.72	2.32	
			Logreg	0.18	-1.71	2.65
		SVM	KDE	0.09	-1.74	3.04
			Logreg	0.09	-1.71	3.01

Table S29. Performance measures of the score-based LR model of the tubing database with log-likelihood-ratio cost (Clr) and minimum and maximum likelihood ratio values with empirical lower and upper bounds (ELUB) before validation.

Elements	Correction	Measure	LR to score	Clr	Min log <sub>10</sub> LR	Max log <sub>10</sub> LR
9	No correction	Manhattan distance	KDE	0.26	-1.16	1.29
			Logreg	0.28	-0.93	1.36
		SVM	KDE	0.15	-1.06	1.52
			Logreg	0.16	-0.95	1.44
		C	Manhattan distance	KDE	0.28	-1.15
			Logreg	0.28	-0.93	1.34
		SVM	KDE	0.25	-1.16	1.65
			Logreg	0.22	-0.94	1.52
		glass	Manhattan distance	KDE	0.31	-1.22
			Logreg	0.26	-1.24	1.51
PVC	No correction	SVM	KDE	0.26	-1.17	1.56
			Logreg	0.24	-0.85	1.64
		Manhattan distance	KDE	0.24	-1.19	1.33
			Logreg	0.24	-1.21	1.42
		SVM	KDE	0.14	-1.06	1.51
			Logreg	0.16	-0.93	1.41
		C, PVC	Manhattan distance	KDE	0.28	-1.19
			Logreg	0.29	-0.93	1.25
		SVM	KDE	0.25	-1.19	1.50
			Logreg	0.19	-1.21	1.52
18	No correction	Manhattan distance	KDE	0.17	-1.31	1.52
			Logreg	0.15	-1.29	1.48
		SVM	KDE	0.06	-1.36	2.08
			Logreg	0.06	-1.26	2.09
		C	Manhattan distance	KDE	0.23	-1.30
			Logreg	0.22	-1.29	1.42
		SVM	KDE	0.13	-1.36	1.85
			Logreg	0.13	-1.28	1.95
		glass	Manhattan distance	KDE	0.19	-1.26
			Logreg	0.17	-1.26	1.74
PVC	No correction	SVM	KDE	0.18	-1.00	1.78
			Logreg	0.14	-0.95	1.78
		Manhattan distance	KDE	0.17	-1.32	1.52
			Logreg	0.15	-1.31	1.44
		SVM	KDE	0.06	-1.37	2.01
			Logreg	0.07	-1.27	1.71
		C, PVC	Manhattan distance	KDE	0.21	-1.29
			Logreg	0.21	-1.29	1.69
		SVM	KDE	0.18	-1.36	1.99
			Logreg	0.14	-1.29	1.85

Table S30. Performance measures of the score-based LR model of the wires database with log-likelihood-ratio cost (Cllr) and minimum and maximum likelihood ratio values with empirical lower and upper bounds (ELUB) before validation.

Elements	Correction	Measure	LR to score	Cllr	Min log <sub>10</sub> LR	Max log <sub>10</sub> LR
9	No correction	Manhattan distance	KDE	0.34	-1.49	2.12
			Logreg	0.22	-1.48	2.34
		SVM	KDE	0.47	-1.50	2.54
			Logreg	0.35	-1.49	2.39
	C	Manhattan distance	KDE	0.43	-1.49	2.16
			Logreg	0.23	-1.48	2.37
		SVM	KDE	0.49	-1.50	2.52
			Logreg	0.33	-1.49	2.48
glass	Manhattan distance	KDE	0.32	-1.49	2.16	
			Logreg	0.22	-1.48	2.34
		SVM	KDE	0.47	-1.50	2.52
			Logreg	0.33	-1.49	2.39
	PVC	KDE	0.42	-1.49	2.20	
			Logreg	0.21	-1.49	2.34
		SVM	KDE	0.45	-1.50	2.54
			Logreg	0.31	-1.49	2.39
C, PVC	Manhattan distance	KDE	0.43	-1.49	2.18	
			Logreg	0.22	-1.48	2.37
		SVM	KDE	0.49	-1.50	2.52
			Logreg	0.34	-1.49	2.48
	18	No correction	KDE	0.09	-1.49	2.28
			Logreg	0.06	-1.48	2.41
		SVM	KDE	0.34	-1.50	2.59
			Logreg	0.13	-1.49	2.41
C	Manhattan distance	KDE	0.35	-1.49	2.31	
			Logreg	0.14	-1.49	2.48
		SVM	KDE	0.34	-1.50	2.56
			Logreg	0.14	-1.49	2.39
	glass	KDE	0.05	-1.49	2.28	
			Logreg	0.07	-1.49	2.41
		SVM	KDE	0.34	-1.50	2.59
			Logreg	0.13	-1.49	2.39
PVC	Manhattan distance	KDE	0.05	-1.49	2.28	
			Logreg	0.06	-1.49	2.41
		SVM	KDE	0.34	-1.50	2.62
			Logreg	0.10	-1.49	2.34
	C, PVC	KDE	0.26	-1.49	2.30	
			Logreg	0.12	-1.49	2.48
		SVM	KDE	0.34	-1.50	2.58
			Logreg	0.13	-1.49	2.39

Table S31. Performance measures of the score-based LR model of the jerrycans database with log-likelihood-ratio cost (Clrr) and minimum and maximum likelihood ratio values with empirical lower and upper bounds (ELUB) before validation.

Elements	Correction	Measure	LR to score	Clrr	Min log <sub>10</sub> LR	Max log <sub>10</sub> LR
9	No correction	Manhattan distance	KDE	0.77	-1.34	1.88
			Logreg	0.79	-1.33	2.24
		SVM	KDE	0.71	-1.38	2.32
			Logreg	0.74	-1.38	2.27
	C	Manhattan distance	KDE	0.38	-1.19	1.85
			Logreg	0.38	-0.99	1.95
		SVM	KDE	0.37	-1.29	2.30
			Logreg	0.37	-1.28	2.17
glass	Manhattan distance	KDE	0.43	-1.37	1.88	
			Logreg	0.45	-1.35	2.22
		SVM	KDE	0.40	-1.39	2.30
			Logreg	0.44	-1.38	2.27
	PVC	KDE	0.59	-1.32	2.22	
			Logreg	0.59	-1.32	2.22
		SVM	KDE	0.70	-1.38	2.32
			Logreg	0.71	-1.38	2.27
C, PVC	Manhattan distance	KDE	0.50	-1.19	1.85	
			Logreg	0.43	-0.99	1.95
		SVM	KDE	0.54	-1.29	2.30
			Logreg	0.52	-1.05	2.16
	18	No correction	KDE	0.78	-1.38	2.16
			Logreg	0.82	-1.38	2.32
		SVM	KDE	0.83	-1.39	2.34
			Logreg	0.80	-1.39	2.30
C	Manhattan distance	KDE	0.38	-1.30	2.30	
			Logreg	0.37	-1.32	2.25
		SVM	KDE	0.41	-1.39	2.41
			Logreg	0.40	-1.35	2.34
	glass	KDE	0.40	-1.39	2.20	
			Logreg	0.40	-1.38	2.32
		SVM	KDE	0.37	-1.39	2.38
			Logreg	0.41	-1.39	2.27
PVC	Manhattan distance	KDE	0.51	-1.38	2.25	
			Logreg	0.53	-1.38	2.32
		SVM	KDE	0.45	-1.39	2.38
			Logreg	0.49	-1.38	2.30
	C, PVC	KDE	0.41	-1.30	2.30	
			Logreg	0.39	-1.32	2.25
		SVM	KDE	0.40	-1.37	2.40
			Logreg	0.42	-1.34	2.32

## Disclaimer

Certain commercial equipment, instruments, or materials are identified in this paper in order to specify the experimental procedure adequately. Such identification is not intended to imply recommendation or endorsement by the National Institute of Standards and Technology, nor is it intended to imply that the materials or equipment identified are necessarily the best available for the purpose.

## References

- [1] K. Lambert, S. Montero, A. Akmeemana, R. Corzo, G. Gordon, E. Haase, P. Jiang, O. Ovide, K. Prasch, K. Redman, T. Scholz, T. Trejos, J. Webb, P. Weis, W. Wiarda, S. Wilczek, H. Xie, P. Zoon, J. Almirall, An interlaboratory study to evaluate the forensic analysis and interpretation of glass evidence, *Forensic Chemistry* 27 (2022). <https://doi.org/10.1016/j.forc.2021.100378>.
- [2] A. Bolck, C. Weyermann, L. Dujourdy, P. Esseiva, J. van den Berg, Different likelihood ratio approaches to evaluate the strength of evidence of MDMA tablet comparisons, *Forensic Sci Int* 191 (2009) 42–51. <https://doi.org/10.1016/j.forsciint.2009.06.006>.
- [3] G. Zadora, A. Martyna, D. Ramos, C. Aitken, *Statistical Analysis in Forensic Science: Evidential Value of Multivariate Physicochemical Data*, Wiley, 2014.
- [4] C.G.G. Aitken, D. Lucy, Evaluation of trace evidence in the form of multivariate data, 2004. <http://www.blackwellpublishing.com/rss>.
- [5] M. de Bruin-Hoegée, J. Schoorl, P. Zoon, M.J. van der Schans, D. Noort, A.C. van Asten, A novel standard for forensic elemental profiling of polymers by LA-ICP-TOF-MS, *Forensic Chemistry* 35 (2023). <https://doi.org/10.1016/j.forc.2023.100515>.